Lowering lattice forces of crystalline bases

Dissertation zur Erlangung des
naturwissenschaftlichen Doktorgrades der
Julius-Maximilians-Universität Würzburg

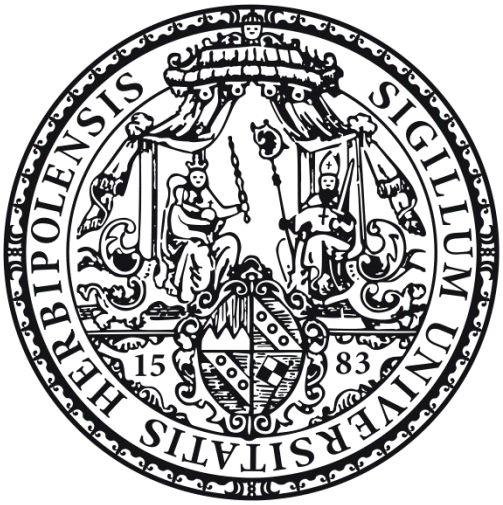

Dissertation zur Erlangung des naturwissenschaftlichen Doktorgrades an
der Fakultät für Chemie und Pharmazie
Der Julius-Maximilians-Universität Würzburg

vorgelegt

von

Maude Reggane
aus **Genf**, **Schweiz**

Würzburg, im **APRIL** 2018

Eingereicht bei der Fakultät für Chemie und Pharmazie am

_____

Gutachter der Dissertation

1. Gutachter: _____

2. Gutachter: _____

Prüfer des öffentlichen Promotionskolloquiums

1. Prüfer: _____
2. Prüfer: _____
3. Prüfer: _____

Tag des öffentlichen Promotionskolloquiums

_____

Doktorurkunde ausgehändigt am

_____

Die vorliegende Arbeit wurde unter Anregung und Anleitung von

Herr Prof. Dr. Dr. Lorenz Meinel

Lehrstuhl für Pharmazie und Lebensmittelchemie der Julius-Maximilians-Universität Würzburg und

Herr Dr. Bruno Galli
Herr Dr. Cornelius Harlacher

Novartis Pharma AG, TRD, Basel
angefertigt

Teile dieser Arbeit wurden bereits in folgender Form veröffentlicht:

Publikationen:

Reggane, M.; Wiest, J.; Saedtler, M.; Harlacher, C.; Gutmann, M.; Zottnick, S.H.; Piechon, P.; Dix, I.; Müller-Buschbaum, K.; Holzgrabe, U.; Meinel, L.; Galli, B. Bioinspired co-crystals of Imatinib providing enhanced kinetic solubility. Submitted to EJPB on April 3rd 2018.

Table of Contents

1 Introduction

1.1 Oral absorption and determining factors

The journey of an active pharmaceutical ingredient (API) from the solid oral dosage form to its molecular target is complex. Diverse biological environments and barriers require a fine balance between physicochemical properties for appropriate pharmacokinetics and pharmacodynamics. While permeability through lipidic cellular membranes, and often selective and potent target binding ask for some affinity for lipidic environment, excessive hydrophobicity, in turn, hampers oral delivery. Indeed, a prerequisite for oral absorption is the complete and timely dissolution in the aqueous gastrointestinal environment, thus hydrophilicity and solubility of a compound is key for oral delivery. Yet, achieving complete and timely dissolution in the gastrointestinal tract has become a major challenge for formulation scientists as the number of poorly water-soluble new chemical entities has kept rising over the past few years, triggering the need for new and innovative ways to deliver insoluble APIs.

1.1.1 Solubility

The solubility of a compound is the concentration of dissolved molecules that are in equilibrium with the solid phase in a saturated solution. It represents the dynamic equilibrium that is obtained once the rate of molecules going from the dissolved to the solid state is equal to the rate of molecules going from the solid to the solution state. The thermodynamic solubility implies that the solid form in equilibrium is the most stable form under these conditions. The equilibrium depends on the temperature, the pressure and on the medium. In contrast, the kinetic solubility refers to a metastable state.

The thermodynamic solubility is an intrinsic property that is fixed by the chemical structure of the molecule. Solubility of organic compounds used in the pharmaceutical environment is largely influenced by their hydrophobicity, and to a lesser extent by their melting point, according to the General Solubility Equation predicting the solubility of new chemical entities during drug discovery.[1, 2]

$$logS = 0.5 - 0.01\,(MP - 25) - logP \qquad \textbf{(Equation 1)}$$

S is the molar aqueous solubility, MP is the Celsius melting point and P is the octanol-water partition coefficient.

The General Solubility Equation reflects the unfavorable effect of a high melting point and a high octanol-water partition coefficient on the thermodynamic solubility which is rationalized as follows. Crystals with high lattice forces often display a high melting point. Indeed strong lattice forces increase the required enthalpy input during the solid-liquid phase transition which translates into a higher melting point.

Similarly strong lattice forces translate into a higher amount of energy required to break solid intermolecular bonds during the dissolution process. On the other hand, the solvation of a more hydrophobic molecule is less favorable as the number and strength of the solute-water interactions are reduced (i.e. less hydration of solute)

The thermodynamic solubility of an API can be increased in a medium containing a co-solvent or a solubilizer, such as a surfactant, a hydrotropic agent, cyclodextrins or polymers. The kinetic or apparent solubility, which is a transient state, can be tuned by changing the physical form of the API. Amorphization, salt and co-crystal formation are well-known formulation approaches that can lead to a transient, increased kinetic solubility.

1.1.2 Dissolution

The rate and extent of dissolution are preludes to oral absorption. According to the International Union of Pure and Applied Chemistry, dissolution is "the mixing of two phases with the formation of one new homogeneous phase (i.e. the solution)".[3] In the frame of solid pharmaceutical dosage forms, one of the phases is the drug, or the formulation, and the second phase is an aqueous liquid, i.e. *in vivo* the gastrointestinal environment. Drug dissolution is the mixing of both phases to result in a new, homogeneous drug solution. Dissolution can be broken down into 5 steps.[4] The first step is the wetting of the solid phase by water molecules. The second and third steps are the breaking down of the solid intermolecular interactions within the crystal, and the solvation of individual molecules by water molecules. According to the diffusion layer model, proposed by Noyes and Whitney, a thin layer of unstirred saturated solution is formed at the interface between the solid and the liquid.[5] Consequently the fourth step of dissolution is the diffusion of molecules from the surface of the solid across this boundary layer to the bulk medium. The last step is the convection of the molecules in the bulk liquid.[4]
This model highlights several possibilities to increase dissolution. Lowering the lattice forces within the crystal by amorphization, polymorph modification, or salt and co-crystal formation reduces the amount of energy needed in step 2. Increasing polarity by changing the charge or electron cloud of the molecules (e.g. by salt or co-crystal formation) increases solvation in step 3. Buffering the boundary layer pH (e.g. by salt or co-crystal formation) increases solubility of the API in this layer, thus increases its diffusion.

1.1.3 Dissolution Rate

The dissolution rate is the change of concentration in the medium over time. Based on the model proposed by Noyes and Whitney placing the diffusion through the boundary layer as the rate-limiting step of dissolution, and applying Fick's First Law to this diffusion step, the mathematical representation of the dissolution rate, the Nernst-Brunner equation, becomes:

$$\frac{dM}{dt} = \frac{S \times D}{h} \times (c_s - c_t) \quad \textbf{(Equation 2)}$$

where, dM is the amount of material dissolving during the time interval dt, S is the surface area available for dissolution (i.e. the wetted surface area), h is the thickness of the boundary layer, D is the diffusion coefficient of the solute in the boundary layer (also called the diffusivity), c_s is the concentration of the solute in the boundary layer (i.e. its kinetic solubility in this environment) and c_t is the concentration of the solute in the bulk liquid at time t.[4-6]

Thus, the dissolution rate may be improved by increasing the surface area S by means of particle size reduction or improved wetting. Assuming that dissolution is diffusion-limited, it becomes very clear that the concentration gradient across the unstirred diffusion layer is a key parameter. On one end, the concentration of the drug in this layer, c_s, can be increased by any of the techniques mentioned above (physical state modification, salt and co-crystal formation, solubilization techniques). On the other end, absorption in the gastrointestinal tract by removing dissolved molecules from the bulk solution lowers c_t which has a favorable effect on dissolution rate.

Placing these considerations in a biopharmaceutical context, dissolution of a drug product is influenced by the formulation properties, by the API physichochemical properties and by various physiological factors.

1.1.4 Passive diffusion

Most small molecules are absorbed from the gastrointestinal tract by passive diffusion across the bilayer cellular membrane of enterocytes.[7] Passive diffusion is a gradient-driven mass transport and is based on the Fick's First Law:

$$J = P \times \left(C_{donor} - C_{acceptor}\right) \quad \textbf{(Equation 3)}$$

Where, J is the flux in amount per unit of time, C_{donor} is the concentration in the donor compartment, $C_{acceptor}$ is the concentration in the acceptor compartment, and P is the permeability.

The permeability, P, is an intrinsic property of an API that is dictated mainly by the molecular size and the hydrogen-bonding potential.[8] The molecular weight of most API falling between 200-600 g/mol this parameter has little influence in this context. Thus permeability of small pharmaceutical molecules is mainly driven by hydrogen-bonding potential. Strong intermolecular hydrogen bonds with water molecules require significant energy to be broken before the API can partition through the lipidic bilayer, and

hydrogen bonding with the polar head groups of phospholipids can dock the API slowing down partitioning.[8, 9]

The pH of the medium and ionization constant of the API dictate the ionization state of the API in solution which influence passive absorption as only the neutral form diffuses through the lipophilic membrane of enterocytes.

In some circumstances, the driving force for the flux across the membrane may be non-ideal, i.e. not strictly linked to concentration but rather to the thermodynamic activity or chemical potential of the drug in solution.[10] According to recent evidence, the type of solution generated by different enabling formulation approaches has an impact on diffusion, and the distinction between solubilized solutions and supersaturated solutions must be emphasized.[10, 11] A solubilized solution is thermodynamically stable and the activity of solubilized drug molecules is in general similar to a saturated solution concentration. In contrast, supersaturated states are metastable, and molecules in solution ineluctably move to a more stable state over time (i.e. the API will phase separate and/or nucleate to form a new, more stable solid phase). As a result, the activity of drug molecules in supersaturated solutions is increased as compared to saturated solutions, which drives the diffusive flux to a maximum level.

1.2 Relevant amphiphilicity-driven behaviours: aggregation and hydrotropy

A molecule bearing both hydrophilic and hydrophobic domains is said to be amphiphilic, and a majority of APIs do have some level of amphiphilicity. Amphiphilicity in aqueous media may lead to several phenomena, from which at least two are of interest in the context of oral absorption.

1.2.1 Aggregation

Many amphiphilic drugs display concentration and pH dependent aggregation *in vitro*, and it is very likely that this occurs *in vivo* as well.[12] Aggregation of amphiphilic small molecules in aqueous media is thermodynamically driven by a reduction in the total free enthalpy of the system. Intermolecular binding interactions within the aggregates contribute to a decrease in the enthalpy factor, while shielding hydrophobic groups from the aqueous surroundings disrupt the highly organized water structure around them which is entropically favorable.[13, 14] Molecules aggregate through electrostatic interactions, hydrogen bonding, π- π, or van der Waals interactions and combinations thereof. Aromatic ring systems are present in most of the aggregators and the feature is thought to be key in driving self-association.[15]

The phenomenon of aggregation has been first discovered in pharmacology inhibition screens as compounds that self-aggregate can give false-positive hits in high-throughput screenings by nonspecific sequestration of proteins. Over the past two decades, aggregation has been proposed to influence solubility, diffusion and ultimately also absorption of poorly water-soluble APIs but data published are inconsistent and a proper understanding of this phenomenon and of its impact on oral absorption is lacking. Pioneering work by Arnold et al. on 36 non-nucleoside reverse transcriptase inhibitors evidenced that the size of aggregates had a direct influence on oral absorption.[16] The authors hypothesized that aggregates below 100 nm could "be absorbed by M cells of Peyer's patches of MALT via the lymphatic circulation", leading to an improved bioavailability. Larger aggregates could only be absorbed once their size was reduced by dilution effects along the gastrointestinal tract. In contrast, Owen et al. observed that passive diffusion of aggregates through cell layers might be prevented due to size restriction.[17]

1.2.2 Hydrotropy

Hydrotropy denotes the solubilization of a sparingly soluble molecule by another amphiphilic molecule, called the hydrotrope or hydrotropic agent.[18] This phenomenon is known since a long time[19] but has not been extensively exploited in pharmaceutical formulation. Hydrotropes contain both hydrophilic and hydrophobic domains and self-aggregate, but unlike surfactants they do not form micelles. The concentrations of hydrotropes needed for a solubilization effect are often in the molar range in contrast to surfactants which are effective solubilizers from very low concentrations. Nicotinamide is a well-known example of hydrotrope and has been shown to solubilize a wide range of hydrophobic drugs.[20] From a thermodynamic point of view, the free enthalpy should decrease upon addition of the hydrotrope. Different mechanisms for hydrotropic solubilization have been proposed, and to date no consensus has been reached:

The first theory is based on hydrotrope-API interactions as the driver of solubilization. Initially it was thought that hydrotrope and drug molecule would form stoichiometry complexes.[20, 21] However recently it has been shown that complex formation is rather unlikely, and the hydrotrope-API interactions rather exist in the form of a non-stoichiometric accumulation of hydrotropic molecules around drug molecules, probably driven by various small scale interactions.[22] Based on this assumption, hydrotrope self-aggregation would decrease solubilization efficiency.

The second theory resembles that of micellar solubilization by classical surfactants. Das et al., based on classical molecular dynamics simulation technique, explained that hydrotropic molecules start to aggregate above their minimum hydrotrope concentration and the drug's incorporation into the hydrophobic core of aggregates provides solubilization.[23]

The third theory, the water structure-based hypothesis, is based on the hydrophobic effect. Hydrotropic solubilization would lead to a breakage of the water structure around hydrophobic domains, which is

entropically favoured.[24] Growing skepticism towards this hypothesis in the literature makes it the least likely of the three theories.

1.3 Bile salts

Bile acids are synthesized from cholesterol and conjugated with amino acids in the liver. They contain a hydrophilic side chain linked to a rigid tetracyclic ring system which exhibits a hydrophobic and a hydrophilic face due to the opposite location of the (hydrophobic) methyl and (hydrophilic) hydroxyl substituents. Conjugation of bile acids with taurine or glycine increases their polarity which lowers their pK_as from 5-6.5 to 1-4, and increases their solubility in the small intestine.[25] Bile acids exist as salts of sodium or potassium under physiological conditions. They exhibit a stepwise aggregation[26] with critical micellar formation value of 2-20 mM which is in the concentration range in the intestinal lumen. Bile salts generally form mixed micelles with polar lipids; biliary phospholipids (phosphatidyl choline) in the fasted state and lipid digestion products in the fed state (monoglycerides and fatty acids) in the intestinal lumen.[25]

Two to eighteen grams of bile salts are secreted each day from the gall bladder into the intestine, mostly after meals as the chyme enters the duodenum. As amphiphilic molecules, their primary physiological function is to facilitate the digestion and absorption of dietary fats and lipophilic vitamins. Bile salts emulsify large fat globules (typically 0.5-10 µm) into fine droplets (50-200 nm) which increases the surface available for hydrolysis by lipases, and they solubilize digestion products.[27, 28] Monoglycerides and fatty acids are brought to the enterocytes membrane surface by the micelles and transferred to the mucosal cells while the bile salts remain in the lumen.[29, 30] Bile acids are metabolized by the gut microbiota and reabsorbed in the ileum and recycled via the portal vein back to the liver, a process called the enterohepatic circulation.

The effect of bile and bile salts on the solubility, dissolution and absorption of lipophilic APIs is since long known.[31] Recently NMR studies conducted to characterize the bile salts-API interactions on a molecular level have demonstrated that amphiphilic APIs can form mixed micelles with bile acids solubilizing the API.[32] In addition bile salts can have a strong impact on the fate of the formulation in the intestinal environment. By dispersing lipid colloidal phases, bile salts decrease the solubilization of the drug which may generate supersaturation and drive absorption from lipid-based formulations.[33, 34] Similarly, the release of API from the polymeric micelles is highly dependent on the presence of bile salts and incorporation into mixed micelles has been shown to be key for absorption.[29]

Recent work conducted by the group of L. Taylor evidenced that bile salts can delay the precipitation of API from supersaturated states by interfering with both nucleation and crystal growth.[35-38] Nevertheless,

despite these promising pieces of work and the tremendous potential of bile salts, deliberate incorporation of bile salts into solid oral dosage forms remains scarce.

1.4 Solubility and dissolution of salts and co-crystals

Two third of drug entities are weak electrolytes, and exhibit a pH-dependent solubility.[39] The cost of the free energy of hydration of ionized species is reduced compared to neutral species, given the higher amount of energy released upon formation of ion-dipole interactions, as compared to hydrogen bonds only. To date, salt formation remains the preferred approach to improve inadequate physicochemical properties in particular low solubility and dissolution rate. In dilute aqueous solutions of the same pH conditions, a salt and its free form have the same thermodynamic solubility, which is dictated primarily by the extent of ionization for weak electrolytes (which in turn depends on the ionization constant and pH of the medium; i.e. salt formation does not modify the ionic equilibria that occurs once in solution). However salt forms might have a kinetic solubility advantage over their equivalent free forms if kinetic barriers exist to prevent nucleation of the latter upon dissolution. The effect of this kinetic advantage on absorption processes is enough to significantly improve the bioavailability of a salt form over a free form. Often, the improved kinetic solubility originates from a faster dissolution rate of salts due to their self-buffering effect.[40] Indeed, the pH in the diffusion layer might differ as much as 4 pH units from the bulk pH, which results in an increased concentration of the API in the diffusion layer, and increases the rate of dissolution according to **Equation 2**. The high lattice forces of salts in general confer a high physical stability, and their manufacturing is well understood. The limitation of salt formation is the need for a relatively strong ionization site.

Co-crystals offer an alternative that has generated a lot of interest in the past two decades. While in a salt the API and counterion are held by an electrostatic bound, co-crystal components are held by multiple weaker interactions such as hydrogen bonds, van der Waals interactions and π stacking. Although salts and co-crystals are often considered as different classes, the difference between a salt and a co-crystal may be as tiny as a 1Å-difference in a proton position.[41] Similar to salts, dynamic dissociation processes of co-crystals upon dissolution might lead to precipitation of the API or of a less soluble form. Like salts, co-crystals are high energy forms of API and can generate a higher kinetic solubility but in general salts have higher dissolution rates than co-crystals due to their self-buffering effect.

1.5 Solubility and dissolution of amorphous systems

Amorphization of APIs in the form of amorphous solid dispersions (ASD) or co-amorphous mixtures is a very efficient method to increase the solubility and dissolution rate of APIs, and over the last two decades extensive research has been conducted to comprehend the mechanisms governing physical stability and dynamic *in vitro/in vivo* performance of amorphous pharmaceutical systems.

The amorphous state is defined by a lack of long-range order of the molecules, as opposed to the crystalline state. The sub-optimal packing results in higher intermolecular distances which weakens intermolecular interactions between molecules and confers a higher internal energy to the material. This higher energy state rationalizes the higher dissolution rate and kinetic solubility often observed with amorphous materials as compared to their crystalline counterparts. The obvious downside is that a higher internal energy also translates into a higher molecular mobility which may jeopardize chemical and physical stability of the amorphous state. Amorphous APIs are often kinetically stabilized within polymer matrices (i.e. in ASDs) or with another low molecular weight component (i.e. in co-amorphous mixtures). An increase in the glass transition of the system along with a reduction of molecular mobility and intermolecular interactions kinetically prevent recrystallization of the amorphous API, inferring shelf-life stability.

The next challenge of amorphous formulations is their performance in aqueous environments in terms of dissolution (i.e. the “spring”) and supersaturation duration (i.e. the “parachute”). There is a common view that *in vitro* dissolution profiles should display a fast dissolution (i.e. a good spring) followed by a maintenance of the supersaturation (i.e. a good parachute) to maximize bioavailability *in vivo*. The dissolution rate from an amorphous matrix is dictated by the API physicochemical properties, the drug load, the type of polymer and the material properties, while the resulting *in vitro* profile is governed by the kinetics of dissolution vs. the kinetics of precipitation. Indeed, supersaturation being a metastable state, recrystallization of the API during dissolution and once in solution needs to be mitigated, and this is often achieved by co-dissolving polymers. Through intermolecular interactions with APIs and a local increase in viscosity, polymers hinder diffusion and collision of the API molecules thus interfering with the formation of a stable nucleus. Furthermore, polymer adsorption on growing crystals can slow down crystal growth.[42]

2 Background and Aim of the Thesis

Molecules classified as a Biopharmaceutical Classification System (BCS) class II are frequently encountered in the pharmaceutical industry. These APIs are characterized by a low solubility and a low dissolution rate, which in turn may result in incomplete absorption and low bioavailability. For compounds referred to as “brick dust” (i.e. characterized by a high melting point (> 200°C) and a moderate lipophilicity (log P < 2))[43] solubility and dissolution limitations are often consequences of the strong intermolecular forces between API molecules in the crystalline form. From a thermodynamic point of view, solubility of an API in a solvent is dictated by the difference between Gibbs energy levels of the initial, undissolved solid state, and the final state where the API molecules are in solution. Enthalpic impact on dissolution is favored in exothermic conditions, i.e. the energy required to overcome API-API (and solvent-solvent) molecular interactions is less than what is generated by newly developed API-solvent molecules interactions. From this enthalpic perspective, dissolution is favored when API-API molecule interactions are reduced. Thus, weakening lattice forces is one way to address solubility and dissolution challenges of highly crystalline BCS class II (and IV) compounds.

Previous work focusing on acids and neutrals evidenced that lowering lattice forces does improve dissolution and enhances solubility, and this goes along with an increased exposure after oral application in animal models.[44] In line with these encouraging results, the objective of this thesis was to explore how basic APIs can be likewise functionalized to optimize inadequate physicochemical properties, particularly low solubility and dissolution rate. In the frame of this work, functionalization of the API goes along with its incorporation into multicomponent systems, which comprise one or several “enablers”. The term “enabler” embraces counterions, coformers, surfactants, bile acids or polymers, and its function encompasses both the improvement of the initial phase of dissolution as well as the maintenance of the dissolved state.

The starting points were inspirations from nature. From the storage of aromatic bases in the aqueous environment of the plant’s vacuoles to the solubilization of dietary fats and liposoluble vitamins by the bile salts micellar system nature has evolved to overcome the challenges of low solubility, and mimicking such systems holds great promise in the formulation of poorly water-soluble APIs.

3 Biomimetic co-crystals with increased kinetic solubility

3.1 Introduction

An interesting feature of plants is the sequestration of high concentrations of aromatic bases in the aqueous environment of their vacuoles. Indeed, several plants rely on toxic alkaloids for their defense against pathogens and herbivores and have developed strategies to locally accumulate sufficiently high concentrations to repel predators while avoiding autotoxicity.[45] A key mechanism for sequestration in vacuoles is complexation with polyphenols.[46] The most studied case is the complexation of caffeine with chlorogenic acid in *Coffee Arabica*. This complex was observed the first time in 1907 by Gorter[47], and was later described as a 1:1 complex in which the π systems of caffeine and chlorogenic acid overlap in a parallel direction. More recently 1D and 2D high resolution ^{1}H and ^{13}C Nuclear Magnetic Resonance (NMR) spectroscopy studies on the caffeine-di-O-caffeoylquinic acid complexes in solution confirmed that these complexes were driven by inter-aromatic stacking interactions.[48] Likewise, cocaine associates with chlorogenic acid in the vacuoles of *Erythroxylum coca* through an overlap of the π orbitals of both compounds.[49]

Based on such findings it was hypothesized that π stacking interactions could be exploited to form salts and co-crystals that are sufficiently stable in solution to prolong their kinetic solubility during a biorelevant period of time, thereby maximizing the solubility advantage of salts and co-crystals of otherwise poorly water-soluble APIs. Imatinib was the first selective tyrosine-kinase inhibitor approved for the treatment of cancer and remains the first-line treatment for chronic myeloid leukemia.[50] In view of its aromaticity and relatively flat molecular architecture, Imatinib was deemed a suitable candidate to investigate possible π stacking in solution with phenolic acids. The free Imatinib base (IFB) is poorly water-soluble, while its marketed form is a mesylate salt (IM).

Hydroxybenzoic acid derivatives and hydroxycinnamic acid derivatives were investigated as counterions and/or coformers based on their chemical structure similarity with chlorogenic acid. In depth investigation was carried out with syringic acid (SYA;4-hydroxy-3,5-dimethoxybenzoic acid). SYA is a phenolic acid naturally occurring in some plants *(e.g. Euterpe oleracea* with 1073 mg/L in the oil fraction)[51] and fruits (e.g. strawberries with 2.7 mg/kg)[52]. It is also present in wines (up to 8 mg/kg in red wine)[53]. Its antioxidant properties have been long recognized, and plants containing SYA are used in traditional Chinese medicine and Ayurvedic medicine.[54, 55] In recent years several publications have reported potential antihyperglycemic[56], hepatoprotective[57], neuroprotective[58, 59], antiosteoporotic[60] and anti-cataract

effects.[61] Its crystal structure has been elucidated the first time in 2016[62], and to my knowledge no salts or co-crystals of SYA with APIs have been reported in the literature to date.

The specific objectives of the present study were (1) to engineer pharmaceutical salts or co-crystals of Imatinib with aromatic counterions and coformers (2) to elucidate the dissolution kinetics and phase transformations of selected new forms in solution (3) to understand the mechanisms behind prolonged supersaturation (4) to assess the impact of association on diffusion through artificial membranes.

3.2 Materials and methods

3.2.1 Materials

Imatinib free base (IFB) and Imatinib mesylate (IM) were provided by Novartis Pharma AG (Basel, Switzerland). Sodium chloride and potassium dihydrogen phosphate (EMSURE grade) used for buffer preparation, LiChropur formic acid and LiChrosolv acetonitrile used for mobile phases preparation, and EMSURE grade solvents used for crystallization were purchased from Merck (Darmstadt, Germany). Millipore water was obtained from a Milli-Q dispenser equipped with a Millipal Express 40 0.22 µm filter from Merck KGaA (Darmstadt, Germany). 0.45 µm PVDF centrifugal filters (Ultrafree MC HV) were purchased from Merck & Cie (Schaffhausen, Switzerland). Methanesulfonic acid, syringic acid (SYA), sodium phosphate monobasic monohydrate, and sodium phosphate dibasic heptahydrate, bestatin, glyburide and n-octanol were purchased from Sigma-Aldrich (Buchs, Switzerland). Deuterated water (D_2O, 99.9% D) and deuterated acetic acid-d_4 (99.5% D) were purchased from Deutero GmbH (Kastellaun, Germany), 40% sodium deuteroxide in deuterated water (NaOD, 99% D), 35% deuterium chloride in deuterated water (DCl, 99% D), 85% deuterated phosphoric acid-d_3 in deuterated water (D_3PO_4, 98% D) and deuterated water (D_2O, 99.9% D) containing 0.05% 3-(trimethylsilyl)propionic-2,2,3,3-d4 acid-Na (TSP-d_4), sodium chloride (99%) and monobasic sodium phosphate anhydrous (99%) from Sigma-Aldrich (Schnelldorf, Germany), hexadeuteriodimethyl sulfoxide (DMSO-d_6, 99.8% D) from Euriso-top (Saarbrücken, Germany), monobasic sodium phosphate monohydrate (99%) from Gruessing (Filsum, Germany), dibasic sodium phosphate anhydrous (99%) from Acros Organics (Geel, Belgium) and Tween 80 from Caelo (Hilden, Germany). Standard 5 mm NMR tubes (400 MHz / 900 MHz) and coaxial insert tubes were purchased from Norell (Landisville, PA). Dulbecco's Modified Eagle Medium (DMEM) high glucose, Hank's balanced salt solution with Ca^{2+} and Mg^{2+} (HBSS), and hydroxyethyl piperazineethanesulfonic acid (HEPES) were purchased from Life Technologies (Zug, Switzerland). Albumin bovine serum Fraction V RIA and Elisa grade (BSA) was purchased from Calbiochem (Merck, Schaffhausen, Switzerland).

3.2.2 Methods

Small Scale Screening

An initial small scale screening was performed to obtain new solid forms of Imatinib. A 1:1.1 stoichiometric mixture of IFB and counterion/coformer was weighted in a 16 x 130 cm Schott Duran test-glass (Mainz, Germany). 600 µL of ethanol or isopropanol were added and the mixture was heated to boiling point with a heat gun HL 2010 E from Steinel (Herzebrock-Clarholz, Germany) until complete dissolution. The solution was left on a Syncore orbital shaker from Büchi (Liestal, Switzerland) under light stirring conditions (100 rpm) at room temperature for 48 h. A thick precipitate was recovered, filtered and washed with 2 volumes of ethanol or isopropanol. Formation of a new form (salt or co-crystal) was confirmed by ^{1}H-NMR, DSC, and XRPD.

Preparation of Imatinib Syringate Co-crystals

I-SYA (1:1) co-crystals at gram scale were prepared by cooling crystallization in an EasyMax 102 system from Mettler-Toledo (Greifensee, Switzerland). To prepare I-SYA (1:1) co-crystal, 1:1.1 stoichiometric mixtures of IFB and SYA was dispensed in a 100 ml glass reactor. Seventy grams of n-propanol/water mixture (95/5 w/w) were added to the reactor and the temperature was increased to 80 °C with an overhead stirrer at 150 rpm. Seeds of I-SYA (1:1) co-crystal obtained previously during screening were used to induce crystallization and added to the reactor after cooling down to 55 °C. Three temperature cycles from 55 °C to 15 °C were carried out with a cooling/heating rate of 0.1 K/min to promote crystal coarsening. A final cool down to 0 °C was done at 0.1 K/min. Solids were filtered, washed twice with 10 g of cold n-propanol/water mixture (95/5 w/w) and dried at 60 °C, 10 mbar for 24 h in a SalvisLAB vacuum dryer from Renggli (Rotkreuz, Switzerland) equipped with a Vacuubrand vacuum pump PC 2012 Vario CVC 2000 II (Theilingen, Switzerland).
The same procedure was used to prepare I-SYA (1:2) co-crystal salt with ten temperature cycles. This allowed conversion of the I-SYA (1:1) co-crystal to I-SYA (1:2) co-crystal salt.
Imatinib hydrate (IH) was obtained from the precipitation of IM in 50 mM phosphate buffer at pH 6.8. Solids were filtered and gently dried at 30 °C, 30 mbar for 24 h in the vacuum dryer to preserve the hydrate. Subsequently, a secondary drying was performed at 60 °C, 30 mbar for 24 h to induce the loss of water molecules. Hydrate formation and stoichiometry were investigated by DSC and TGA.

Single Crystal X-Ray Diffraction

Intensity data were collected at 100 K on a Bruker AXS three-circle diffractometer (Madison, WI) with monochromated Cu(Kα)-radiation (Helios MX confocal mirror monochromator), microfocus rotating anode generator, and a Smart 6000 CCD detector using the SMART software V5.632 from Bruker. 13 ω-scans at different ϕ-positions were performed to ensure appropriate data redundancy. Data processing and

global cell refinement were performed with SAINT V7.36A from Bruker. A semi-empirical absorption correction was applied, based on the intensities of symmetry-related reflections measured at different angular settings (Sheldrick GM (2008) SADABS V2008/1, Bruker AXS Inc).
The structure was solved by dual space-recycling methods and subsequent DF syntheses and refined based on full-matrix least-squares on F2 using the SHELXTL program suite (Sheldrick GM (2001) SHELXTL V6.12, Bruker AXS Inc.). Anisotropic displacement parameters were used for all non-hydrogen atoms. Hydrogen atoms were located in DF maps and refined in idealized positions using a riding model.

X-Ray Powder Diffractometry (XRPD)

Dried solids and wet residues from dissolution and solubility experiments were charged between thin-film SpectroMembrane of Kapton from Chemplex Industries (Palm City, FL) in a metallic holder and analyzed with a PANalytical X'Pert PRO powder diffractometer from PANalytical (Zürich, Switzerland) using Cu-Kα radiation (unsplit Kα1+Kα2 doublet, mean wavelength 1.5419 Å) at a power of 40 kV and 40 mA, and a focusing X-ray mirror for Cu radiation. The scattered X-ray went through a 0.04 rad axial Soller slit and a 2.5 mm anti-scattering slit and detection was performed with a X'Celerator detector from PANalytical. Measurements were done in transmission mode in coupled two theta/theta mode with a step size of 0.0084° in 2θ and 25 s measurement time per step in the range of 4 - 40° (2θ). Data analysis was carried out with the software Data Viewer from PANalytical.

Differential Scanning Calorimetry (DSC)

DSC was performed on a Q2000 instrument from TA Instruments (New Castle, DE) using a scanning rate of 20 K/min from 25 to 250 °C for the IFB, IM, IH; and from 25 to 200 °C for the I-SYA co-crystals, under a nitrogen purge (flow rate of 50 ml/min). Two to five mg of the samples was weighted into a non-hermetic closed aluminum crucible (Tzero Pan and Lid from TA Instruments).

Thermogravimetric Analysis (TGA)

TGA of IH was performed on a Discovery TGA instrument from TA Instruments using a scanning rate of 20 K/min from 25 to 250 °C. Two to five mg of the samples was weighted in an aluminum cup (TA Instruments).

Buffer Preparation

Simulated intestinal fluid (SIF) is a 50 mM phosphate buffer pH 6.8. It was prepared according to the United States Pharmacopeia (USP).[63] 0.9 g of sodium chloride and 6.8 g of potassium dihydrogen phosphate were dissolved in 900 mL of Millipore water. The pH was measured with a SevenCompact pH meter from Mettler-Toledo (Greifensee, Switzerland) equipped with an InLab Micro electrode and

adjusted with 1 M HCl or NaOH of Titripur grade from Merck (Darmstadt, Germany). The volume was completed to 1 L with Millipore water.

Equilibrium solubility Measurements

The equilibrium solubility of IFB in phosphate buffer at pH 6.8 was determined by the shake flask method. An excess of solids (5 mg/mL) was added to 3 mL of phosphate buffer and stirred with a magnetic stirrer for 24 h at room temperature. In addition the equilibrium solubility of IFB in physical mixtures with one and two molar equivalents of SYA was measured. After 24 h, the pH was recorded and the samples were filtered through 0.45 µm Polyvinylidene fluoride (PVDF) Ultrafree MC HV centrifugal filters from Merck & Cie (Schaffhausen, Switzerland) in a miniSpin centrifuge from Vaudaux-Eppendorf AG (Basel, Switzerland) at 13.400 rpm for 90 seconds. Filtrates were further diluted with acetonitrile, and the amount of Imatinib and SYA in solution was quantified by UPLC-UV. Excess solids remaining on the filters were analyzed by XRPD. All experiments were performed in triplicate.

pH-Solubility Profile of Imatinib

A pH solubility profile was calculated based on the solubility-pH Henderson-Hasselbalch equation.[64]The pK_as of Imatinib were determined by potentiometric titration using a Sirius T3 (Sirius Analytical, East Sussex, UK) and the intrinsic solubility of Imatinib was determined by equilibration at pH 9. The equilibrium solubility of IFB at room temperature was determined experimentally at three different pHs (6.1, 6.7 and 8.9). An excess amount of Imatinib free base was added to deionized water and the pH was adjusted with a NaOH solution. The suspensions were stirred with a magnetic stirrer at 500 rpm until equilibrium was reached. At equilibrium (equilibrium state was confirmed by repeating the quantification after 1 h) the amount of Imatinib in solution was quantified by UPLC-UV after filtration through filtered 0.45 µm PVDF centrifugal filters. The pH was recorded and the solids in equilibrium with the solution were analyzed by XRPD to confirm that no change of form occurred during the experiment. The equilibrium solubility of IFB at pH below 4.3 could not be determined as a change of form was observed.

Dissolution Profile Measurements

Fifteen or 30 mg substance equivalent to free base were added to 3 mL of 50 mM phosphate buffer pH 6.8 (SIF) at room temperature. Stirring was with a magnetic stirrer at 300 rpm. At predefined time points, 100 µL aliquots were sampled and filtered through 0.45 µm PVDF centrifugal filters from Ultrafree in a miniSpin centrifuge at 13.400 rpm for 90 seconds. Filtrates were diluted with acetonitrile and assayed by UPLC-UV. At the end of the experiment (24 h), solids were filtered and analyzed by XRPD. The pH value was recorded 3 h after the start of the experiments. For IFB no pH change was observed, for IM and I-SYA (1:1) co-crystal the pH changed slightly to 6.5 and for I-SYA (1:2) co-crystal salt decreased to 5.9. For SYA alone a pH of 5.0 was observed. All experiments were performed in triplicate.

Ultra Performance Liquid Chromatography (UPLC)

Quantification of solute concentrations was performed on a 1290 Infinity UPLC from Agilent Technologies (Basel, Switzerland) equipped with a diode array detector (G4212A), an auto sampler (G4226A), a column thermostat (G1330B) and a quaternary pump (G4204A) with an Acquity UPLC BEH C18 1.7 µm (2.1 x 100 mm) column from Waters (Milford, MA). Different methods were used for Imatinib and SYA. For the analysis of Imatinib, the column temperature was set to 35 °C. Mobile phase A was a 10 mM phosphate buffer prepared by dissolving 2.27 g of sodium phosphate monobasic monohydrate and 0.954 g of sodium phosphate dibasic heptahydrate in 2 L of Millipore water. The pH was checked and adjusted to 6.4 with 1N HCl or NaOH solutions, if necessary. The buffer was filtered through Nalgene™ Rapid-Flow™ sterile disposable filter units with 0.2 µm PES membrane (Thermo Fisher Scientific, MA, USA). Mobile phase B was a mixture of acetonitrile and water (95/5; v/v). The gradient profile was as follows for mobile phase B: 0-5 min 10-90%; 5-5.25 min 90-90%; 5.25-5.50 min; 90-10%; 5.50-6.50 min 10-10%. The flow rate was set at 0.6 mL/min and detection was performed at λ = 267 nm. For the analysis of SYA the method was modified. The temperature of the column oven was increased to 40 °C and the mobile phase consisted of 0.1% formic acid in Millipore water (A) and (B) of a mixture of acetonitrile and water (95/5; v/v). Mobile phase A was filtered through Nalgene™ Rapid-Flow™ sterile disposable filter units with 0.2 µm PES membrane (Thermo Fisher Scientific, MA, USA). The gradient profile was as follows for mobile phase B: 0-5 min 10-90%; 5-5.25 min 90-90%; 5.25-5.50 min; 90-10%; 5.50-6.50 min 10-10%. The flow rate was set at 0.6 mL/min and detection was done at λ = 275 nm. For propranolol, the same method as for SYA was used with a detection at λ = 290.6 nm. For enalapril maleate, mobile phase A was a 10 mM KH_2PO_4 buffer adjusted to pH 2.4 with phosphoric acid. Mobile phase B was a mixture of acetonitrile and water (95/5; v/v). The gradient profile was as follows for mobile phase B: 0-5 min 10-90%; 5-5.25 min 90-90%; 5.25-5.50 min; 90-10%; 5.50-6.50 min 10-10%. The flow rate was set at 0.6 mL/min and detection was performed at λ = 210 nm.

Nuclear Magnetic Resonance Experiments

A 50 mM buffer with of dibasic sodium phosphate in D_2O was prepared and the pH was adjusted with NaOD or D_3PO_4 to pD 7.81 (= pH 7.4). The critical aggregation concentration (CAC) was determined by ^{1}H NMR concentration dependent measurements as previously described.[65] The supersaturated state was simulated by increasing the nominal concentration to 1000 µM Imatinib. Briefly, a 100 mM stock solution of IM, IFB, I-SYA (1:1) co-crystal and I-SYA (1:2) co-crystal salt in deuterated dimethyl sulfoxide (DMSO-d6) was prepared and 15 µl was added to 1500 µl buffer (solvent switch method). The following concentration scheme was used (1000 µM, 1000 µM + surfactant (tween 80), 500 µM, 250 µM, 125 µM , 62.5 µM). The concentration dependent 1H NMR spectra were recorded on a Bruker Avance 400 MHz spectrometer (Karlsruhe, Germany) operating at 400.13 MHz with a BBO BB-H 5 mm probe head, and data processing was done with the software TopSpin 3.0. The temperature was adjusted with a BCU-05 (Bruker) temperature control unit. The following acquisition parameters were applied for the ^{1}H NMR:

number of scans 1024, at a temperature of 300 K, flip angle 30°, spectral width 20.55 ppm, and transmitter offset at 6.175 ppm. The acquisition time was set to 3.985 seconds followed by a relaxation delay of 1.0 seconds with collection of 64000 data points at a sample spinning frequency of 20 Hz. Processing was done using an exponential line broadening window function of 0.3 Hz, automatic baseline correction and manual phasing. The spectra were referenced to the external standard 0.05% sodium trimethylsilylpropionate in D_2O (TSP-d_4) filled in a coaxial insert tube.

2D rotational nuclear overhauser effect spectroscopy (ROESY) spectra were recorded with a Bruker 600 MHz Avance III HD NMR spectrometer using a 5 mm cryo-probe and the pulse sequence roesyphpp.2 in the phase-sensitive mode with cw spinlock for mixing and a purge pulse before d1 to avoid total correlated spectroscopy (TOCSY) cross peaks. A manual phase correction and an automatic baseline correction in both dimensions were performed.

For the ROESY experiments the 1000 µM I-SYA (1:2) co-crystal salt sample in deuterated buffer pH 7.4 was degassed by three freeze-thaw cycles filled in a 5 mm LPV tube from Wilmad-LabGlass, (Vineland, NJ) and measured after preparation, i.e., in supersaturated state and after 72 h (in equilibrium).

In vitro Permeation Studies

In vitro permeation studies were carried out using Side-Bi-Side Cells from PermeGear, (Hellertown, PA) consisting of 3.4 mL donor and acceptor compartments and a 0.9 mm orifice diameter. The cells were placed on a 9-Station Horizontal Cell Stirrer from SES GmbH (Bechenheim, Germany). Artificial membranes (PVDF, 0.45 µm, 0.78 cm^2) were purchased from Pion (Billerica, MA) and loaded with 25 µL of gastrointestinal tract (GIT) lipid purchased from Pion. Temperature was at 37 °C throughout the experiment. The membranes were mounted between the two compartments and pre-heated phosphate buffer (37 °C) was added to the acceptor compartment.

This system was validated for its discriminatory power between low and highly permeable compounds. Propranolol was used as a high permeability model compounds and enalapril maleate was used as a low permeability compound. These two model compounds were also used to assess the lipidic membrane integrity in presence of 0.025% of Tween 80.

In the first experiment, 100 µM (equivalent to Imatinib free form) clear solutions of IFB, IM, I-SYA (1:1) co-crystal and I-SYA (1:2) co-crystal salt were transferred into the donor compartment. Clear solutions were chosen instead of suspensions to control for the amount of Imatinib in solution. The maximum concentration of IFB in the acceptor compartment was 10 times below its equilibrium solubility, thus ensuring sink conditions. At predefined time points 50 µL aliquots were sampled from the acceptor compartment, diluted with acetonitrile and analyzed by UPLC-UV. All experiments were performed in triplicate. In a second experiment the diffusion of SYA and Imatinib were monitored from a 10 mM solution of Imatinib syringate co-crystal I-SYA 1:1. In a third experiment 0.025% of Tween 80 was added to a 1000 µM IM solution, to assess the effect of aggregation on diffusion.

Low Efflux Madin-Darby Canine Kidney (LE-MDCK) cells Permeation Assay

The LE-MDCK permeation assay was performed in apical to basolateral direction. A Corning HTS Transwell 96 well plate with 1.0 µm polyethylene terephthalate (PET) membrane (#3392) was seeded with 75 µL of a 500'000 MDCK-low efflux clone E9_1 cells/ml DMEM solution to reach 37'500 cells pro well, and were incubated for four days at 37°C + 5% CO_2. Before the assay, cells were washed twice with HBSS (pre-warmed to 37°C) and incubated for 30 minutes at 37°C and 5% CO_2. 5 and 50 µM IM, I-SYA (1:1), I-SYA (1:2) and SYA solutions in HBSS incl 10 µM bestatin, 0.02% BSA, 0.3% DMSO and 10 mM HEPES were prepared and centrifuged 10 min at 1000g. HBSS solution was removed from the upper transwell and lower reservoir and 75 µL of compound solutions were dispensed in the donor plate while 235 µL of HBSS solution including 0.02% BSA, 0.3% DMSO and 10 mM HEPES were dispensed into the acceptor plate. The sandwich plate was incubated for 2 h at 37°C. After incubation 10 µL of sample were mixed with 70 µL of a 31/69 (v/v) solution of acetonitrile and 0.625 µM glyburide (internal standard) in H2O and analyzed for quantification. The separation was done on a LC-MS with a PAL System (CTC Analytics, Zwingen, Switzerland) and an Allegro pump (Allegro Industries, SC, USA) with a Synergi RP-Polar 50x2.1 mm column of 2.5 µm diameter (Phenomenex, Basel, Switzerland). The over temperature was set to 60°C, mobile phase A was 0.1% formic acid in water and mobile phase B was 0.1% formic acid in acetonitrile. The injection volume was 3 µL and the gradient was set as followed for mobile phase B: 0-0.3 min 5%; 0.3-1.0 min 5-100%; 1.0-2.5 100%; 2.5-2.6 min 100-5%; 2.6-3.0 min 5% with a flow of 0.45 mL/min. The detection was done on a MSMS ThermoTSQ Quantum Discovery (Thermo Scientific, MA, USA) using a Heated Electrospray Ionization (HESI-II) source, a spray voltage of 4000V in positive mode and 3000 V in negative mode, and a capillary temperature of 350°C. All compound parameters such as parent mass, product mass, tube lens and others were obtained using the autotuning step of the QuickQuan application. The scan time was 0.02s

$logD_{6.8}$ determination

The $logD_{6.8}$ of Imatinib and SYA was determined by the shake flask method. Briefly, SIF buffer was presaturated with n-octanol and n-octanol was presaturated with SIF buffer overnight. 200 µM stock solutions of Imatinib and SYA were prepared in n-octanol and vigorously mixed with SIF buffer over 24 h. After phase separation, 100 µL of the organic phase and 100 µL of the aqueous phase were sampled and diluted with acetonitrile. The amount of Imatinib and SYA in the two phases was quantified by UPLC-UV. All experiments were performed in triplicate.

3.3 Results and discussion

3.3.1 Small scale screening

Twelve acids were screened for salt or co-crystal formation with Imatinib (**Figure 1 and 2**). Five hits were obtained with SYA, vanillic acid (VAN), caffeic acid, dihydrocaffeic acid, and gallic acid. Salt/co-crystal formation was confirmed by XRPD, DSC and ^{1}H-NMR (**Figure 3 and Table 1**). The form with SYA was selected for further investigation based on its superior intrinsic dissolution rate (data not shown).

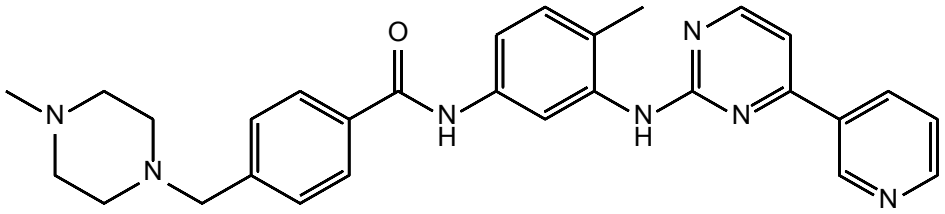

Figure 1. *Molecular structure of Imatinib*

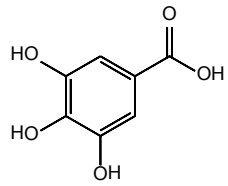

Gallic acid

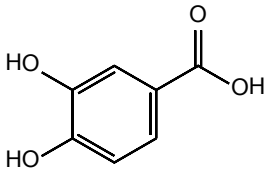

Protocatechuic acid

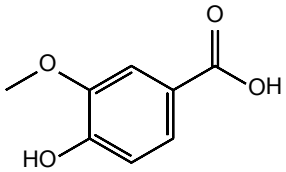

Vanillic acid (VAN)

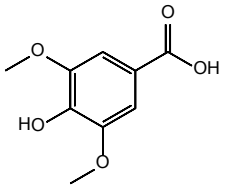

Syringic acid (SYA)

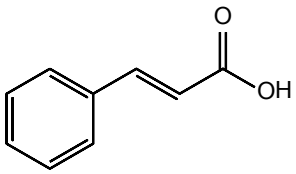

Cinnamic acid

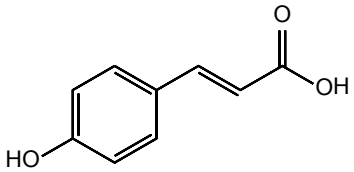

Coumaric acid

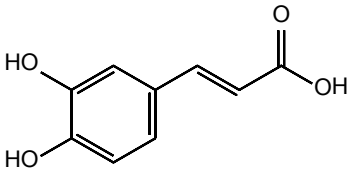

Caffeic acid

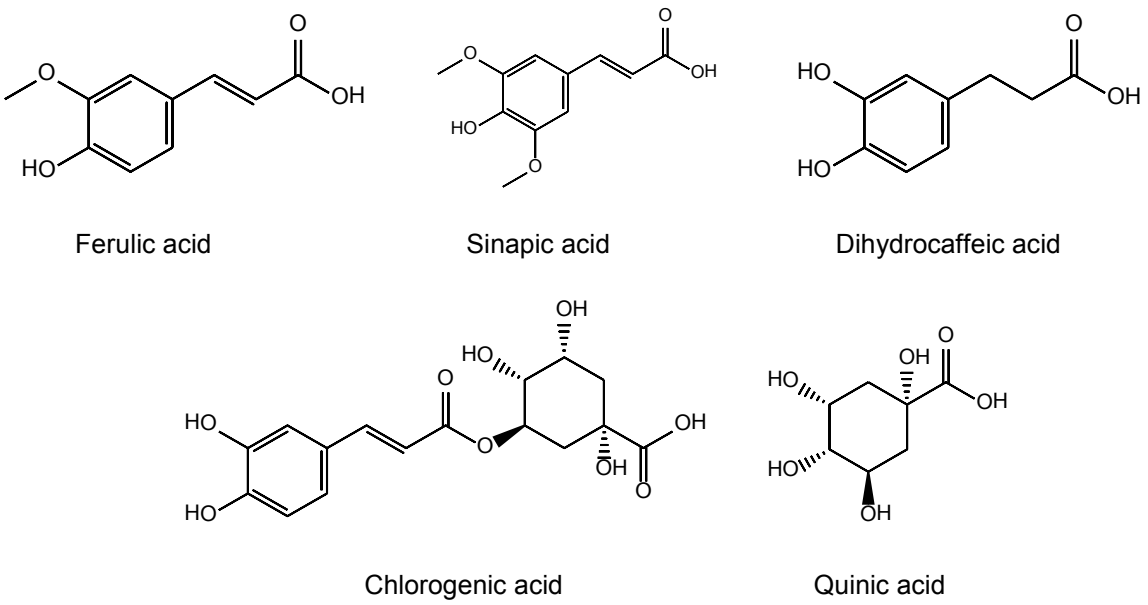

Figure 2. *Molecular structure of selected acids for initial screening*

Table 1. *Thermal and spectroscopic analysis of the new forms with the references*

	DSC		**^{1}H-NMR**
	Mp counterion (CI) (°C)	**Mp new form (°C)**	**Imatinib:CI ratio**
Syringic acid	207.6	164.9	1:1
Vanillic acid	210.5	78.9	1:1
Gallic acid	260.0	212.5	1:1
Caffeic acid	241.7	163.4	1:1
Dihydrocaffeic acid	139.3	203.9	1:1

STI571-reggama1-002-007

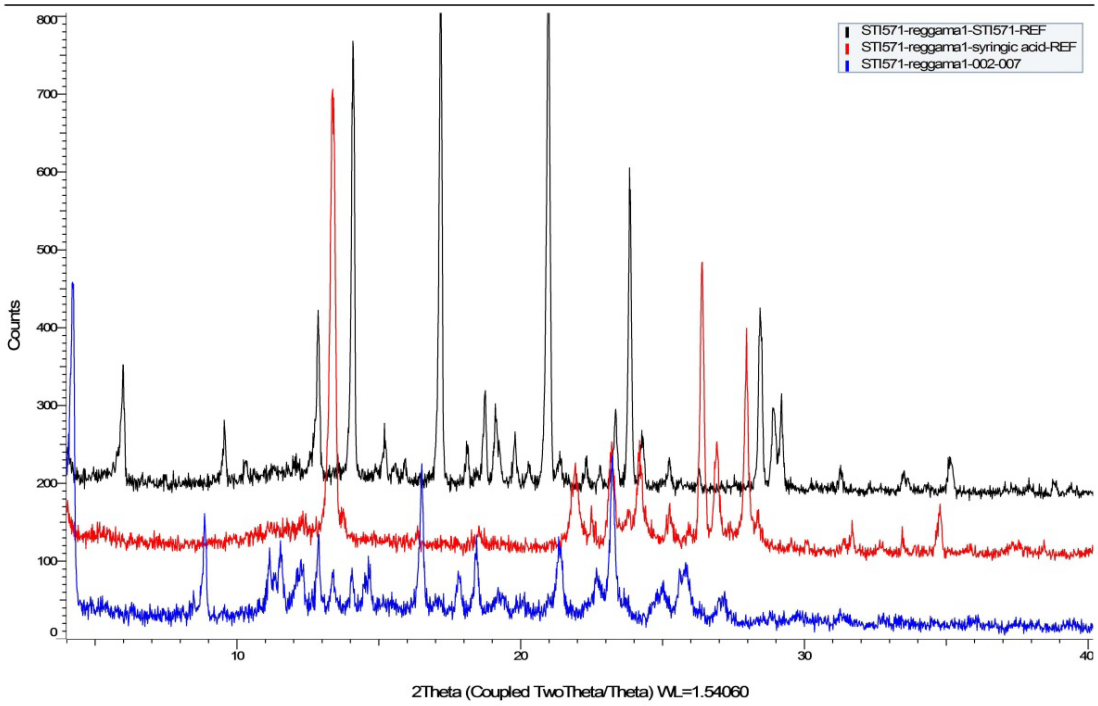

STI571-reggama1-002-015

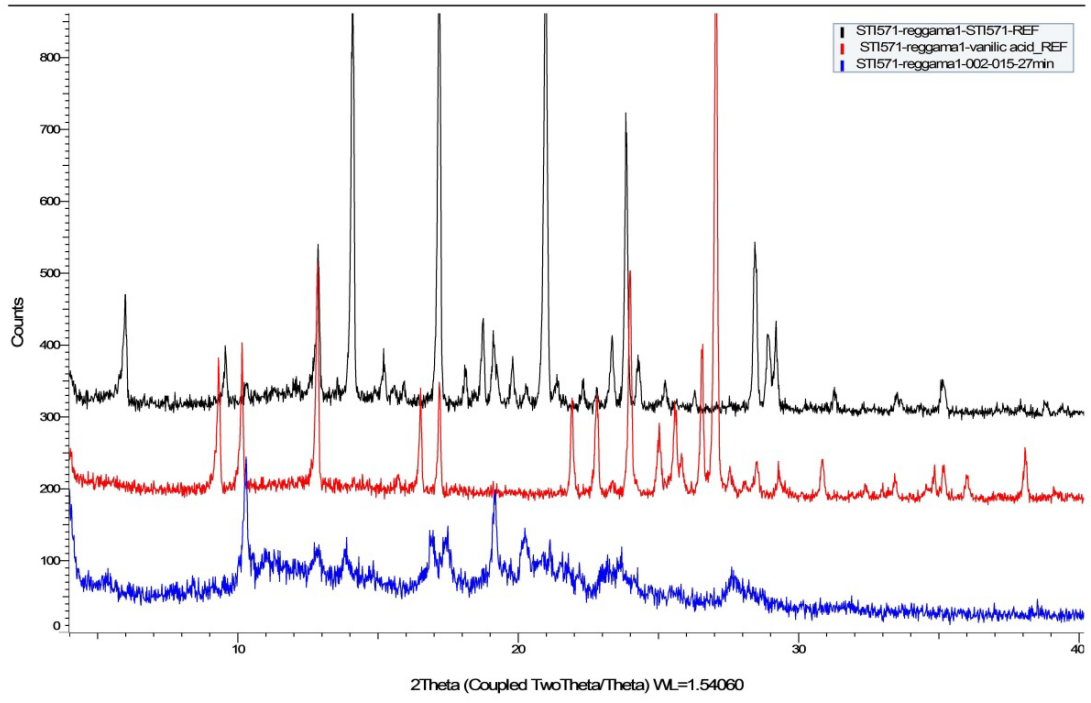

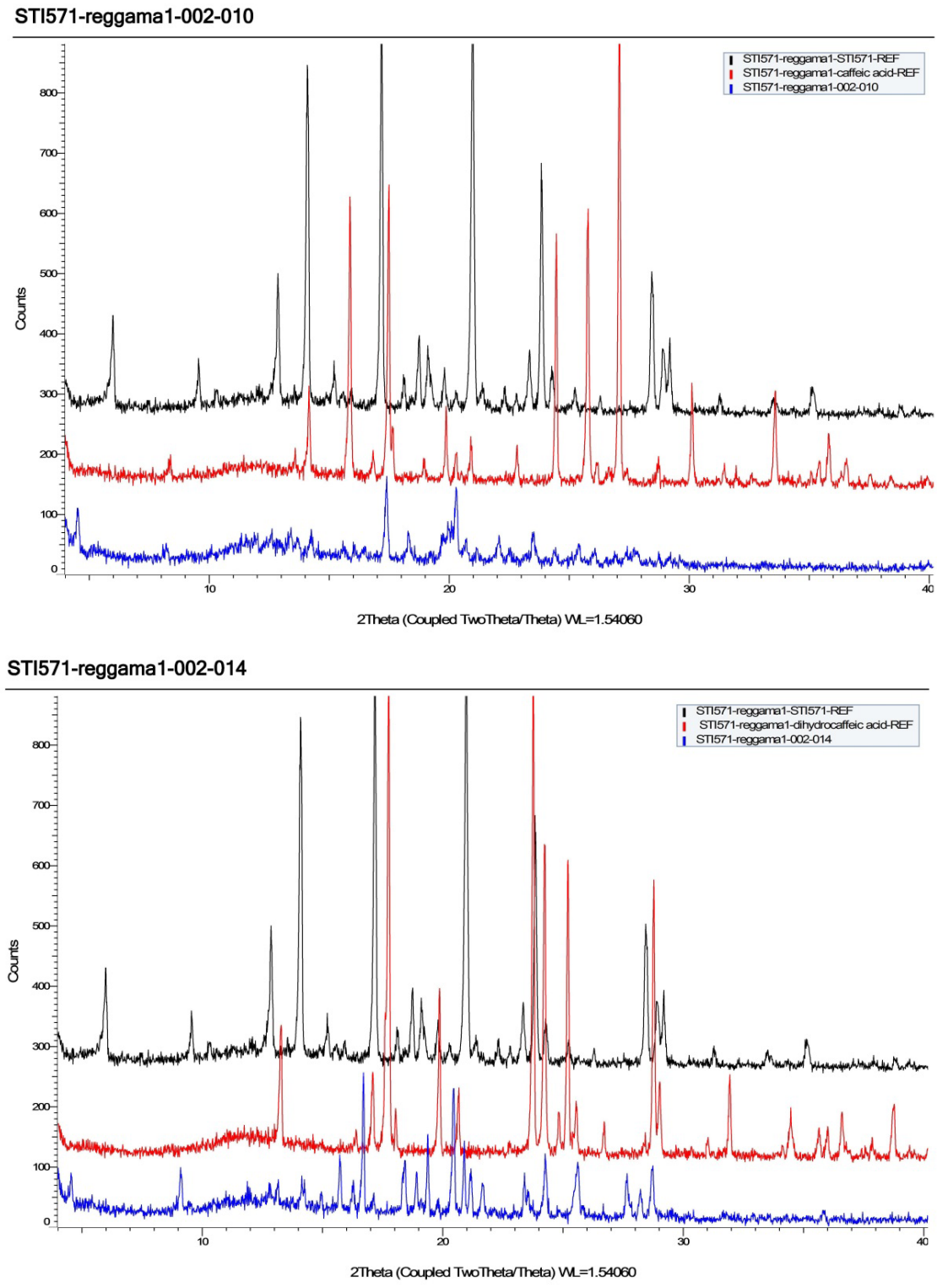

Figure 3. *XRPD diffractograms of Imatinib free base (IFB; black), the counterions (red) and the new forms (blue). The samples were named as follows: STI571-reggama1-002-007 with syringic acid; -015 with vanillic acid; -010 caffeic acid; -014 with dihydrocaffeic acid*

3.3.2 Structural Studies

The following data and text are part of a manuscript (Bioinspired co-crystals of Imatinib providing enhanced kinetic solubility) submitted to the European Journal of Pharmaceutics and Biopharmaceutics.

"Imatinib and SYA co-crystallized in the triclinic crystal system in the space group ($P\bar{1}$) with Z = 2 in a ratio of 1:1 (referred to as I-SYA (1:1) co-crystal, **Figure 4A, Table 2**). The carboxylic function COOH (H 49) of SYA formed a hydrogen bond with the pyridine nitrogen (N 2) of Imatinib (*d*: 1.84 Å; *θ*: 173.4°, **Table 3**) and the hydroxyl group (H 38) of SYA with the piperazine nitrogen (N 31) of Imatinib (*d*: 2.00 Å; *θ*: 149.8°, **Table 3**). The Imatinib molecules adopted a head-to-tail conformation with hydrogen bonds between N-H 13 and O 23 (*d*: 2.11 Å; *θ*: 153.9°) and N-H 21 and N 10 (*d*: 2.24 Å; *θ*: 163.2°), and π stacking of the aromatic functions (**Figure 4C, Table 3**). [66]

The co-crystal salt of Imatinib and SYA with a ratio of 1:2 crystallized in the monoclinic crystal system in the space group ($P2_1/c$) with Z = 4 (referred to as I-SYA (1:2) co-crystal salt, **Figure 4B, Table 2**). The acid of the first SYA molecule was activated as a carboxylate as the proton (H 63) was transferred to the piperazine nitrogen (N 34) of Imatinib (*d*: 1.76 Å; *θ*: 166.6°, **Table 3**), which yielded a salt. The second SYA molecule remained neutral and the same hydrogen bond between the carboxylic group (H 49) of SYA and the pyridine nitrogen N 2 of Imatinib as for the non-salt I-SYA (1:1) was observed (*d*: 1.92 Å; *θ*: 160.6°, **Table 3**). Imatinib molecules adopted the same head-to-tail conformation as observed for the I-SYA (1:1) co-crystal (**Figure 4D**).

Increasing SYA stoichiometry went along with an increased measured density (1.269, 1.299, and 1.369 g/cm^3 for IFB, I-SYA (1:1) and I-SYA (1:2), respectively) which suggested lower lattice forces of the co-crystals." The aspect of both co-crystals was thin, long needle-like.

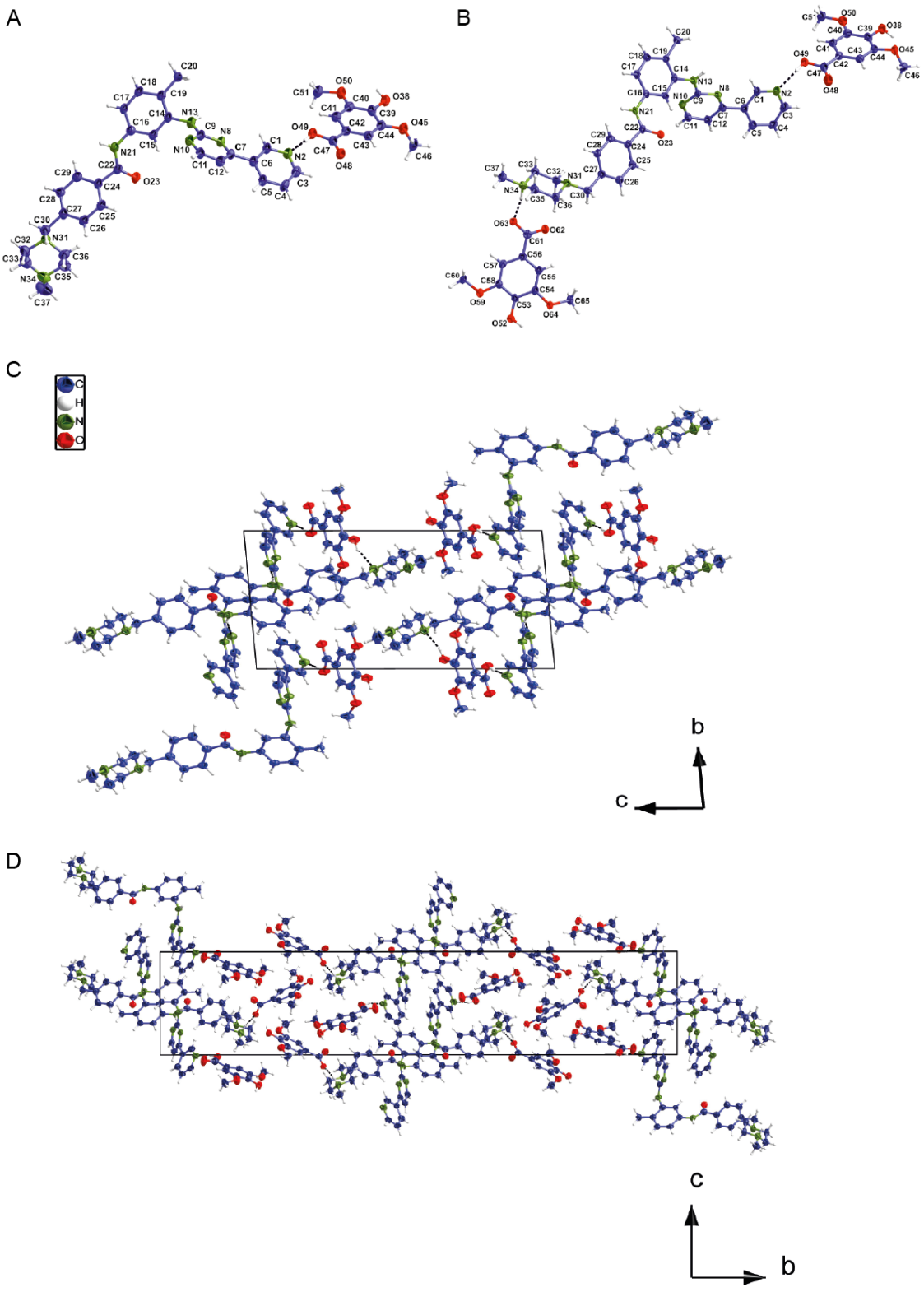

Figure 4. *(A) Crystal structure of the Imatinib syringate co-crystal I-SYA (1:1), and (B) the Imatinib co-crystal salt I-SYA (1:2), (C) crystal packing of the I-SYA (1:1) co-crystal and (D) the I-SYA (1:2) co-crystal salt*

Table 2. *Crystallographic parameters of the Imatinib syringate co-crystal I-SYA (1:1) and the Imatinib co-crystal salt I-SYA (1:2)*

Compound	I-SYA (1:1)	I-SYA (1:2)
emp formula	$C_{38}H_{41}N_7O_6$	$C_{47}H_{51}N_7O_{11}$
formula wt	691.78	889.95
crystal system	triclinic	monoclinic
T/K	100	100
space group	$P\bar{1}$	$P2_1/c$
***a*/Å**	7.950(3)	8.021(2)
***b*/Å**	10.938(4)	51.402(11)
***c*/Å**	20.753(9)	10.586(2)
***α*/°**	84.56(3)°	90
***β*/°**	84.55(3)°	98.400(13)
***γ*/°**	81.06(3)°	90
volume (Å^3)	1768.8(12)	4317.7(16)
Z	2	4
D_{calcd} (g cm^{-3})	1.299	1.369
***μ* (mm $^{-1}$)**	0.732	0.817
F(000)	732	1880
total ref	39128	77674
unique ref	6371	7752
R_{int}	0.2293	0.2025
R_1 ($I > 2\sigma(I)$)	0.0775	0.0669
***w*R_2**	0.1809	0.1565
completeness (%)	97.1	97.9
goodness-of-fit	0.999	1.010
2*θ* range (°)	2.15-68.77	3.44-68.28

Table 3. *Hydrogen bond lengths and angles of <O-H...O of the Imatinib syringate co-crystal I-SYA (1:1) and the Imatinib co-crystal salt I-SYA (1:2) (Å)*

	D-H…A	d(D-H)	d(H…A)	d(D…A)	<(DHA)
I-SYA (1:1)	N(13)-H(13)...O(23)#1	0.88	2.11	2.921(4)	153.9
	N(21)-H(21)...N(10)#2	0.88	2.24	3.094(5)	163.2
	O(38)-H(38)...N(31)#3	0.84	2.00	2.761(5)	149.8
	O(38)-H(38)...O(50)	0.84	2.30	2.727(4)	111.8
	O(49)-H(49)...N(2)	0.84	1.84	2.677(5)	173.4
I-SYA (1:2)	N(13)-H(13)...O(23)#1	0.88	2.01	2.874(4)	166.8
	N(21)-H(21)...N(10)#2	0.88	2.22	3.077(4)	164.0
	N(34)-H(34)...O(63)	0.93	1.76	2.669(4)	166.6
	O(38)-H(38)...O(62)#3	0.84	1.91	2.726(3)	164.3
	O(49)-H(49)...N(2)	0.84	1.92	2.723(4)	160.6
	O(52)-H(52)...O(63)#4	0.84	1.91	2.697(3)	156.0
	O(52)-H(52)...O(64)	0.84	2.31	2.711(3)	110.1

3.3.3 Thermal Analysis

Both co-crystals (I-SYA (1:1) and I-SYA (1:2)) exhibited a melting point at 164°C (**Figure 5**). IFB, IM, and SYA melted at 211°C, 219°C and 208°C, respectively (**Figure 5**).

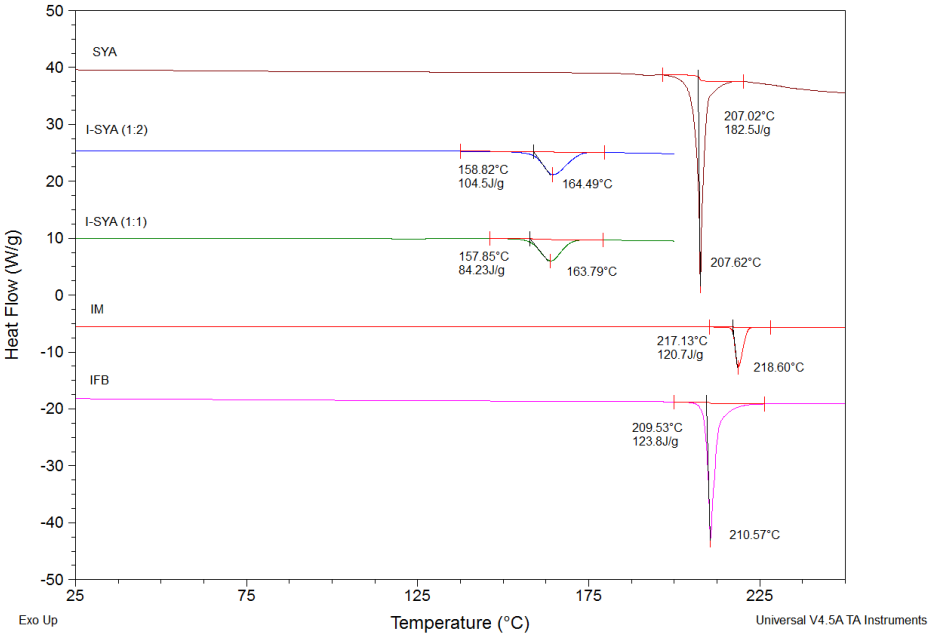

Figure 5. *DSC thermograms of Imatinib free base (IFB), Imatinib mesylate (IM), Imatinib syringate co-crystal I-SYA (1:1), Imatinib syringate co-crystal salt I-SYA (1:2) and syringic acid (SYA)*

3.3.4 Powder dissolution studies

Understanding the kinetics of dissolution, supersaturation, form conversion and recrystallization in aqueous environments requires close monitoring of these events over time. Powder dissolution under non-sink conditions (with respect to IFB) were conducted in simulated intestinal fluid (SIF), which is a 50 mM phosphate buffer with a pH of 6.8.[63] To place these experiments in a biopharmaceutical context, the dynamics were followed over a period of 3 h, and then a final measure was made after 24 h to observe the system evolution towards its equilibrium.

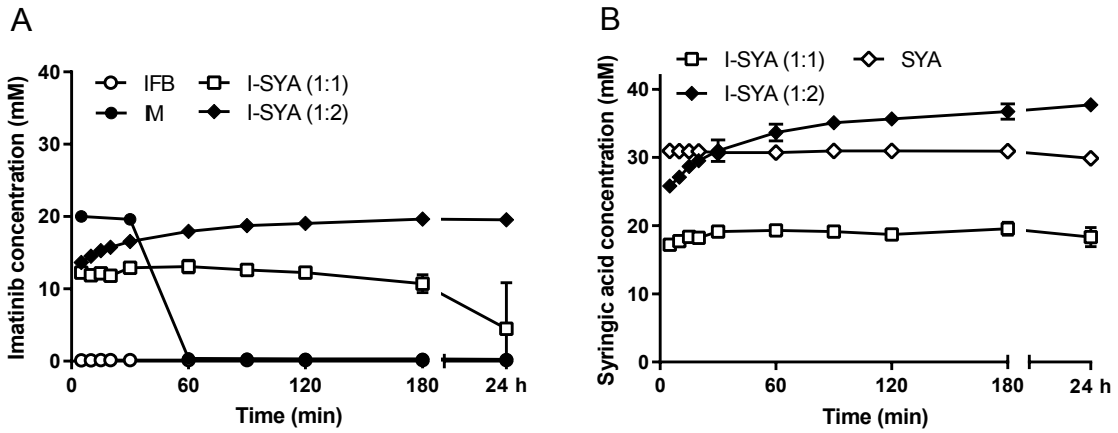

Figure 6. *Dissolution profiles of Imatinib free base (IFB), Imatinib mesylate (IM), Imatinib syringate co-crystal I-SYA (1:1), Imatinib syringate co-crystal salt I-SYA (1:2), and Syringic acid (SYA) in simulated intestinal buffer (SIF) at pH 6.8 (n=3). (A) Imatinib concentrations (B) SYA concentrations*

The IM and the co-crystals generated high concentrations, with the initial dissolution of the IM salt being slightly faster than that of the syringate co-crystals (**Figure 6**). The IFB dissolved only to low concentrations, in line with its low equilibrium solubility at pH 6.8. Once in solution IM and I-SYA (1:1) converted to a less soluble hydrate form (IH, **Figure 7**). Hydrate formation was confirmed by DSC and TGA (data not shown). The kinetics of conversion differed largely between the forms (**Figure 6A**); while IM precipitated within 1 h the dissolved fraction of I-SYA (1:1) remained for more than 3 h. Liquid-liquid phase separation (LLPS) occurred from the dissolved I-SYA (1:1); an Imatinib-rich phase (ratio 2.5:1 Imatinib to SYA) separated from the aqueous continuous phase which was enriched with SYA (ratio 1:1.5 Imatinib to SYA). Over time IH nucleated from the Imatinib-rich phase.

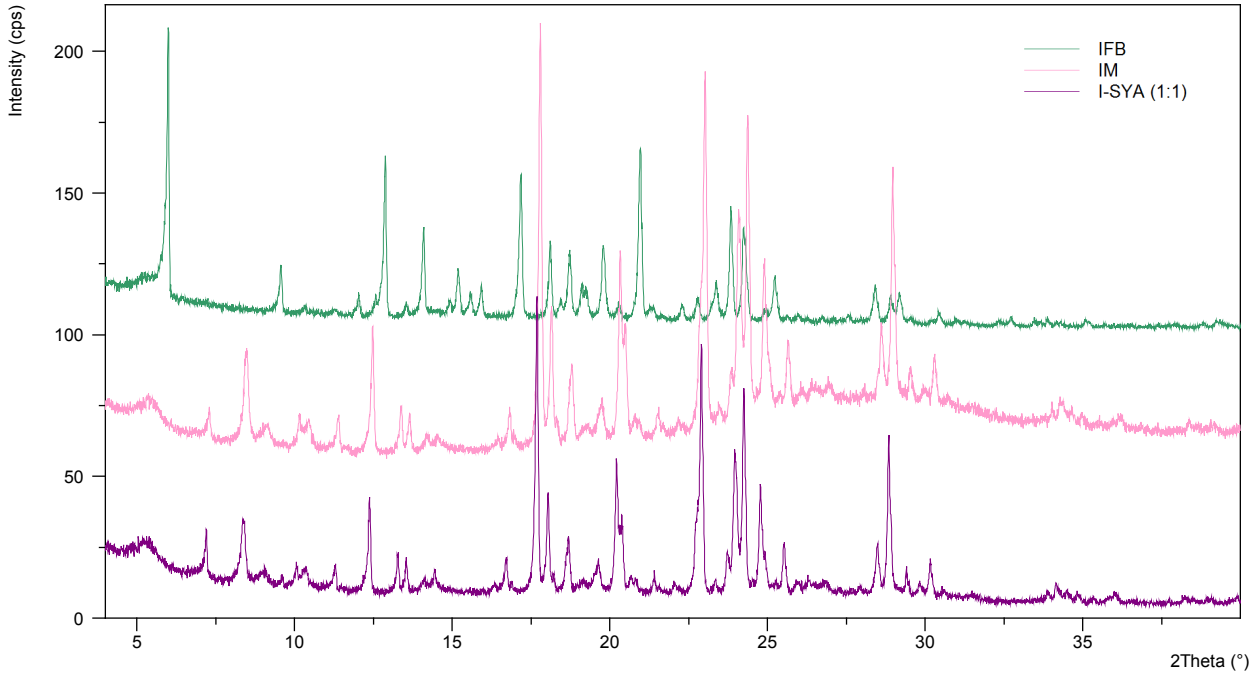

Figure 7. *XRPD diffractograms of collected solids at the end (24 h) of powder dissolution studies for Imatinib free base (IFB), Imatinib mesylate (IM) and Imatinib syringate co-crystal I-SYA (1:1)*

A congruent dissolution of Imatinib and SYA was observed from the I-SYA (1:2) co-crystal (**Figure 8A and 8B**). Concomitant LLPS prevented the evaluation of the congruency in the release from the I-SYA (1:1) co-crystal (**Figure 8C**). Monitoring of the dissolution of SYA from these forms revealed that while IH precipitated, SYA remained in solution (**Figure 6B**).

The next step was to understand whether solubilization or supersaturation governed the high concentrations of Imatinib (I-SYA (1:1) and I-SYA (1:2)) in solution. Whether a drug is solubilized or supersaturated may have profound implications for absorption. While a supersaturated solution is thermodynamically unstable but can drive passive diffusion through membranes at a maximum level, a thermodynamically stable solubilized solution might actually have a lower flux as the free drug concentrations is typically not increased. SYA having a molecular architecture similar to hydrotropic agents (e.g. benzoic acid) could solubilize Imatinib by hydrotropic solubilization.[22, 23, 67]

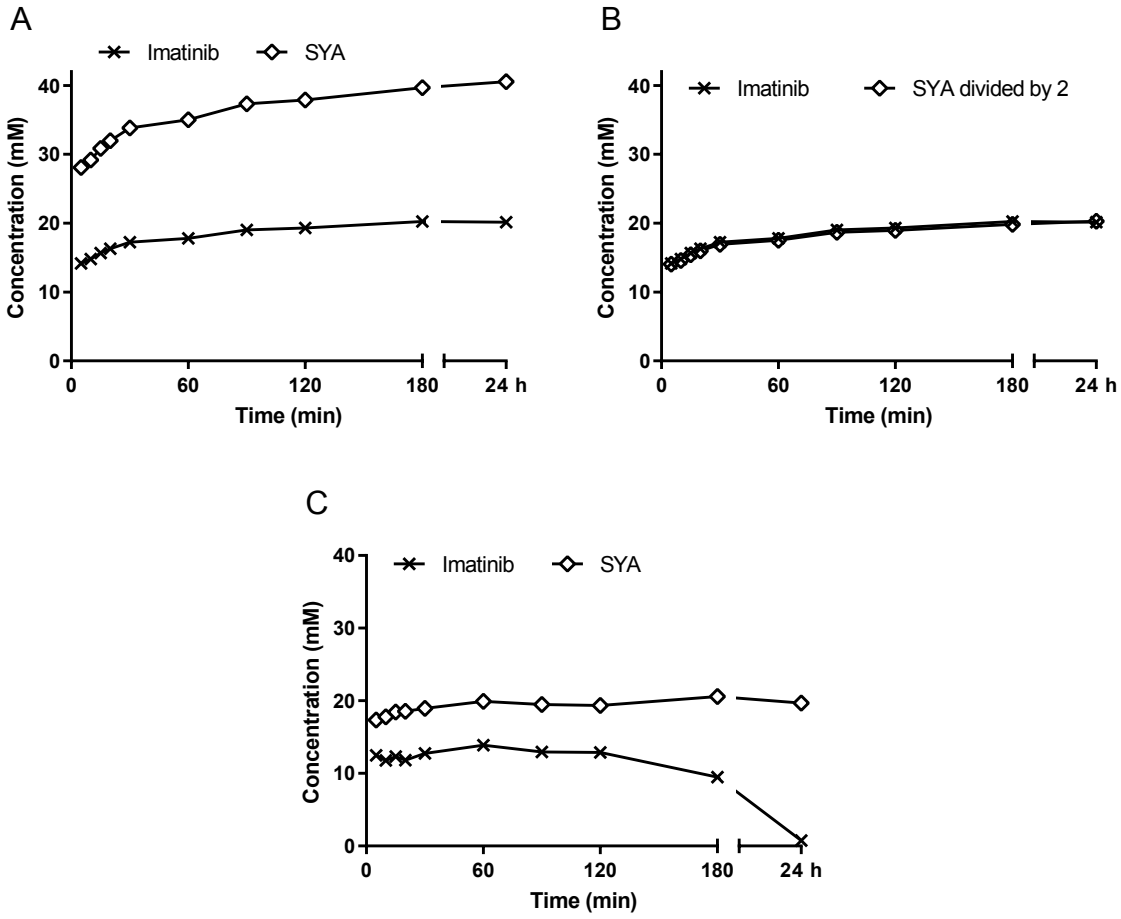

Figure 8. *Individual dissolution profiles of Imatinib and syringic acid (SYA) from (A, B) Imatinib syringate co-crystal salt I-SYA (1:2) and (C) Imatinib syringate co-crystal I-SYA (1:1) in SIF buffer at pH 6.8. In (B) the concentration of SYA has been divided by two to highlight congruency*

In a first step, IFB was slurried with one and two molar equivalents of SYA as physical mixtures in SIF buffer. After 24 h, the amount of Imatinib in solution was four and twenty times higher than the IFB equilibrium solubility, with one and two stoichiometric equivalents of SYA, respectively (**Figure 9**). There was no change of form during equilibration (**Figure 10**).

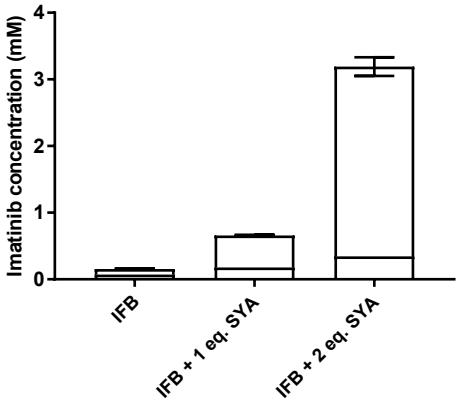

Figure 9. *Concentration of Imatinib in a physical mixture of Imatinib free base (IFB) with syringic acid (SYA) in the molar ratio 1:1 and 1:2 (IFB:SYA) compared to native IFB slurried in SIF buffer for 24 h (n=3)*

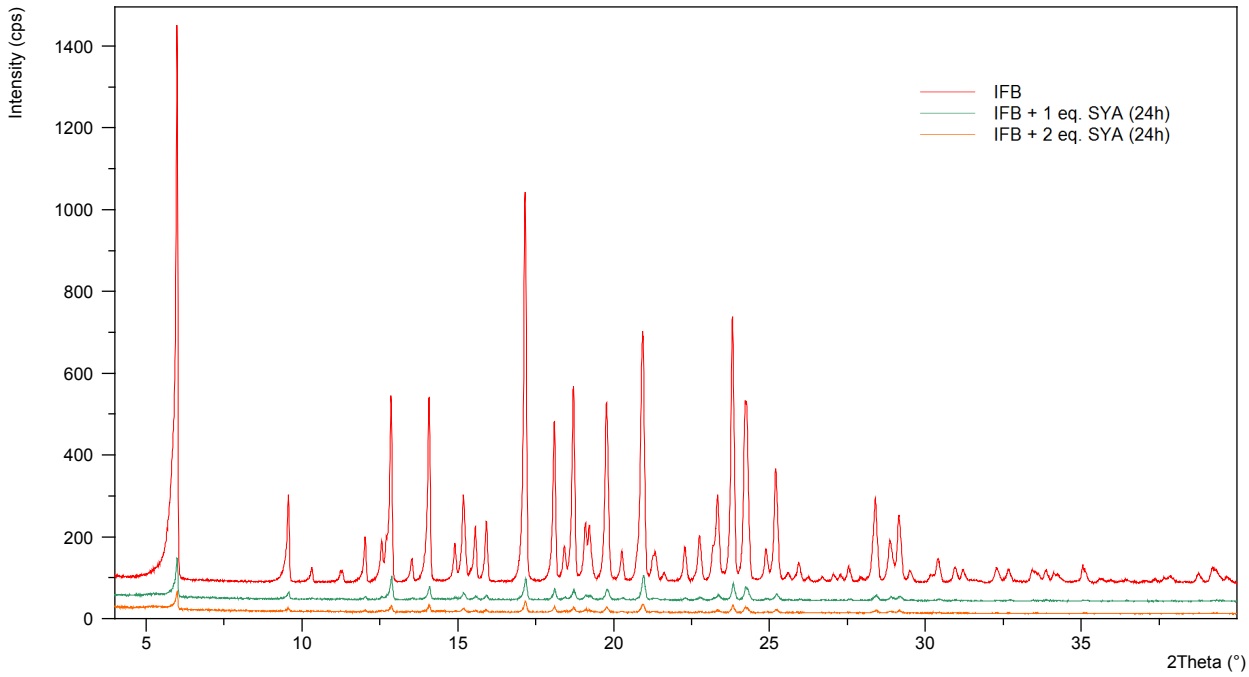

Figure 10. *XPRD of solids collected after 24 h equilibration of the physical mixtures of Imatinib free base (IFB) with syringic acid (SYA) (1:1 and 1:2 molar ratio IFB:SYA) and native IFB in SIF buffer pH 6.8*

To rule out that the increase in solubility was a pH effect (as the pH decreased to 6.4 and 6.1 with one and two molar equivalent of SYA, respectively), the pH solubility profile of IFB was measured (**Figure 11**).

The theoretical profile was calculated based on the Henderson-Hasselbalch equation and was in good agreement with experimental data. The horizontal lines in the bars in **Figure 9** represent the theoretical

equilibrium solubility of Imatinib at pH 6.8, 6.4 and 6.1. The difference between the theoretical solubility of Imatinib at these pHs and the concentration measured in presence of SYA indicated that increased solubility originated mostly from a solubilization effect by SYA and only to a minor extend from the change of pH.

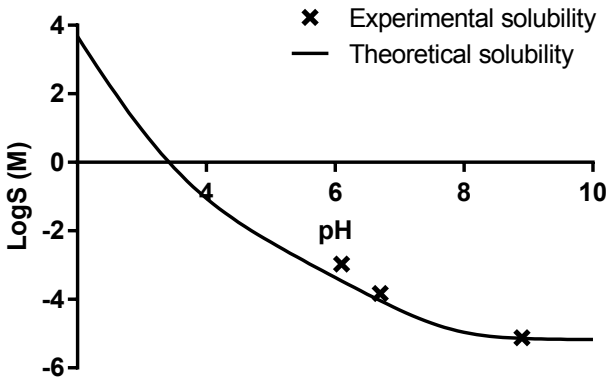

Figure 11. *Experimental and theoretical pH solubility curve of Imatinib free base*

In a second step, 10 mM clear solutions of IM, I-SYA (1:1) or I-SYA (1:2) were seeded either with IFB or IH. Seeding with IFB did not induce any desupersaturation (**Figure 12A**). However, seeding with crystals of IH was followed by a rapid precipitation of IM, I-SYA (1:1) and I-SYA (1:2) into the hydrate form (**Figure 12B and Figure 13**). This experiment demonstrated that SYA interfered with the nucleation of the IH, but when the nucleation barrier is overcome (e.g. by seeding), SYA had very little effect in preventing crystal growth of IH and desupersaturation occured.

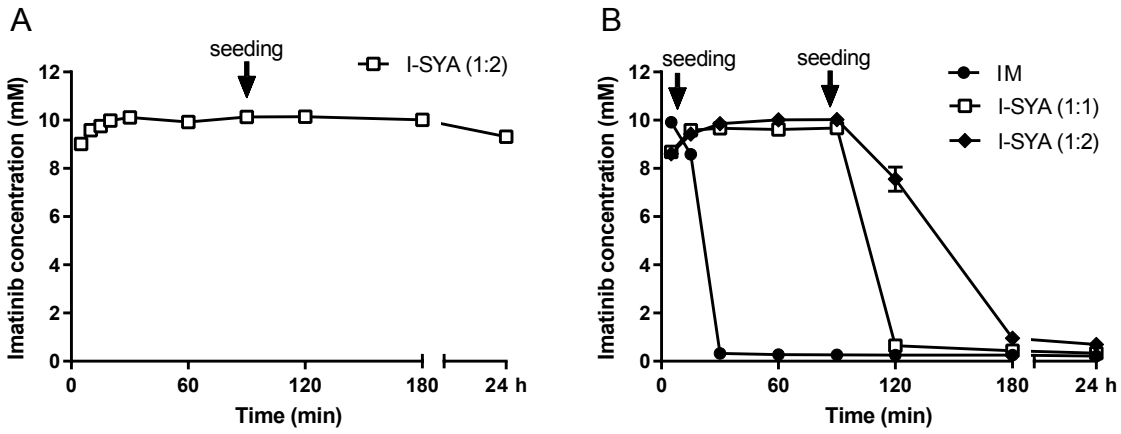

Figure 12. *(A) Seeding experiments of the 10 mM Imatinib syringate co-crystal salt I-SYA (1:2) solution with Imatinib free base (IFB) seeds and (B) seeding experiments of 10 mM Imatinib mesylate (IM), Imatinib syringate co-crystal I-SYA (1:1), and Imatinib syringate co-crystal salt I-SYA (1:2) solutions with Imatinib hydrate (IH) seeds. The arrows indicate seeding: (A) IFB seeds were added after 90 min, (B) IH seeds were added in the IM solution after 10 min and in the I-SYA (1:1) and I-SYA (1:2) solutions after 90 min*

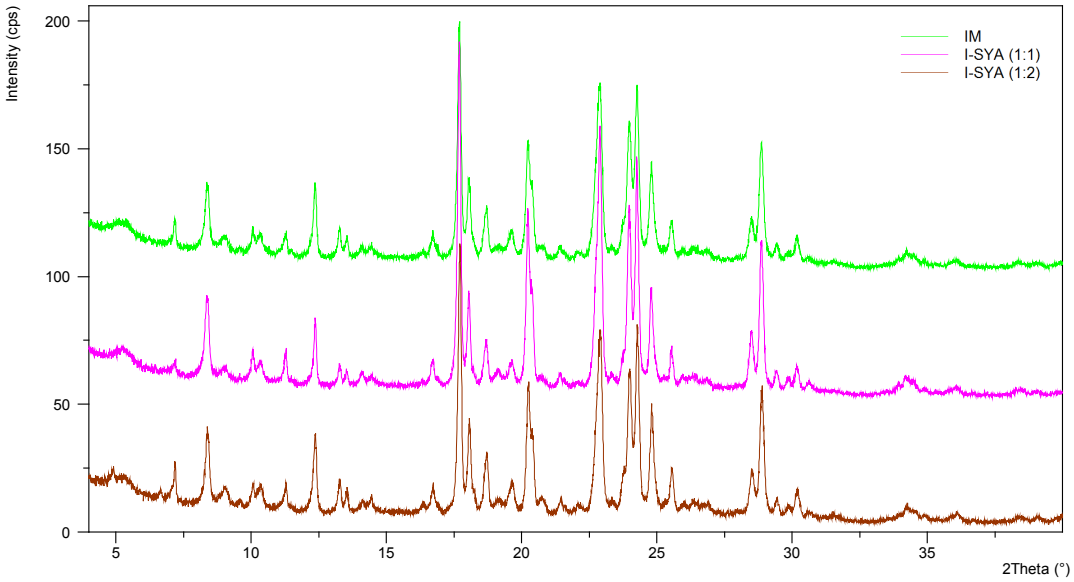

Figure 13. *XRPD of solids collected at the end (24 h) of the seeding experiment with Imatinib hydrate (IH)*

3.3.5 Solution ^{1}H NMR studies

The following data and text have been kindly provided by Dr. Johannes Wiest, and are part of a manuscript (Bioinspired co-crystals of Imatinib providing enhanced kinetic solubility) submitted to the European Journal of Pharmaceutics and Biopharmaceutics.

"Molecular self-aggregation in solution was studied by ^{1}H NMR. [65, 68] Imatinib self-aggregated at pH 7.4, as indicated by concentration dependent shifts of the ^{1}H signals (critical aggregation concentration (CAC) ≈ 25 – 50 µM) for IFB, IM, I-SYA (1:1) co-crystal and I-SYA (1:2) co-crystal salt (**Figure 14-17**). Neither the mesylate counterion nor the co-crystal former SYA prevented Imatinib aggregation in solution. Supplementation of a surfactant (Tween 80) reverted the shifts for Imatinib reflecting the breakup of the Imatinib aggregates by the surfactant (**Figure 14-17**).

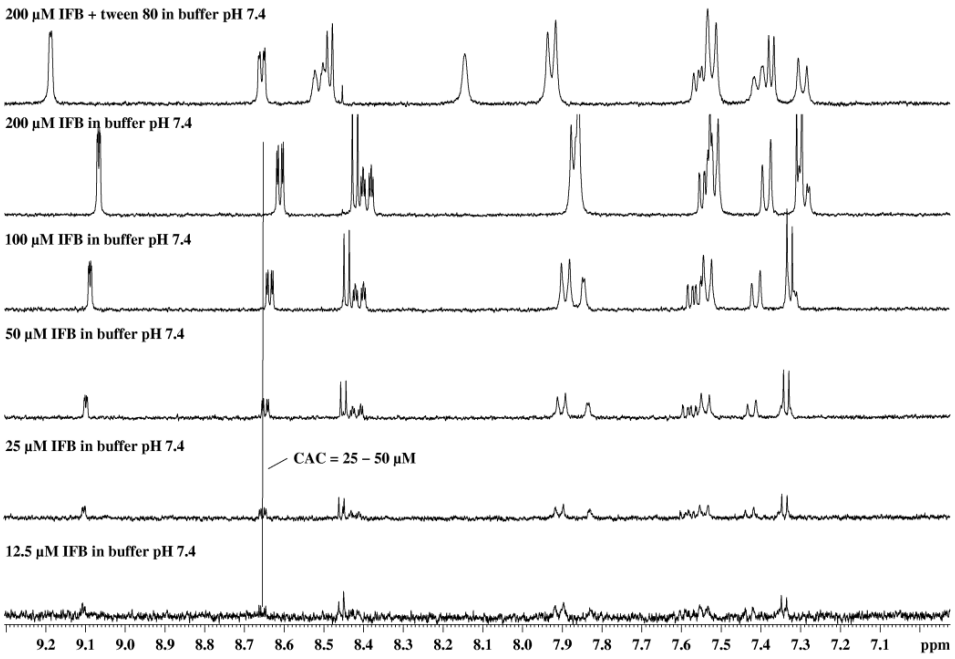

Figure 14. *Determination of the critical aggregation concentration (CAC) by concentration dependent ^{1}H NMR spectroscopy of Imatinib free base (IFB) at pH 7.4*

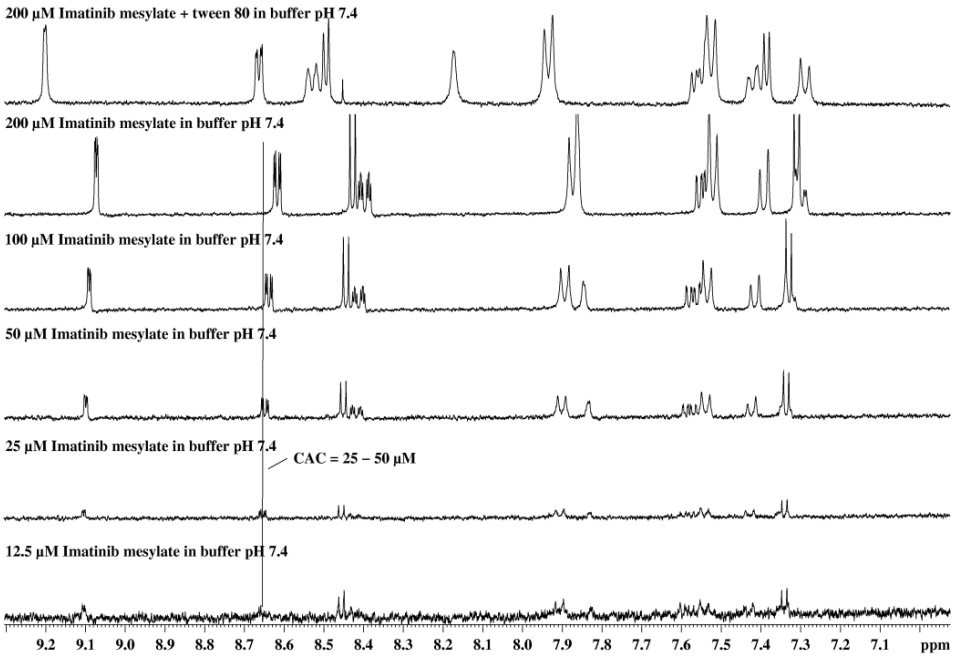

Figure 15. *Determination of the critical aggregation concentration (CAC) by concentration dependent ^{1}H NMR spectroscopy of Imatinib mesylate (IM) at pH 7.4*

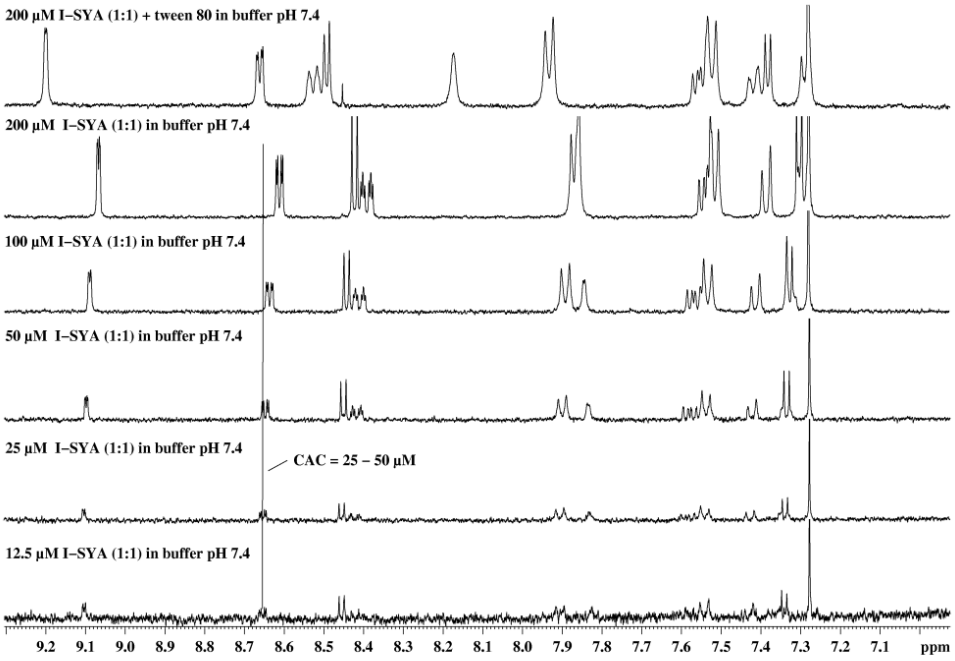

Figure 16. *Determination of the critical aggregation concentration (CAC) by concentration dependent ^{1}H NMR spectroscopy of Imatinib syringate co-crystal I-SYA (1:1) at pH 7.4*

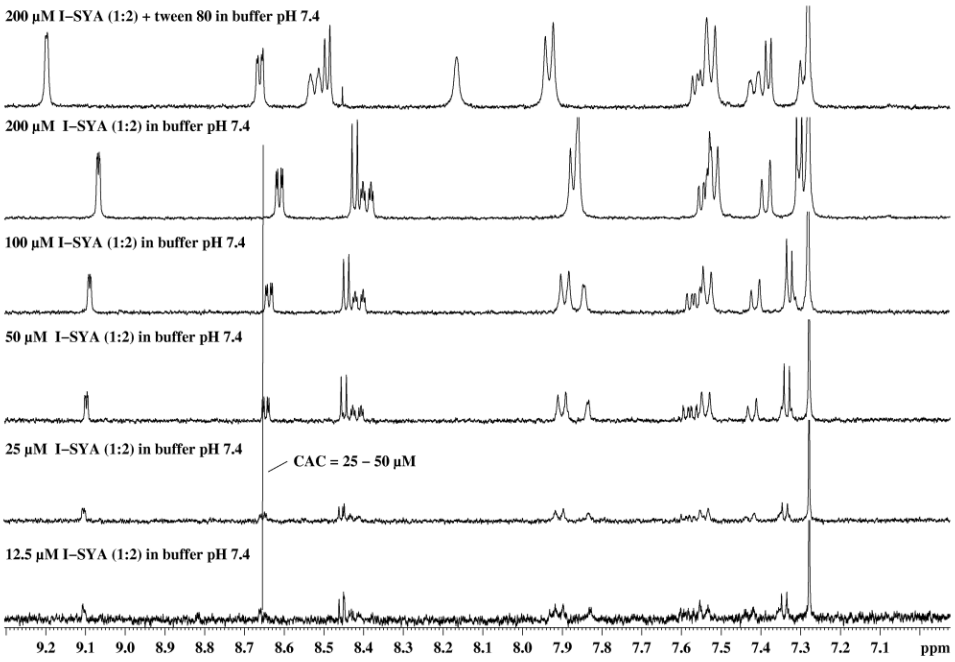

Figure 17. *Determination of the critical aggregation concentration (CAC) by concentration dependent ^{1}H NMR spectroscopy of Imatinib co-crystal salt I-SYA (1:2) at pH 7.4*

At the highest nominal concentration of 1000 µM almost identical chemical shifts were observed for Imatinib's ^{1}H signals for IFB, IM and I-SYA (1:1) co-crystal, whereas for the I-SYA (1:2) co-crystal salt the signals were shifted to higher field (**Figure 18A and Figure 19A**). Sharp signals were recorded indicating a small size of the aggregates due to fast tumbling rate.[65]

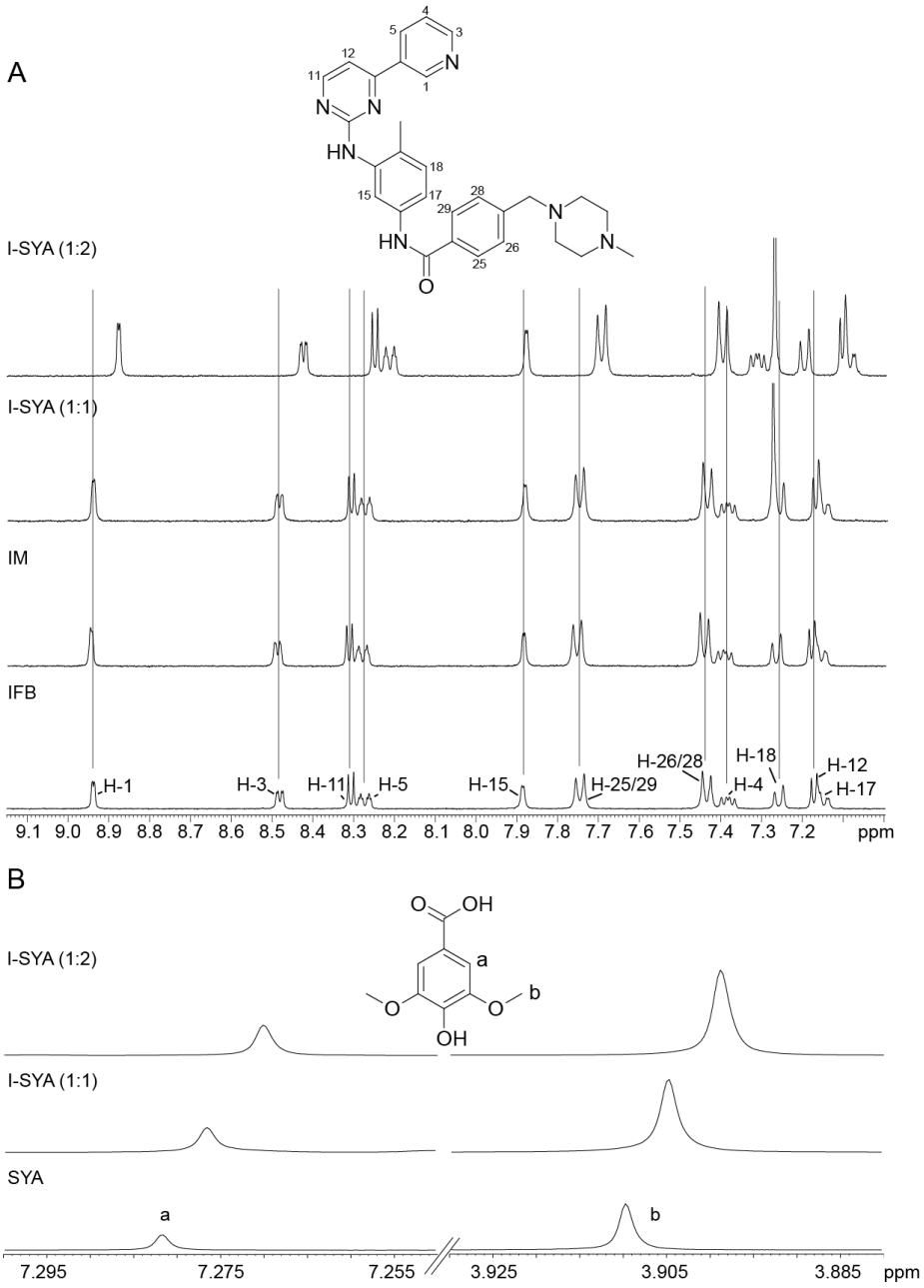

Figure 18. *(A) Aromatic range of the ^{1}H NMR spectra of Imatinib free base (IFB), Imatinib mesylate (IM), Imatinib syringate co-crystal I-SYA (1:1), and Imatinib syringate co-crystal salt (1:2), and (B) the ^{1}H signals of protons a and b of syringic acid (SYA), I-SYA (1:1) and I-SYA (1:2) at the nominal concentration of 1000 µM in deuterated phosphate buffer at pH 7.4*

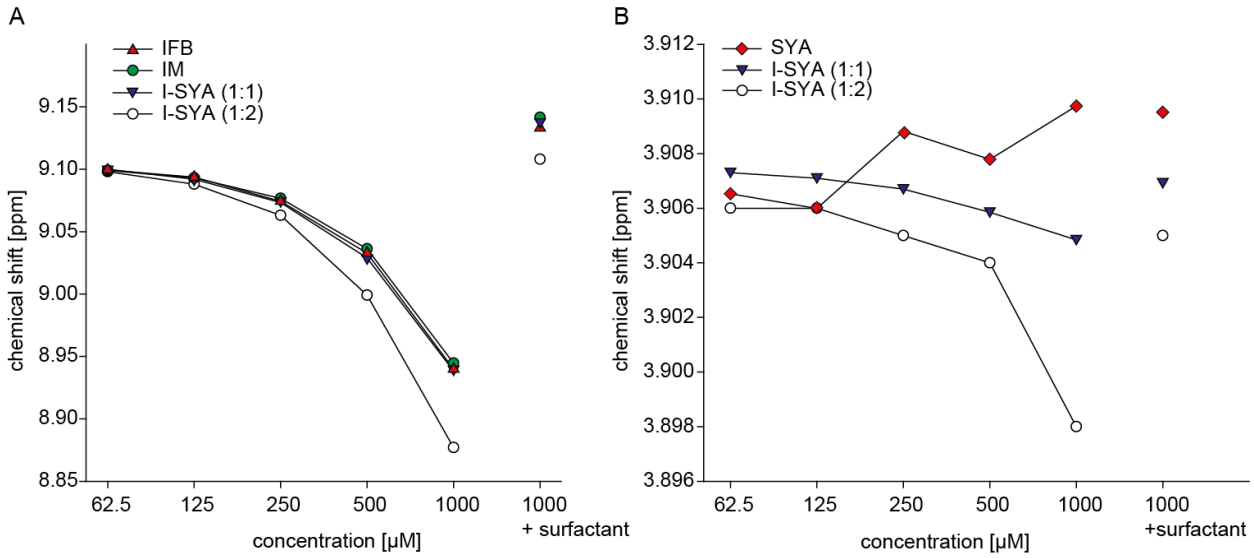

Figure 19. *Concentration dependent chemical shifts of the ^{1}H signals of (A) Imatinib (H-1), and (B) syringic acid (SYA) (H-b). Additional to the nominal concentration of 1000 µM surfactant (Tween 80) was added, which broke up the Imatinib aggregates as indicated by the reversed shift*

Similar to Imatinib, SYA displayed concentration dependent chemical shifts (CAC ≈ 25 – 50 µM) with sharp signals, but the aggregates did not respond to the supplementation of surfactant possibly reflecting aggregates with low aggregation numbers and similar hydrophilicity than SYA alone, i.e., the surfactant was ineffective (**Figure 20**). In presence of Imatinib the ^{1}H signals of SYA shifted to higher field in contrast to SYA alone (**Figure 18B**), and upon surfactant supplementation the shifts for SYA reverted to the initial state for I-SYA (1:1) co-crystal and I-SYA (1:2) co-crystal salt (**Figure 19B**). This is suggesting at least in part close arrangement of SYA molecules to Imatinib aggregates as the chemical shifts of SYA were affected by the ring current effects of Imatinib's aromates. As reported (*vide supra*) the IH form precipitated directly from IM but not from I-SYA (1:1) solution for which LLPS was observed (**Figure 6**) reflecting kinetically hindered displacement of the SYA molecules from Imatinib by water."

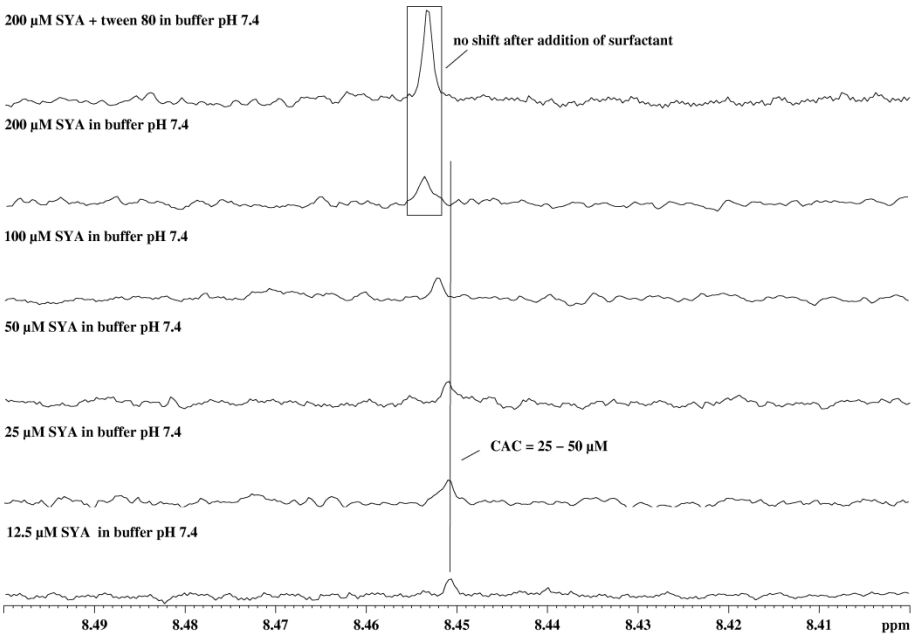

Figure 20. *Determination of the critical aggregation concentration (CAC) by concentration dependent ^{1}H NMR spectroscopy of syringic acid (SYA) at pH 7.4*

Aggregation of Imatinib with SYA could be driven by two different mechanisms. The first hypothesis is based on the existence of intermolecular interactions between Imatinib and SYA that persist in solution. These interactions could be in the form of hydrogen bonds, π-π stacking, van der Waals interactions and/or electrostatic interactions, Imatinib and SYA being oppositively charged at pH 6.8. A shift in the signal of the aromatic protons from NMR studies suggests participation of the aromatic rings of both Imatinib and SYA in the aggregation. The existence of so called supramolecular synthons in solution has already been suggested in several reports. Banik et al. argued that the synthon structure can be maintained upon dissolution and acts as a precipitation inhibitor which extends the kinetic solubility of co-crystals. The term “synthon-extended-spring-and-parachute model” was coined to describe this behaviour.[69] Another example comes from Cherukuvada et al. who reported a nitrofurantoin-p-aminobenzoic acid co-crystal that formed a stable solution in water for more than 3 days, and this was ascribed to a stabilization of the API nitrofurantoin towards precipitation of the hydrate form by the coformer p-aminobenzoic acid.[70]

The second hypothesis relies on the hydrophobic effect. SYA could be included into the Imatinib aggregates due to its relative hydrophobicity. This inclusion in turn prevents Imatinib molecules within aggregates to reorganize into nuclei while preventing water molecules to take place, hence sustains supersaturation. A similar case has been monitored by ^{1}H-NMR studies on HPMC-AS and nifedipine.[71]

HPMC-AS was shown to distribute into nifedipine-rich phase during aggregation, which in turn prolonged supersaturation. It was noticed that a lower aqueous solubility of the polymer (e.g. by decreasing the pH which neutralizes the carboxyl groups of the polymer) augmented its inclusion.
In fact, both mechanisms might be at play; inclusion of SYA into Imatinib aggregates could be driven by its hydrophobicity, and strengthened by intermolecular interactions with Imatinib in the aggregates.

There seems to be a relationship between the hydrophilicity of the coformer and the solution stability of the resulting co-crystals with poorly water-soluble APIs.[72] Co-crystals with little soluble coformers tend to have a better solution stability (i.e., to be less prone to dissociation) than co-crystals with highly soluble coformers. Indeed, both moderately soluble coformers and poorly soluble APIs are often amphiphilic and hydrophobic and these properties might drive association in solution.[73]

Relative stability in solution is thought to be important for bioavailability enhancement and different strategies to stabilize solutions from co-crystals have been reported. Most focused on polymeric precipitation inhibitors and surfactants.[74, 75] For example Wang et al. have shown that the duration of supersaturation from a dihydromyricetin-caffeine co-crystal could be extended in the presence of polyvinylpyrrolidone K30. This formulation resulted in a higher bioavailability compared to the neat co-crystal when dosed in dogs.[76] Surfactants in micellar concentration can thermodynamically stabilize co-crystals in solution or decrease the drive for recrystallization by decreasing the supersaturation degree.[77] For instance, dissolution of a saccharin co-crystal in presence of a sufficiently high sodium lauryl sulfate concentration in the medium prevented crystallization of a poorly soluble indomethacin polymorph.[78] Combined approaches have also been employed to maximize the kinetic solubility of co-crystals. Childs et al. used a combination of hydroxylpropyl cellulose as precipitation inhibitor, and vitamin E d-α-tocopheryl polyethylene glycol 1000 succinate as solubilizer to formulate a danazol-vanillin co-crystal.[79] In rats the bioavailability of this optimized formulation was increased more than five fold over the neat co-crystal. Engineering co-crystals or salts with amphiphilic coformers such as the hydroxybenzoic acid derivatives to generate association in solution like it was done in the present work could be an effective alternative to maximize the kinetic solubility of salts and co-crystals.

3.3.6 Permeation Studies

Absorption of a drug from the intestinal lumen to the blood circulation depends on the interplay between solubility and permeability (which are dictated by opposite physicochemical properties). Passive diffusion through membranes depends on the activity of the drug rather than on its total concentration.[10, 11]. Thus, it is important to understand the impact of aggregation and association in solution on the thermodynamic activity of the API, and on resulting diffusion gradients and flux through membranes. Permeation studies were performed (1) to investigate whether Imatinib and SYA could diffuse as aggregates/complexes and

the impact thereof on the rate of diffusion, (2) to assess the consequence of a potentially reduced free drug concentration/fraction due to aggregation on diffusion.

Artificial membranes

In vitro diffusive flux through artificial membranes was investigated with gastrointestinal tract (GIT) lipid-loaded PVDF membranes loaded in 3 mL Side-Bi-Side cells. The amount of API and coformer that diffused through the membrane from the donor compartment to the acceptor compartment was quantified over 3 h and the slope obtained from the time-concentration profiles between 30 min and 3 h was used to calculate the flux.

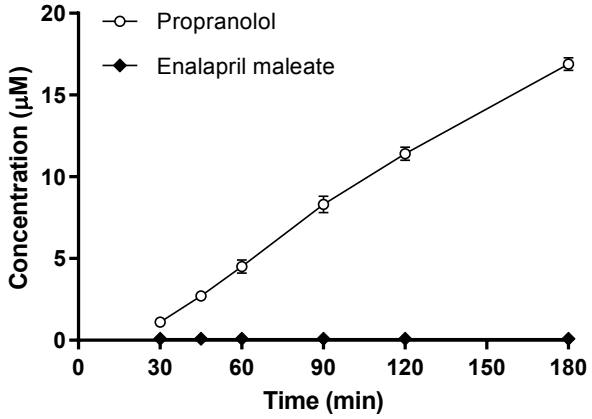

Figure 21. *Acceptor concentration due to diffusion of Propranolol and Enalapril maleate through artifical membranes (n=3)*

First this system was validated for its discriminatory power with propranolol a highly permeable compound, and enalapril maleate a low permeable compound. The diffusion of these two standards was very different, e.g. after 3 h the concentration of Propranolol in the acceptor reached 16.9 µM while that of Enalapril maleate was below 0.1 µM (**Figure 21**). Thus, the GIT lipid membrane system has a large discriminatory power and is suitable to compare permeation of the different forms.

To isolate the effect of the counterion/coformer on the permeability of Imatinib from any diffusion enhancement generated by an increased kinetic solubility of the co-crystals, all diffusion studies were conducted at the same molar solutions (100 µM equivalent to free base). All forms showed practically the same diffusion rate (**Figure 22A**), thus, the diffusion of Imatinib through an artificial membrane was neither influenced by the presence of SYA nor by methanesulfonic acid.

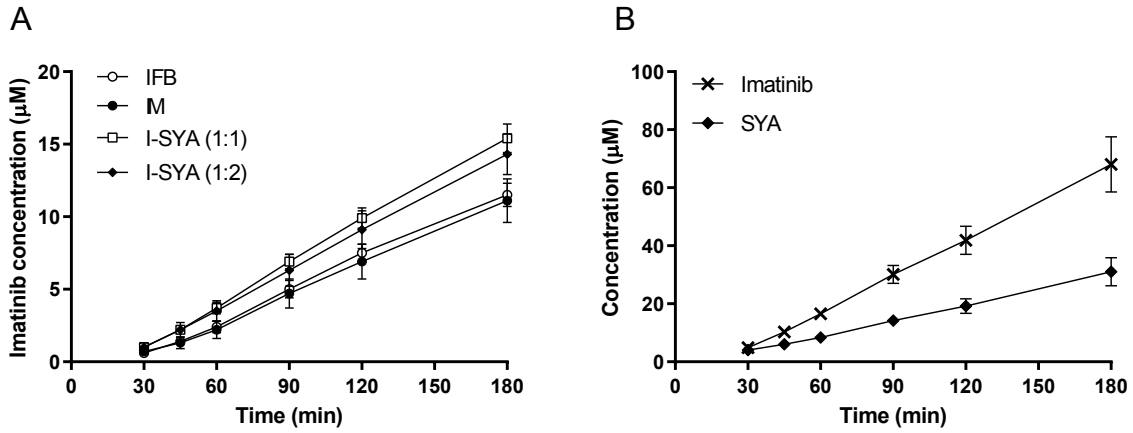

Figure 22. *Acceptor concentration due to diffusion through artificial membranes of (A) Imatinib from Imatinib free base (IFB), Imatinib mesylate (IM), Imatinib syringate co-crystal I-SYA (1:1) or Imatinib syringate co-crystal salt I-SYA (1:2) solutions (100 µM as equivalent free base), and of (B) Imatinib and syringic acid (SYA) from an Imatinib syringate co-crystal I-SYA (1:1) solution (10 mM as equivalent free base) (n=3)*

To compare the diffusion of Imatinib and that of SYA from the co-crystal a 10 mM solution of the I-SYA (1:1) was used (**Figure 22B**). No evidence of a co-permeation of Imatinib with SYA as aggregates or as stoichiometric complexes was found. Imatinib diffused faster than SYA which is in line with its higher permeability conferred by a higher $logD_{6.8}$ (2.5 vs. -1.28, respectively, as determined by shake-flask). Therefore, Imatinib and SYA interacted individually with the membrane surface according to their intrinsic physicochemical properties and did not influence each other's permeability and diffusion rate. Consequently, co-crystals increase diffusion only through increased local moiety concentrations at the membrane surface.[80]

The permeation of Imatinib from a 1000 µM IM solution with addition of 0.025% Tween 80 was investigated to elucidate the effect of aggregation on permeation. A pre-experiment with propranolol and enalapril maleate was performed to ensure that addition of a surfactant to the medium would not compromise the membrane integrity. After 3 h the Propranolol concentration in the acceptor compartment was ca. 18.6 µM and that of Enalapril maleate below 0.1 µM indenpendently of Tween 80 presence which confirmed that membrane integrity was kept in presence of surfactant (**Figure 23A**). Addition of Tween 80 to a 1000 µM Imatinib solution was known to break up Imatinib aggregates as evidenced by ^{1}H-NMR. Diffusion experiments showed that the aggregation state of Imatinib did not prevent rapid partitioning into the membrane as the flux did not increase in presence of Tween 80 (**Figure 23B**). This contrasts with previous reports describing that colloidal species could not cross cellular membranes by passive diffusion due to their large size.[17] The relative affinity of the compounds to the membrane and to the aggregates, and the strength, structure, and dynamics of aggregation in solution might influence diffusion of colloidal

species. In the present case the association between SYA and Imatinib might be weak and/or dynamic enough to allow the free species to diffuse independently.

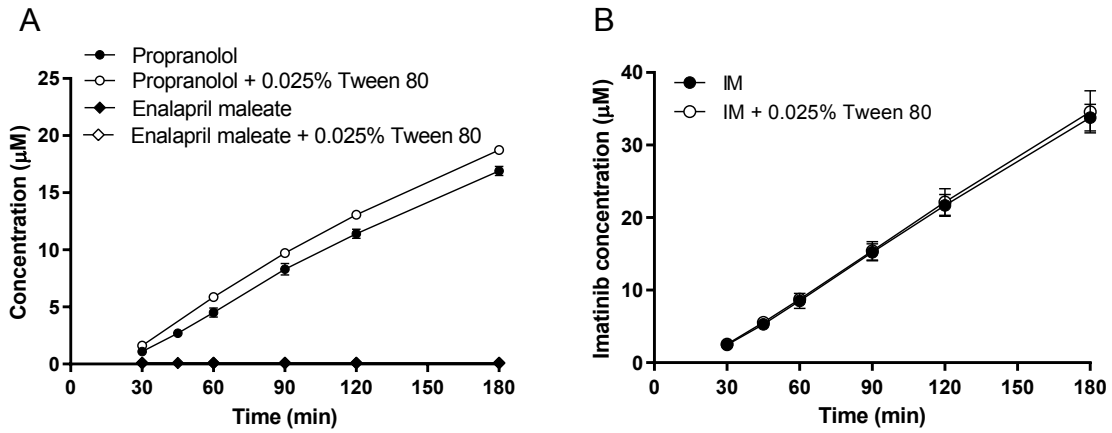

Figure 23. *Acceptor concentration due to diffusion of (A) Propranolol and Enalapril maleate from 100 µM solutions with and without Tween 80 (B) Imatinib from a 1000 µM solution of Imatinib mesylate (IM) with and without Tween 80 (n=3)*

Cellular membranes – LE-MDCK cells

Diffusion was further investigated through cellular membranes using Low Efflux Madin-Darby Canine Kidney (LE-MDCK) cell lines. To assess the impact of aggregation on diffusion, assays were performed at two different concentrations; one below the CAC (i.e. 5 µM) and one above the CAC (i.e. 50 µM). To compare results across different nominal concentration, the results are presented as the apparent permeability (P_{app}) which was calculated according to **Equation 4**.

$$P_{app} = \frac{\Delta Q}{\Delta t} \times \frac{1}{AC_0} \qquad \textbf{(Equation 4)}$$

Where, $\Delta Q/\Delta t$ is the total amount transported from the donor compartment to the acceptor compartment over time, A is the surface area of the cell monolayer, and C_0 is the nominal concentration in the donor compartment.

No significant difference was observed between the different forms (**Figure 24**) which is in line with the results obtained from artificial membranes. Diffusion was not reduced at concentrations above the CAC of Imatinib which also confirmed previous observations from artificial membranes.

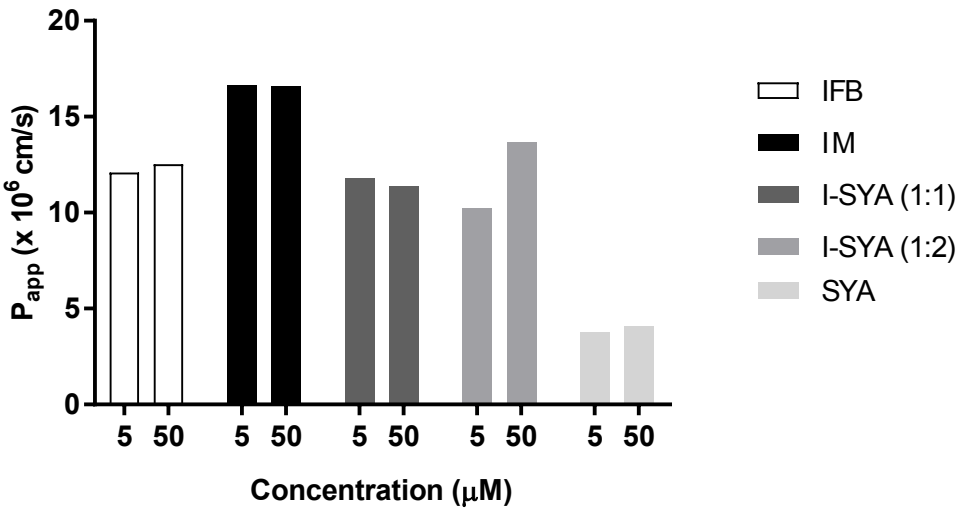

Figure 24. *Apparent permeability of Imatinib free base (IFB), Imatinib mesylate (IM), Imatinib syringate co-crystal I-SYA (1:1), Imatinib syringate co-crystal salt I-SYA (1:2) and Syringic acid (SYA) through LE-MDCK cells from 5 μM and 50 μM solutions*

A decrease in passive diffusion through enterocytes membranes due to aggregation under physiological conditions would have been one hypothesis to explain the late and variable T_{max} of Imatinib mesylate in patients.[81] Indeed, if aggregates would be physically excluded from passive diffusion in the upper intestine, dilution and breakage of aggregates along transit would result in a late T_{max}.

A different hypothesis could be that aggregates are absorbed via the lymphatic route. This theory was proposed by Janssen et al. when they observe high drug concentration in lymph tissues after oral administration of non-nucleoside reverse transcriptase inhibitors to dogs.[16] Colloidal species and particles can be taken up by the M cells in Peyer's patches of the mucosa-associated lymphoid tissue of the intestine and drained by the lymph fluid until the thoracic lymph duct to enter the systemic circulation.[82] However, since no evidence that aggregation prevents diffusion was found in this work, both above hypotheses probably do not hold and the root cause for the peculiar pharmacokinetics of Imatinib remains to be elucidated.

3.4 Conclusion

Two co-crystals of Imatinib with SYA were engineered and their structure was elucidated by single crystal diffractometry. Upon dissolution in aqueous media, the syringate co-crystals generated Imatinib concentrations that were 60x higher than that of the free base. Due to their amphiphilicity, Imatinib and SYA aggregated in solution, which prevented rapid precipitation of Imatinib hydrate from the solution

state, while this effect was missing in the mesylate case. Diffusion of Imatinib through cellular and artificial membranes was not impacted by aggregation and assays revealed that the association of Imatinib and SYA was weak enough to allow an individual interaction with the membrane. This piece of work demonstrated the value of using hydrotropic agents, like hydroxybenzoic acid derivatives to engineer solution-stable co-crystals of poorly water-soluble APIs. Further studies in animals or humans are desirable to evaluate the *in vivo* translation of this “parachute” effect.

4 Ternary amorphous solid dispersions

4.1 Introduction

The release of an amorphous, molecularly dispersed API from a polymeric matrix is a highly complex phenomenon which comprises several steps. The first prerequisite is the wetting of the amorpous solid dispersion (ASD) powder or compact.[83] Then, water ingress and hydration of the API and polymer enable dissolution. If the polymer is insoluble in the dissolution medium, or has a tendency to swell, the API has to diffuse through the viscous layer before it is released to the bulk medium. The sum of these events determines the dissolution rate of the ASD which is often referred to as the "spring". Each step depends on a number of factors including the type of polymer, the API physicochemical properties, the drug loading, the manufacturing process, and the medium characteristics (pH, viscosity, ionic strength, hydrodynamics etc.). The drug loading often determines if the dissolution process is drug-controlled, polymer-controlled or both[84], and has a strong influence on wetting. The manufacturing process will define key material characteristics such as porosity, surface area and surface properties. As a result, it is often difficult to predict the dissolution rate of ASDs and their optimization remains empirical and time-consuming.

A high initial release rate from ASDs, or forceful spring, might be beneficial in several instances. A boost release at the site of absorption (i.e. in the upper part of the small intestine) might avoid portioning from the stomach and result in the generation of higher concentrations at the site of absorption. This might be particularly relevant for drugs whose efficacy is C_{max} driven. Secondly, for basic compounds a fast release in the upper part of the gastrointestinal tract may counteract rapid precipitation upon the pH shift during transfer from the stomach to the small intestine. While a strong spring might be easily achieved with hydrophilic polymers like polyvinylpyrollidones or copovidone, swelling polymers like hydroxypropylmethylcellulose (HPMC) and their derivatives typically slow down release. Yet, HPMC derivatives are widely used as polymeric carriers for ASDs due to their superior precipitation inhibition ability. Thus, it is of interest to investigate new approaches to improve API release from such matrices.

To this end it was investigated whether inclusion of hydrotropic agent in polymeric ASDs could boost the spring. The hypothesis was that hydrotropic agents, having some surface properties similar to classical surfactants, could enhance wetting of ASDs, and improve dissolution and solvation of poorly water-soluble APIs which could, in turn, result in a faster API release from HPMC derivatives ASDs. While inclusion of classical surfactant in ASDs has been thoroughly investigated, hydrotropic agents have received little attention. Ciprofloxacin (CPX), a poorly water-soluble compound was used as a model compound for this investigation.

4.2 Material and methods

4.2.1 Materials

Ciprofloxacin, nicotinamide, vanillic acid (VAN), vanillin, p-aminobenzoic acid (PABA), sodium taurocholate (NaTC), acetic acid and trifluoroacetic acid were purchased from Sigma-Aldrich (Buchs, Switzerland). Sodium chloride, sodium hydroxide, and potassium dihydrogen phosphate (EMSURE grade), sodium dihydrogen phosphate used for buffer preparation, and LiChrosolv acetonitrile used for mobile phases preparation were purchased from Merck (Schaffhausen, Switzerland). Millipore water was obtained from a Milli-Q dispenser equipped with a Millipal Express 40 0.22 µm filter from Merck KGaA (Darmstadt, Germany). 0.45 µm PVDF centrifugal filters (Ultrafree MC HV) were purchased from Merck & Cie (Schaffhausen, Switzerland). Ready-to-use fasted simulated intestinal fluid (FaSSIF V1) powder was purchased from Biorelevant (London, UK). HPMC 603, HPMC-AS-LF and HPMC-P55 were obtained from Novartis Stein (Switzerland).

4.2.2 Methods

Preparation of Amorphous Solid Dispersions (ASDs) by Freeze-drying

ASDs were prepared by freeze-drying in a VirTis adVantage laboratory benchtop freeze-dryer from SPScientific (NY, USA) equipped with a RZ 6 vaccuum pump from vacuubrand (Theilingen, Switzerland). Five weight percent stock solutions of polymers, counterions/coformers, NaTC and CPX were prepared in acetic acid. The stock solutions were combined in 50 mL Wheaton glass serum bottle from Sigma (Buchs, Switzerland) to prepare ASDs of different drug load and compositions. The samples were lyophilized with the following program: The pressure was lowered to ca. 2 mbar and the temperature was reduced from room temperature to -30°C over 40 min and held at -30°C during 90 min. During the primary drying, the temperature was increased to 20°C and the pressure was decreased to 0.5 mbar over 180 min. The temperature was increased to 25°C and the pressure was decreased to 0.2 mbar over 120 min and these conditions were held for 120 min. Then the pressure was increased to 2.5 mbar until samples were unloaded. The condenser temperature was set to -40°C.

X-Ray Powder Diffractometry (XRPD)

ASDs prepared by freeze-drying were charged between thin-film SpectroMembrane of Kapton from Chemplex Industries (Palm City, FL) in a metallic holder and analyzed with a PANalytical X'Pert PRO powder diffractometer from PANalytical (Zürich, Switzerland) using Cu-Kα radiation (unsplit Kα1+Kα2 doublet, mean wavelength 1.5419 Å) at a power of 40 kV and 40 mA, and a focusing X-ray mirror for Cu radiation. The scattered X-ray went through a 0.04 rad axial Soller slit and a 2.5 mm anti-scattering slit

and detection was performed with a X'Celerator detector from PANalytical. Measurements were done in transmission mode in coupled two theta/theta mode with a step size of 0.0084° in 2θ and 25 s measurement time per step in the range of 4 - 40° (2θ). Data analysis was carried out with the software Data Viewer from PANalytical.

SIF and FaSSIF Preparation

50 mM phosphate buffer pH 6.8 (= simulated intestinal fluid (SIF)) was prepared accordingly to the United States Pharmacopeia (USP).[63] 0.9 g of sodium chloride and 6.8 g of potassium dihydrogen phosphate were dissolved in 1L of Millipore water. The pH was measured with a SevenCompact pH meter from Mettler-Toledo (Greifensee, Switzerland) equipped with an InLab Micro electrode and adjusted with 1 M HCl or NaOH of Titripur grade from Merck (Darmstadt, Germany).
Fasted simulated intestinal fluid (FaSSIF; V1) was prepared according to the instructions from Biorelevant (London, UK). To prepare 1 L of FaSSIF, 2.24 g of ready to use powder was dissolved in 1 L of NaH_2PO_4 anhydrous buffer (0.42 g of NaOH, 3.44 g of NaH_2PO_4 and 6.19 g of NaCl).

Solubility Measurements

The equilibrium solubility of CPX in phosphate buffer at pH 6.8 was determined by the shake flask method. An excess of solids (5 mg/mL) was added to 3 mL of phosphate buffer and stirred with a magnetic stirrer for 24 h at room temperature. In addition the equilibrium solubility of CPX in physical mixtures with HPMC-AS (3 mg/ml) and/or VAN (one or two molar equivalents) was measured. After 24 h, the pH was recorded and the samples were filtered through 0.45 µm PVDF Ultrafree MC HV centrifugal filters from Merck & Cie (Schaffhausen, Switzerland) in a miniSpin centrifuge from Vaudaux-Eppendorf AG (Basel, Switzerland) at 13.400 rpm for 90 seconds. Filtrates were further diluted with acetonitrile, and the amount of CPX in solution was quantified by UPLC-UV. Excess solids remaining on the filters were analyzed by XRPD.

Powder Dissolution in SIF and FaSSIF

Fifteen mg substance equivalent to CPX free form of freeze-dried ASDs were added to 3 mL of 50 mM phosphate buffer pH 6.8 (SIF) at room temperature. A magnetic stirrer at 300 rpm was used to provide agitation. At predefined time points, 100 µL aliquots were sampled and filtered through 0.45 µm PVDF centrifugal filters from Ultrafree in a miniSpin centrifuge at 13.400 rpm for 90 seconds. Filtrates were diluted with acetonitrile and assayed by UPLC-UV.

Ultra Performance Liquid Chromatography (UPLC)

Quantification for the solubility measurements was performed on a 1290 Infinity UPLC from Agilent Technologies (Basel, Switzerland) equipped with a diode array detector (G4212A), an auto sampler (G4226A), a column thermostat (G1330B) and a quaternary pump (G4204A) with an Acquity UPLC BEH C18 1.7 µm (2.1 x 100 mm) column from Waters (Milford, MA). For the analysis of CPX and VAN, the column temperature was set to 35 °C. Mobile phase A was a 95/5/0.05 (v/v/v) water/acetonitrile/trifluoroacetic acid mixture. Mobile phase B was a 95/5/0.05 (v/v/v) acetonitrile/water/trifluoroacetic acid mixture. The gradient profile was as follows for mobile phase B: 0-5 min 10-90%; 5-5.25 min 90-90%; 5.25-5.50 min; 90-10%; 5.50-6.50 min 10-10%. The flow rate was set at 0.6 mL/min and detection was performed at λ = 279 nm.

4.3 Results and discussion

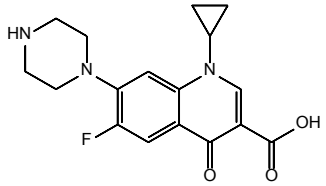

Figure 25. *Molecular structure of ciprofloxacin (CPX)*

CPX free form is a zwitterion with two pK_a of 6.09 and 8.74.[85] At pH 6.8 CPX is predominantly in its zwitterionic form with the carboxylic acid and the piperazine ionized. CPX is classified as a BCS class IV compound due to its low solubility in water and relatively poor permeability, and the high doses required for an effective antibiotic treatment.[86] It is marketed as the hydrochloride salt. Once in water, CPX converts to different hydrate forms, which are less soluble than the free form.[87]

4.3.1 Screening of different counterions

Four hydrotrope-like compounds[88] and one bile salt were screened for their ability to improve initial release of CPX from HPMC amorphous solid dispersions (ASDs; **Figure 26 and 27**). The hydrotrope-like compounds were selected based on their known hydrotropic behavior (nicotinamide and vanillic acid (VAN)) or their structural analogy with hydrotropes (vanillin and p-aminobenzoic acid (PABA)). Sodium taurocholate (NaTC) was selected based on previous work on bile salts (see **Chapter 3**). For a fast screening, a low drug load of 20% and a 1:1 mass ratio between CPX and the hydrotropes were chosen. The high melting point of CPX (275°C) and its poor solubility in most organic solvents precluded the use

of hot melt extrusion and spray drying to manufacture the ASDs. Thus, freeze-drying from acetic acid solutions was selected.

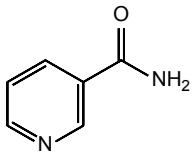

Nicotinamide

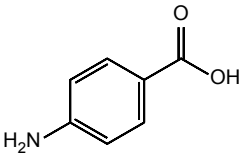

p-aminobenzoic acid (PABA)

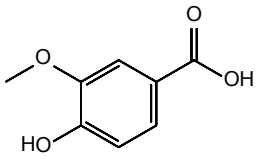

Vanillic acid (VAN)

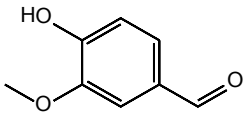

Vanillin

Figure 26. *Molecular structure of selected hydrotropic and hydrotropic like agents*

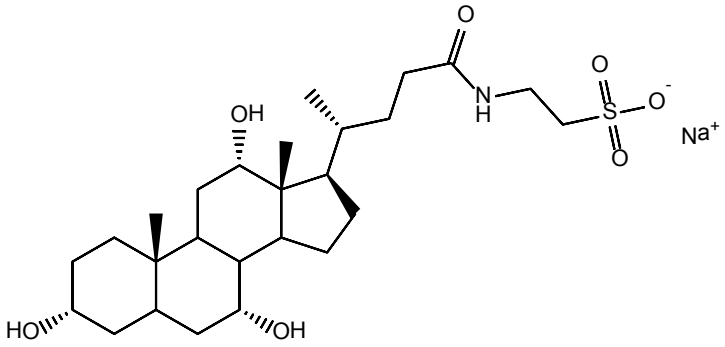

Figure 27. *Molecular structure of sodium taurocholate (NaTC)*

Turning CPX into an ASD is a promising approach to increase its dissolution and solubility at neutral pH (**Figure 28**). However, the release from a binary CPX/HPMC ASD was limited to about 5%. During the assay formation of a viscous polymer plug was observed, which was probably slowing down further release. There was a significant difference in the performance of HPMC ASDs containing different hydrotropes and bile salt (**Figure 28**). While addition of Nicotinamide, NaTC and PABA did not improve initial release, 60% of the API was released from the ASD containing VAN within the first 5 min. Vanillin had a small effect on the release. A high release was achieved with PABA between 30 min and 60 min and this could not be explained. Once in solution CPX precipitated as a different form in all cases (probably as the hydrate form as described in the literature) except for the VAN containing ASD from which a new form precipitated. Differences between hydrotropes might be explained by different intermolecular interactions with CPX, although this was not investigated in the present work. The lack of effect of NaTC might reflect poor affinity of CPX with bile salts, which could be consistent with the lack of positive food effect for this compound. Based on this screening, VAN and PABA were selected for the next step.

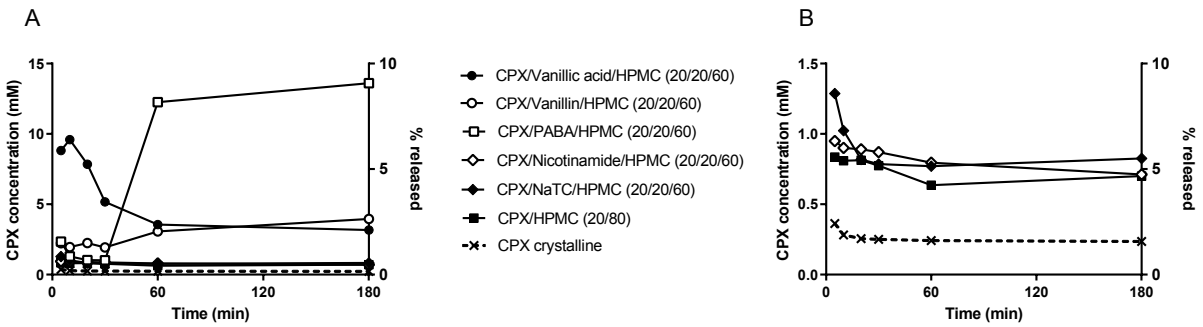

Figure 28. *(A) Dissolution of amorphous solid dispersions containing 20% of Ciprofloxacin (CPX) in SIF buffer pH 6.8 (B) zoom in the low concentrations (0 to 1.5 mM)*

4.3.2 Screening of different polymers

The next step was to screen three different cellulosic polymers: HPMC, HPMC acetate succinate (HPMC-AS) and HPMC phthalate (HPMC-P). For all polymers, addition of VAN or PABA improved the release (**Figure 29**) from ASDs. The highest release was obtained with HPMC-AS and VAN, thus this system was selected for further investigation.

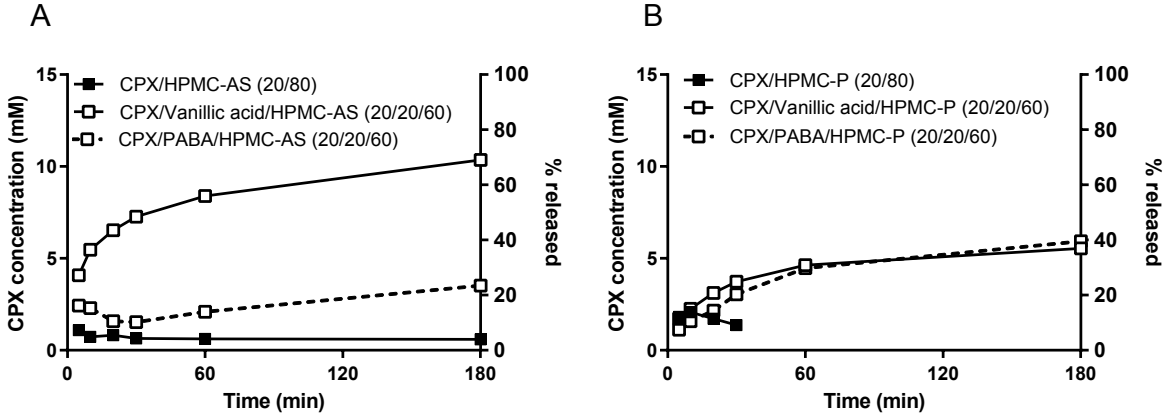

Figure 29. *Dissolution of (A) HPMC-AS based amorphous solid dispersions (ASDs) and (B) HPMC-P based ASDs containing 20% of Ciprofloxacin (CPX) in SIF buffer pH 6.8*

4.3.3 Solid state characterization

A total of 8 compositions with different CPX/VAN/HPMC-AS ratios were prepared by freeze-drying and characterized by XRPD (**Table 4**).

Table 4. *Overview of the different Ciprofloxacin (CPX) compositions prepared by freeze-drying and characterization by XRPD*

Composition n°	CPX (%)	VAN (%)	HPMC-AS (%)	XRPD
1	100	0	0	crystalline
2	20	0	80	different form amorphous
3	40	0	60	some crystallinity
4	20	80	0	different form crystalline VAN reflections
5	40	60	0	crystalline VAN reflections
6	20	20	60	amorphous
7	20	60	20	crystalline VAN reflections
8	40	40	20	amorphous

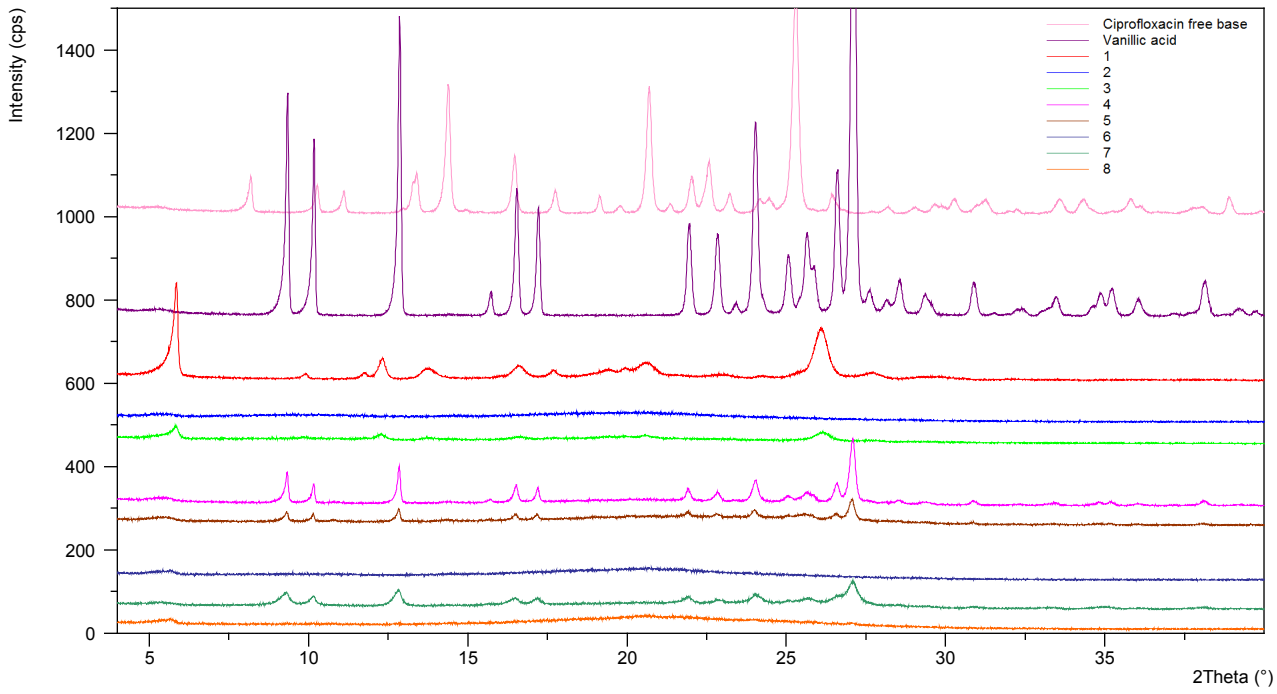

Figure 30. *XRPD diffractograms of the different compositions of Ciprofloxacin prepared by freeze-drying*

Pure amorphous CPX could not be obtained by freeze-drying (**Figure 30**). Instead a different polymorph was obtained. HPMC-AS stabilized the amorphous form up to a drug load of 20% (Composition 2). At a higher drug load traces of crystalline material were detected (Composition 3). Presence of VAN prevented CPX polymorph recrystallization and enabled the preparation of ASDs up to a drug load of 40% (Composition 8). Excess VAN (based on a mass ratio between VAN and CPX; Compositions 4, 5 and 7) recrystallized. These observations may indicate intermolecular interactions between CPX and VAN in the

solid state that stabilized both CPX and VAN against recrystallization from the amorphous state, i.e., an optimum ratio between CPX and VAN requiring only a minimal amount of polymer for solid state stability.

4.3.4 Dissolution studies

To evaluate the dissolution and supersaturation of the different compositions, powder dissolution experiments were performed in two different media and conditions: SIF buffer pH 6.8 at 25°C, and fasted simulated intestinal fluid (FaSSIF) pH 6.5 at 37°C.

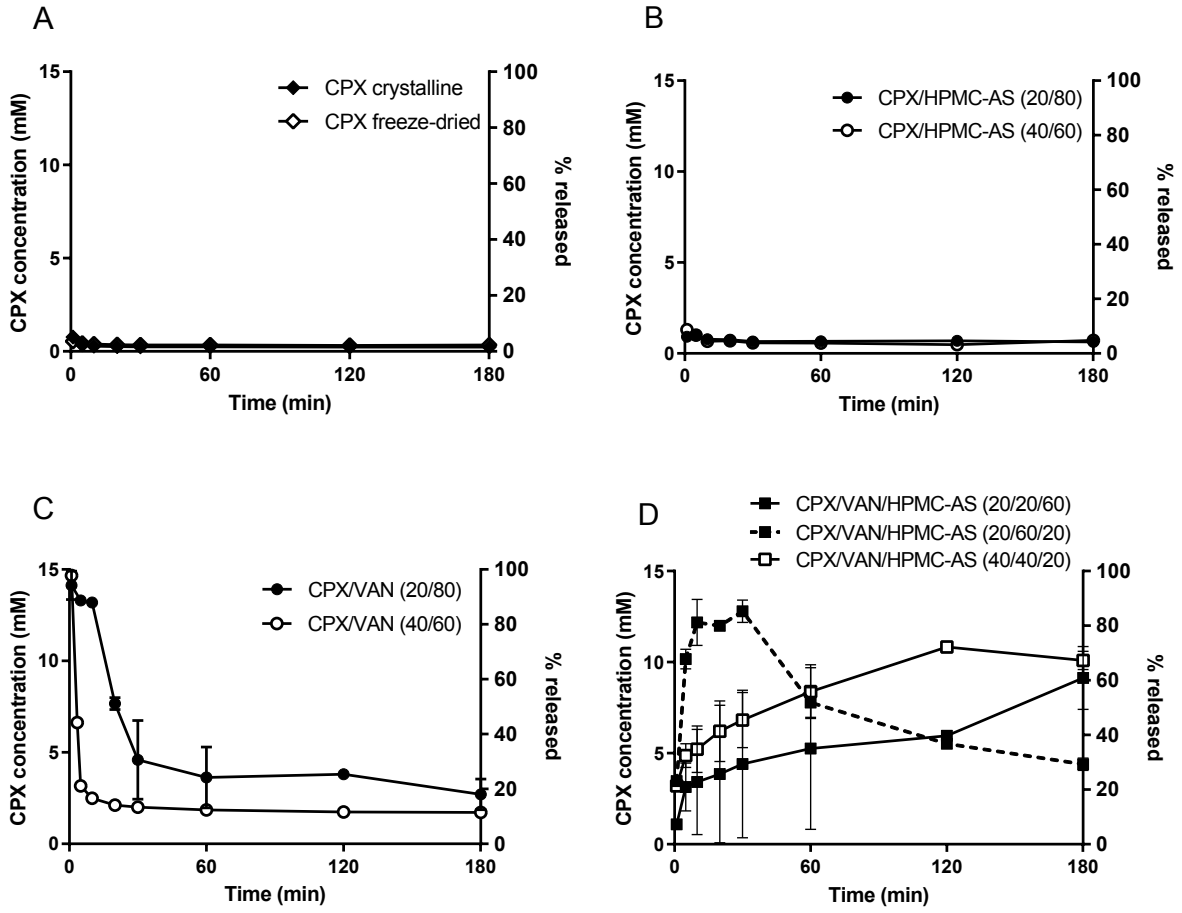

Figure 31. *Powder dissolution of the different compositions in SIF buffer at room temperature. (A) Crystalline CPX (reference) and freeze-dried CPX (B) Freeze-dried binary solid dispersions of CPX /HPMC-AS (C) Freeze-dried co-mixtures of CPX/VAN (D) Freeze-dried ternary solid dispersions of CPX/VAN/HPMC-AS*

The freeze-dried CPX (which was not amorphous but was a different polymorph than the starting material; **Figure 30**) completely dissolved within seconds and immediately precipitated. The first time point at 10 seconds could not capture its initial dissolution, but it was visually observed (**Figure 31A**). The polymorphic form obtained by freeze-drying must be a higher energy form which dissolves rapidly. However without any precipitation inhibitor, CPX rapidly precipitates as a stable hydrate form.[87] A similar observation was made with the co-mixtures of CPX with VAN (**Figure 31C**). These freeze-dried co-mixtures dissolved rapidly but CPX precipitated within a few minutes, while VAN remained in solution (VAN data not shown*).* CPX release and dissolution from binary composition with HPMC-AS (Compositions 2 and 3) was very limited in SIF (**Figure 31B**). In contrast, combining VAN and HPMC-AS allowed to tune the dissolution profile of solid dispersions (**Figure 31D**). Solid dispersion (SD) 7 which contained the highest amount of VAN (60%) showed the fastest release while the slowest release occurred with the ASD 6 that contained the highest amount of polymer (60%). All ternary SDs (Compositions 6, 7, 8) could maintain high concentrations during the course of the experiment (3 h) even with low levels of HPMC-AS (20%). Indeed, HPMC-AS is one of the most potent polymeric precipitation inhibitor and this property has been ascribed to its amphiphilicity and the presence of hydrophobic domain which promotes interactions with hydrophobic APIs.[89, 90] In addition, Li et al. have shown that HPMC was able to prevent CPX hydrate formation.[87]

The dissolution profiles were markedly different in FaSSIF, a medium which contains a bile salt, sodium taurocholate (NaTC), and lecithin. Major differences were observed with the binary HPMC-AS ASDs (Composition 2) and with the co-mixtures (Compositions 4 and 5; **Figure 32**) as compared to the dissolution profiles in SIF.

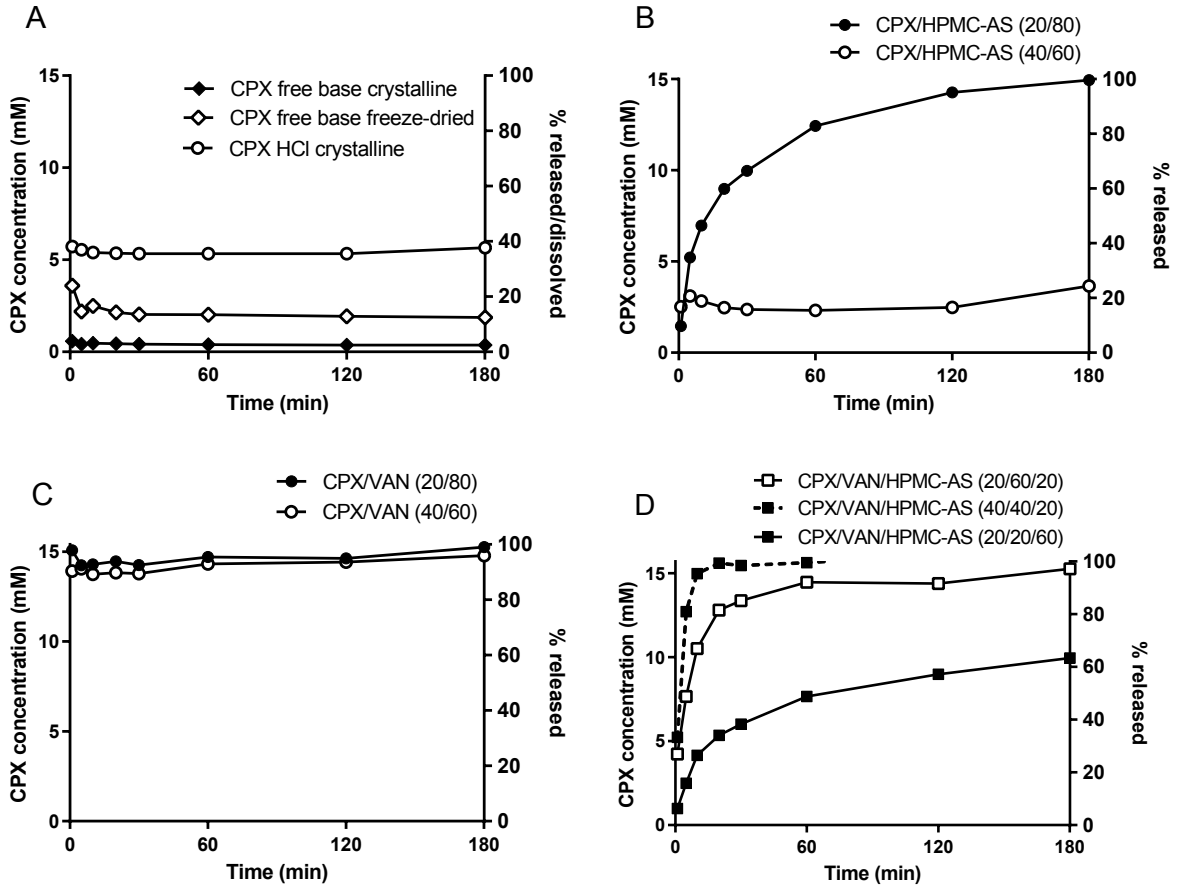

Figure 32. *Powder dissolution of the different compositions in FaSSIF at 37°C (A) CPX free base crystalline, CPX HCl salt, CPX free base freeze-dried (B) Freeze-dried binary solid dispersions of CPX /HPMC-AS (C) Freeze-dried co-mixtures of CPX/VAN (D) Freeze-dried ternary solid dispersions of CPX/VAN/HPMC-AS*

First, a sustained release from composition 2 was observed and the ASD was completely dissolved at the end of the assay (**Figure 32B**), while in SIF buffer only around 5 % CPX had been released after 3 h (**Figure 31B**). The solubility of CPX was not notably different in FaSSIF than in SIF buffer (0.37 vs. 0.23 mM, respectively) hence improved release was not caused by an increase in solubility. One hypothesis for the enhanced release in FaSSIF could be that HPMC-AS has a higher solubility in this medium and/or that the wetting of the ASD powder was improved in the bile salts-rich medium. Indeed, wettability is a key factor determining dissolution of ASDs and was shown to directly correlate with dissolution rate.[83] Bile salts being endogenous surfactants must contribute to a large increase in wettability.

The low performance of composition 3 (**Figure 32B**) could be explained by the presence of crystalline CPX in the solid dispersion (**Figure 30**) as concentrations are similar to freeze-dried CPX which was the same polymorph (**Figure 32A**).

The co-mixtures of CPX with VAN (Compositions 4 and 5) did not precipitate in FaSSIF over 3 h (**Figure 32C**). This contrasts the fast precipitation observed in SIF buffer, and could be due to a crystallization inhibition effect by NaTC present in FaSSIF. Recently bile salts have been shown to be effective precipitation inhibitors for a number of drugs.[35-38] Interestingly, bile salts are able to delay nucleation both in the monomeric and micellar state. The anti-nucleation effect seems to be compound- and bile salt-specific. Li et al. attempted to study the nucleation inhibition effect on a molecular level by molecular dynamics simulations and their work revealed the importance of hydrophobic interactions and hydrogen bonding between APIs and bile salts.[36] In addition, the bulky hydrophobic group and the lack of flexibility of bile salts combined with their amphiphilicity are suggested to be important features for the nucleation inhibition of APIs.[91] Interestingly, bile salts also act in synergy with polymers to delay nucleation.
The release profiles of the ternary SDs (SDs 6, 7 and 8) was also improved in FaSSIF, but the rank order remained the same as in SIF buffer, with SD 7 (containing 60% VAN) showing the fastest release and ASD 6 (containing 60% polymer) showing the slowest release (**Figure 32D**). In summary, in both media inclusion of a hydrotropic agent enhanced both the spring and the parachute of SDs.

Hydrotropic agents have received only little attention in the field of ASDs, nevertheless the scarce data published is promising. Paidi et al. prepared ternary ASDs of atorvastatin calcium trihydrate with nicotinamide and HPMC.[92] Similar to our observations, they witnessed a decrease in dissolution rate with an increased amount of polymer, and ascribed it to an increased thickness of the gel layer due to polymer swelling which retarded drug diffusion. An increased nicotinamide/API ratio led to an increased percentage of API released after 15 min. This effect was accredited to nicotinamide's hydrotropic effects which increased atorvastatin solubility and improved wetting of the spray dried powder. Another interesting effect of hydrotropes is the modification of the pH-dependant solubility of polymers. For instance, a ternary ASDs of Nitrazepam, saccharin and Eudragit E, a basic polymer insoluble at neutral pH, was able to generate supersaturation at pH 6.8.[93] The authors suggested that hydrophilic interactions between saccharin and Eudragit E enabled dissolution of the later at neutral pH. Similar observations were made with Eudragit E and a Novartis compound (data not shown).

4.3.5 Equilibrium solubility

To understand if the boost release was due to a solubilization of CPX by VAN, its equilibrium solubility was measured in presence of VAN, HPMC-AS and a combination of both. HPMC-AS solubilized CPX only to a limited extend, as it is often the case with polymers (**Figure 33**). In contrast, in presence of one and two molar equivalent of VAN, the concentration of CPX was 4.6 and 6.5 fold higher than its equilibrium solubility in SIF buffer, respectively, which could indicate a hydrotropic solubilization. In addition there was a synergistic effect of VAN and HPMC-AS with CPX concentrations 8.4 fold higher than the reference.

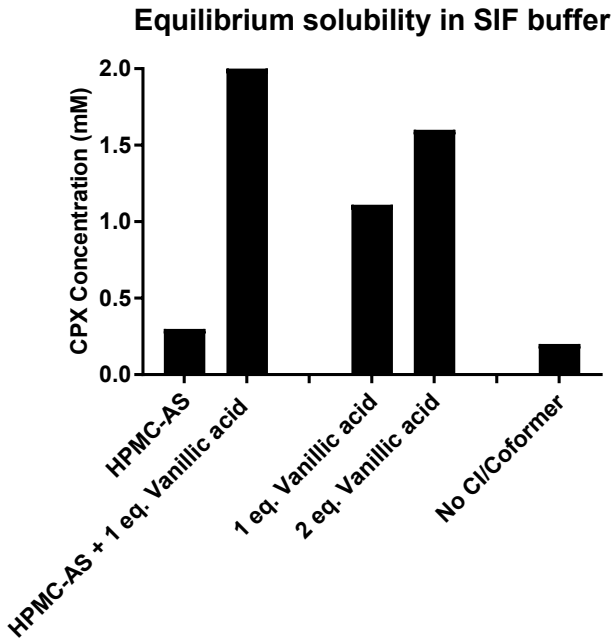

Figure 33. *Equilibrium solubility of CPX in SIF buffer pH 6.8 in presence of predissolved HPMC-AS (3 mg/ml) and/or different molar ratio of VAN (1:1 and 1:2 CPX:VAN) with native reference*

Therefore, a solubilization of CPX by VAN and HPMC-AS is probably one mechanism responsible for the high spring release of the ternary ASDs. An increased solubility of CPX in the diffusion layer certainly leads to a higher concentration gradient and thus a faster dissolution according to **Equation 2**. Although this has not been investigated further in the present work, another very likely mechanism for an enhanced spring is the improved wetting of the ASDs powders containing VAN.[83]

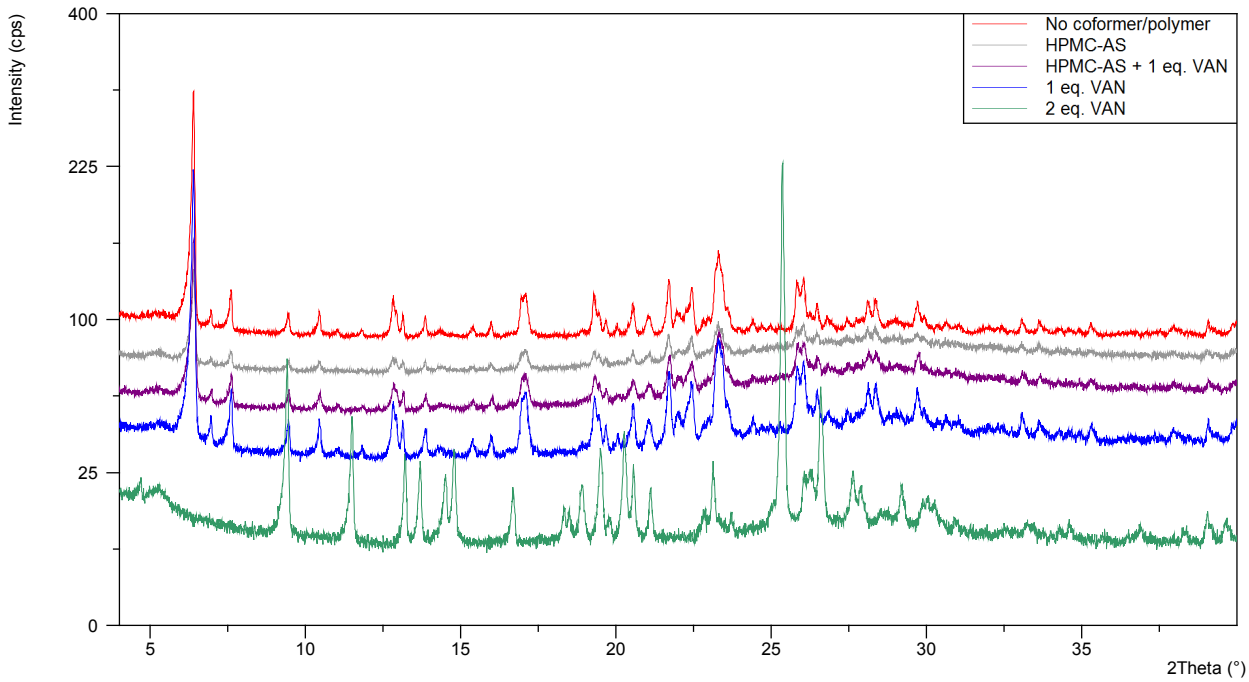

Figure 34. *XRPD diffractograms of collected solids at the end of the equilibrium solubility determination in SIF buffer pH 6.8 at room temperature (24 h)*

Upon dissolution in an aqueous medium, CPX converted to different forms (**Figure 34**). Interestingly presence of VAN altered CPX phase transformations in solution. While CPX converted to the hydrate form in presence of one stoichiometric equivalent of VAN and in presence of HPMC-AS, in presence of two stoichiometric equivalents of VAN, nucleation of a different form was preferred.

Although this investigation is still in its preliminary stage, it brings two important considerations. The first one is the consideration of hydrotropic agents in the formulation of ASDs of poorly water-soluble APIs. First, hydroptropes could enhance physical stability of ASDs through intermolecular interactions with the API, thereby reducing mobility and recrystallization. Miscibility of the API in the amorphous matrix is improved and the drug load can be increased which reduces the size of the final dosage form.
Furthermore, addition of hydrotropes within the amorphous matrix of ASDs improves their dissolution performance in aqueous environments. Hydrotropic solubilization on one hand increases dissolution rate by increasing the solubility of the API in the boundary layer, and by increasing the wetted surface area available by dissolution. On the other hand this solubilization effect may delay precipitation of the API from solution state by decreasing supersaturation levels. If precipitation occurs, hydrotropes can favor one form over the other, which could bring a biopharmaceutical advantage if this precipitated form has a higher solubility or faster re-dissolution rate.

The second consideration is the parachute effect provided by bioendogenous components. Indeed, the observation that co-mixtures which precipitated rapidly in SIF buffer did not precipitate in FaSSIF questions the parachute paradigm. While some artificial parachute effect might be needed in some cases, the effect of endogenous precipitation inhibitors must be considered. It should be emphasized that FaSSIF contains only one bile salt in contrast to the pool of bile salts present *in vivo*, thus, the parachute effect from bioendogenous components is likely underestimated in FaSSIF, as multiple bile salts typically have a superior precipitation inhibition ability as compared to single one.[38]

4.4 Conclusion

Binary ASDs of CPX and HPMC-AS, ternary ASDs of CPX, VAN and HPMC-AS, and co-mixtures of CPX and VAN were prepared by freeze-drying and their dissolution and supersaturation were assessed in SIF buffer and in FaSSIF. The release of CPX from binary HPMC-AS ASDs in SIF buffer was very low and addition of VAN provided a forceful spring, probably through an improvement of wetting and a solubilization effect. While the co-mixtures dissolved immediately, in SIF buffer initial dissolution was followed by a rapid precipitation. Interestingly, rapid precipitation of the co-mixtures did not occur in FaSSIF, probably due to an interaction of CPX with NaTC and/or lecithin present in this medium. In addition, release from binary HPMC-AS ASD with a low drug load was largely improved in FaSSIF. This study highlights the potential of hydrotropic agents to enhance release from matrices of swelling polymers from the HPMC family, and their effect on solution mediated phase transformations of poorly water-soluble APIs. Furthermore, the differences in release profiles and supersaturatoion duration observed between SIF buffer and FaSSIF question the need for a strong parachute in supersaturating drug delivery systems. *In vivo* studies are required to evaluate the biorelevance of these findings.

5 Bile salts to enhance bioavailability in the fasted state

5.1 Introduction

Concomitant food intake can alter a drug's pharmacokinetics by different mechanisms; the absorption of the drug can be enhanced via an increase in dissolution rate and solubility, a stimulation of bile flow, a delayed gastric emptying, an increase in splanchnic blood flow or an enhanced lymphatic uptake.[94] On the other hand, absorption can be reduced by physical or chemical interactions with food components (e.g. sequestration) or by an increase in intestinal mobility. The BCS classification has an impact on the propensity to be subject to a food effect, and the majority of BCS class II and IV have a positive food effect. The formulation might have a significant impact on food effect and can be tailored to mitigate food effects. For example an enabling formulation for the drug Aprepitant consisting of spray-coated nanoparticles eliminated the positive food effect by increasing the bioavailability.[95]

Compound A is a highly crystalline base (melting point > 200°C) BCS class IV compound. Its bioavailability has a strong dependance on food intake with AUC and C_{max} increasing more than a factor two after a high fat meal. Such an increase in pharmacokinetic parameters brings safety concerns for the patients as C_{max} might be associated with severe side effects. In view of its extremely low solubility at neutral pH (< 0.02 µg/ml), the likelihood that solubility is the driving factor for the food effect is high. The bioavailability of a pH 1.2 solution after oral administration is only 50% which could reflect precipitation upon transfer from the stomach to the small intestine. Thus, the aim of the work presented in this chapter was to (1) identify the root cause of the food effect (2) develop a formulation principle which was less sensitive to food intake than the reference formulation of Compound A.

5.2 Materials and Methods

5.2.1 Materials

Compound A free base and Compound A hydrochloride monohydrate were obtained from Novartis (Basel, Switzerland). HPMC 603, HPMC-AS-LF, HPMC-P55, mannitol and PVP XL were supplied by Novartis Stein (Schaffhausen, Switzerland). Soluplus and PVPVA64 were purchased from BASF (Ludwishafen, Germany). Eudragit E and Eudragit L100-55 were purchased from Evonik Industries (Essen, Germany). Size 00 hard gelatin capsule shells were purchased from Capsugel (Colmar, France). Acetic acid, maleic acid, sodium taurocholate (NaTC), L-α-Phosphatidyl choline from egg yolk were purchased from Sigma-Aldrich (Buchs, Switzerland). FeSSIF was prepared in house by freeze drying. Ready-to-use fasted simulated intestinal fluid (FaSSIF-V2) powder was purchased from Biorelevant (London, UK). Sodium chloride (NaCl), sodium hydroxide (NaOH), and potassium dihydrogen phosphate (EMSURE grade), sodium dihydrogen phosphate used for buffer preparation, and LiChrosolv acetonitrile used for mobile phases preparation were purchased from Merck (Schaffhausen, Switzerland). Millipore water was obtained from a Milli-Q dispenser equipped with a Millipal Express 40 0.22 µm filter from Merck KGaA (Darmstadt, Germany). 0.45 µm PVDF centrifugal filters (Ultrafree MC HV) were purchased from Merck & Cie (Schaffhausen, Switzerland).

5.2.2 Methods

Preparation of Amorphous Solid Dispersions (ASDs) by Freeze-drying

ASDs were prepared by freeze-drying in a VirTis adVantage laboratory benchtop freeze-dryer from SPScientific (NY, USA) equipped with a RZ 6 vaccuum pump from vacuubrand (Theilingen, Switzerland). Five weight percent stock solutions of polymers and NaTC, and one weight percent stock solutions of Compound A were prepared in acetic acid. The stocks solutions were combined in 50 mL Wheaton glass serum bottle from Sigma (Buchs, Switzerland) to prepare ASDs of different drug load and compositions. The samples were lyophilized with the following program: The pressure was lowered to ca. 2 mbar and the temperature was reduced from room temperature to -30°C over 40 min and held at -30°C during 90 min. During the primary drying, the temperature was increased to 20°C and the pressure was decreased to 0.5 mbar over 180 min. The temperature was increased to 25°C and the pressure was decreased to 0.2 mbar over 120 min and these conditions were held for 120 min. Then the pressure was increased to 2.5 mbar until samples were unloaded. The condenser temperature was set to -40°C.

X-Ray Powder Diffractometry (XRPD)

ASDs prepared by freeze-drying, and samples placed in stability were charged between thin-film SpectroMembrane of Kapton from Chemplex Industries (Palm City, FL) in a metallic holder and analyzed with a PANalytical X'Pert PRO powder diffractometer from PANalytical (Zürich, Switzerland) using Cu-Kα radiation (unsplit Kα1+Kα2 doublet, mean wavelength 1.5419 Å) at a power of 40 kV and 40 mA, and a focusing X-ray mirror for Cu radiation. The scattered X-ray went through a 0.04 rad axial Soller slit and a 2.5 mm anti-scattering slit and detection was performed with a X'Celerator detector from PANalytical. Measurements were done in transmission mode in coupled two theta/theta mode with a step size of 0.0084° in 2θ and 25 s measurement time per step in the range of 4 - 40° (2θ). Data analysis was carried out with the software Data Viewer from PANalytical.

Differential Scanning Calorimetry (DSC)

DSC was performed on a Q2000 instrument from TA Instruments (New Castle, DE) using a scanning rate of 20 K/min from 25 to 200, 250 or 300 °C under a nitrogen purge (flow rate of 50 ml/min). A second heating cycle was done to evidence glass transition temperatues (T_g). Two to five mg of the samples was weighted into a non-hermetic closed aluminum crucibles (Tzero Pan and Lid from TA Instruments).

SIF, FaSSIF and FeSSIF Preparation

50 mM phosphate buffer pH 6.8 (= SIF buffer) was prepared according to the United States Pharmacopeia (USP).[63] 0.9 g of sodium chloride and 6.8 g of potassium dihydrogen phosphate were dissolved in 1L of Millipore water. The pH was measured with a SevenCompact pH meter from Mettler-Toledo (Greifensee, Switzerland) equipped with an InLab Micro electrode and adjusted with 1 M HCl or NaOH of Titripur grade from Merck (Darmstadt, Germany).

Fasted Simulated Intestinal Fluid (FaSSIF-V2) was prepared according to the instructions from Biorelevant (London, UK). To prepare 1 L of FaSSIF, 1.79 g of ready-to-use FaSSIF-V2 powder was dissolved in 1 L of pH 6.5 maleic acid buffer (1.39 g of NaOH, 2.22 g of maleic acid and 4.01 g of NaCl to 1L of water).

Fed simulated intestinal fluid (FeSSIF) was prepared in house by freeze drying. Sodium taurocholate 538.7 mg, Lipoid E PCS 155 mg, Glyceryl molooleate 178.3 mg and sodium oleate 24.4 mg in 100 mL of water. The same amount was reconstituted 2 h before use with 3'500 mg of a maleic buffer pH 5.8. The maleic buffer was prepared by dissolution of 0.7334 g of NaCl and 0.6388 g of NaOH in 100 mL of water. The pH was measured with a SevenCompact pH meter from Mettler-Toledo (Greifensee, Switzerland) equipped with an InLab Micro electrode and adjusted with 1 M HCl or NaOH of Titripur grade from Merck (Darmstadt, Germany).

Precipitation Inhibition Assay

One mg/mL polymer stock solutions of HPMC-P, HPMC-AS, Eudragit E and Eudragit L100-55 were prepared in SIF buffer and stirred overnight. One hundred mg of Compound A free base were dissolved in 1 mL of acetic acid. Ten µL of the Compound A stock solution were added to 10 mL of either pure SIF buffer or the polymeric stock solutions. At predefined time points, 100 µL aliquots were sampled and filtered through 0.45 µm PVDF centrifugal filters from Ultrafree in a miniSpin centrifuge at 13.400 rpm for 90 seconds. Filtrates were diluted with acetonitrile and assayed by UPLC-UV. The pH value was recorded 3 h after the start of the experiments. The final pH varied between 6.0 and 6.2.

Powder dissolution in SIF, FaSSIF and FeSSIF

0.3 mg substance equivalent to free base were added to 3 mL of 50 mM phosphate buffer pH 6.8 (SIF) or FaSSIF-V2 or FeSSIF media at room temperature. Stirring was with a magnetic stirrer at 300 rpm. At predefined time points, 100 µL aliquots were sampled and filtered through 0.45 µm PVDF centrifugal filters from Ultrafree in a miniSpin centrifuge at 13.400 rpm for 90 seconds. Filtrates were diluted with acetonitrile and assayed by UPLC-UV. The pH value was recorded 3 h after the start of the experiments. Due to the low nominal amount of product, no pH change greater than 0.1 units was observed.

Ultra Performance Liquid Chromatography (UPLC)

Quantification of Compound A in the solubility and dissolution assays was performed on a 1290 Infinity UPLC from Agilent Technologies (Basel, Switzerland) equipped with a diode array detector (G4212A), an auto sampler (G4226A), a column thermostat (G1330B) and a quaternary pump (G4204A) with an Acquity UPLC BEH C18 1.7 µm (2.1 x 100 mm) column from Waters (Milford, MA). The column temperature was set to 35 °C. Mobile phase A was a pH 6.2 10 mM phosphate buffer. To prepare 2 L of buffer, 2.27 g of sodium phosphate monobasic monohydrate and 0.954 g of sodium phosphate dibasic was dissolved in 1.90 L of water. The pH was measured with a SevenCompact pH meter from Mettler-Toledo (Greifensee, Switzerland) equipped with an InLab Micro electrode and adjusted, if necessary, with 1 M HCl or NaOH of Titripur grade from Merck (Schaffhausen, Switzerland). The volume was filled up to 2.0 L with water. The buffer was filtered through Nalgene Rapid-Flow sterile disposable filter units with 0.2 µm PES membrane (Thermo Fisher Scientific, MA, USA). Mobile phase B was a 95/5 (v/v) acetonitrile/water mixture. The gradient profile was as follows for mobile phase B: 0-5 min 10-90%; 5-5.25 min 90%; 5.25-5.50 min; 90-10%; 5.50-6.50 min 10%. The flow rate was set at 0.6 mL/min and detection was performed at λ = 267 nm.

Stability Study

Freeze-dried samples were stored under different conditions to assess physical stability.
Open glass bottles containing pure freeze-dried Compound A free base and Compound A HCl were stored in a dessicator with silica beads and in a dessicator with a saturated solution of NaCl (providing 75% relative humidity) in a Mermmert oven at 80°C (Thermotec, Kaiseraugst, Switzerland). XRPD and DSC analysis was done at time 0, after three days and after one month.
Open glass bottles containing the two selected ASDs Compound A HCl/NaTC/Eudragit E and Compound A HCl/NaTC/HPMC-P were stored in dessicators with silica beads in 40°C and 60°C Kelvitron t chambers from Heraeus Instruments (Geneva, Switzerland), in a ThermoTEC at 25°C/60%RH chamber from TTWE (Kaiseraugst, Switzerland) and in a Pharma climatic test chamber at 40°C/75%RH from CTS (Hechingen, Germany). After one month, XRPD analysis was carried out to detect the presence of recrystallized material.

Freeze-dried Material Compression and Milling

Powders obtained by freeze-drying were compressed with an hydraulic press using the intrinsic dissolution rate apparatus. Briefly, approximatively 100-150 mg of freeze-dried material was filled in the 8 mm diameter die cavity and the punch was placed into the chamber. The powder was compressed on a SEPAC hydraulic press for 1 min at 2 tons. The disc obtained was removed from the die by disassembly and milled with a mortar and pestle. The milled material was then sieved through 0.25, 0.5 and 1 mm hand screens. Different fractions were collected in different vials.

Capsules Filling

Size 00 capsules were filled manually with the sieved fraction ≥ 250 µm to ≤ 1000 µm of compressed and milled freeze-dried material. For ASD 1, two capsules per dog were filled each with 130 mg of ASD powder which represents 25.0 mg equivalent Compound A free base per capsule. For ASD 2, four capsules per dog were filled each with 131.5 mg of ASD powder which represents 12.5 mg equivalent Compound A free base per capsule.

Capsules Dissolution

Capsules dissolution was performed in a Sotax USP 2 paddle apparatus (Aesch, Switzerland). One liter vessels were filled with 900 mL of either SIF buffer, or HCl 0.1 M solution. The media were degased with helium for one min per liter, and pre-heated to 37°C with the paddle speed set at 100 rpm. The capsules were placed in a sinker and dropped into the media at time 0. After 15, 30, 45 and 60 min, 2 mL were sampled and filtered through 0.45 µm PVDF Ultrafree MC HV centrifugal filters from Merck & Cie

(Schaffhausen, Switzerland) in a miniSpin centrifuge from Vaudaux-Eppendorf AG (Basel, Switzerland) at 13.400 rpm for 90 seconds. Filtrates were further diluted with acetonitrile, and the amount of Compound A in solution was quantified by UPLC-UV.

Capsules Disintegration

Disintegration of capsules was performed on a Sotax DT2 disintegration tester (Aesch, Switzerland). 1000 mL Schott beakers were filled with 900 mL of either SIF buffer, either HCl 0.1 M solution. The media were degassed with helium for one min per L, and pre-heated to 37°C. Capsules were placed in the basket and disks were used to prevent floating. The basket-rack assembly was immersed at a constant frequency rate of 30 cycles per minutes. The process of disintegration was visually observed and the time for complete disintegration was recorded.

In vivo Study

Two Compound A ASDs in capsules (ASD 1 and ASD 2) were administered to four male Beagle dogs originated from Marshall Bio Resources (USA) in a cross-over design. The dose was 50 mg/dog of active moiety. Dogs were fasted overnight before the study start and were given their standard diet (300 - 350 g; Art. Nr. 3353 Provimi KlibaSA, Kaiseraugst, Switzerland) approximately 4 hours post dose. All animals had free access to tap water. When receiving ASD 1, dogs were treated with pentagastrin to decrease the pH in the stomach. For the preparation of the pentagastrin solution, pentagastrin (Sigma-Aldrich) was dissolved in 10% PEG400 in sterile water at a concentration of 80 µg/mL. The dosing volume was 0.075 mL/kg (i.m. using a 23 g needle) and the final dose 6 µg/kg. The pentagastrin administration was executed 45 min before capsule administration. When receiving ASD 2, dogs were treated with ranitidine to increase the pH of the stomach. Ranitidine (ZANTIC Inj Lösung 50 mg/5 mL, GlaxoSmithKline AG, Münchenbuchsee, Switzerland) was administered intravenously at a dose of 2 mg/kg 1 h before capsule administration. Following pretreatment, capsules were administered with approximately 20 mL of tap water to facilitate swallowing. Swallowing of the complete dose was checked visually.

Blood samples were collected from the vena cephalica into tubes containing no anticoagulant at 0.25, 0.5, 1, 1.5, 2, 4, 8, 12, 24, 30 and 48 h after capsule administration. After collection, the blood samples were allowed to clot at room temperature (approx. 30 min). Serum was prepared by centrifugation (3000 g, 10 min, 4°C) and was transferred in individual tubes with barcodes. The samples were stored at -80°C.

Quantification was done by Liquid Chromatography-tandem Mass Spectrometry (LC-MS/MS) using Electrospray Ionization (ESI) in positive ion mode. Pharmacokinetic parameters were calculated by means of the Phoenix software (WinNonlin, Pharsight Corp., Mountain View, CA, USA) using the noncompartmental approach.

5.3 Results and Discussion

5.3.1 Cause of the positive food effect

Powder dissolution experiments conducted in fasted simulated intestinal fluid (FaSSIF) and fed simulated intestinal fluids (FeSSIF) revealed that the solubility of Compound A free base and its hydrochloride salt was significantly increased in FeSSIF (**Figure 35**). Thus, the positive food effect is probably caused by an increased solubility in the fed environment, rich in bile salts, lecithin and monoglycerides. The bell shape curve suggested a conversion to a less soluble form over the course of dissolution.

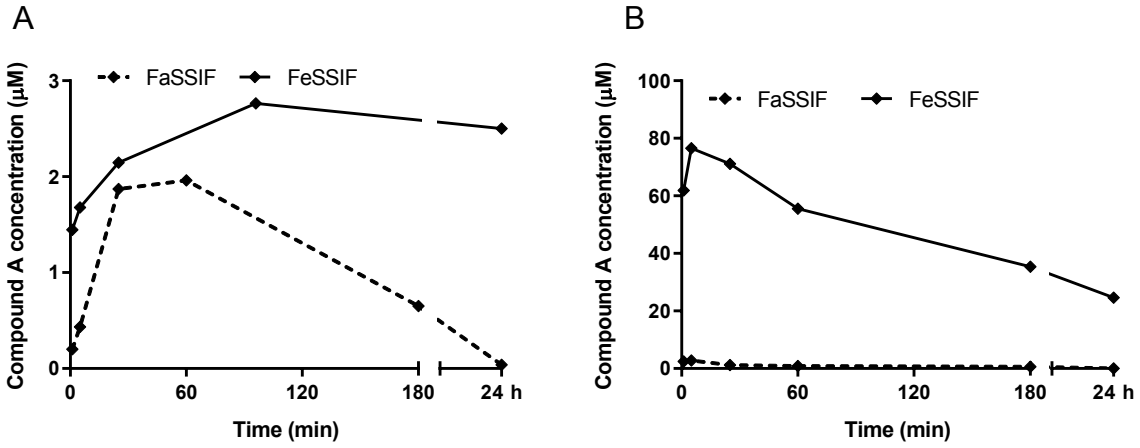

Figure 35. *Powder dissolution of (A) Compound A free base and (B) Compound A HCl monohydrate salt in FaSSIF and FeSSIF media*

The FeSSIF medium contained sodium taurocholate (NaTC), phosphatidylcholine, glyceryl monooleate and sodium oleate. Powder dissolution was studied in the maleic buffer used to reconstitute the FeSSIF medium (pH 5.8) in presence of each of the single components individually (**Figure 36A**). None of the components, on an individual level, solubilized Compound A to a similar level as when combined in FeSSIF (i.e. maximum concentration in FeSSIF 76.5 µM), which indicated a synergistic solubilization of Compound A by the different components of FeSSIF. Nevertheless, on an individual level NaTC, a bile salt, showed the highest solubilization, however only at high concentrations (0.2 mM) (**Figure 36B**).

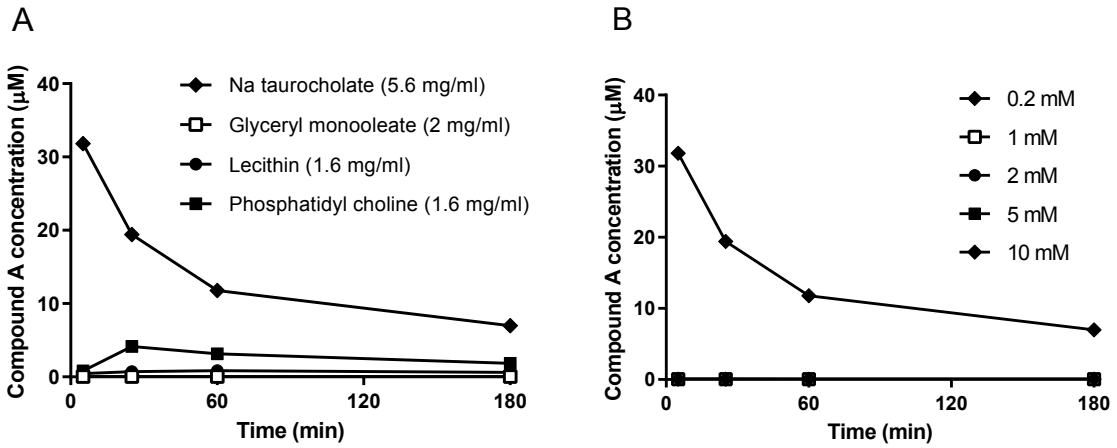

Figure 36. *(A) Dissolution of crystalline Compound A HCl salt in maleic acid buffer pH 5.8 (reconstitution buffer for FeSSIF medium) in presence of single FeSSIF components (B) Dissolution of crystalline Compound A HCl salt in maleic acid buffer with different concentrations of predissolved NaTC.*

Thus, bile salts have to be combined with another enabling formulation principle. In view of the extremely low solubility of Compound A, ASD preparation was chosen as it is one of the most powerful approaches to increase dissolution and the kinetic solubility of APIs.

5.3.2 Amorphous solid dispersion development

Solubility and Powder Dissolution Studies

Seven polymers (Eudragit E, Eudragit L100-55, HPMC-AS, HPMC-P, PVP VA 64, HPMC and Soluplus) were screened in a step-wise approach for they solubilization efficiency (**Figure 37A**), their precipitation inhibition efficiency (**Figure 37B**) and API release (**Figure 38A**).

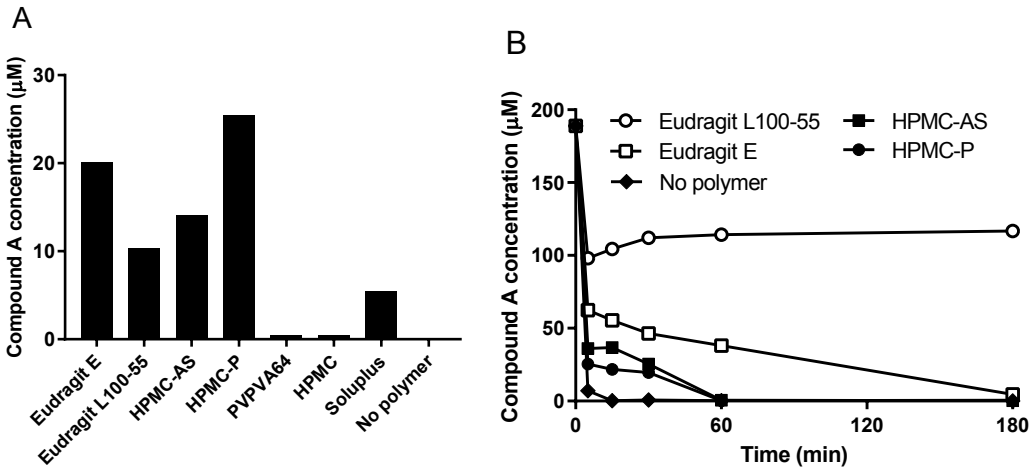

Figure 37. *(A) Equilibration of crystalline Compound A free base in SIF buffer pH 6.8 in presence of 1 mg/ml pre-dissolved polymer and (B) Precipitation inhibition of Compound A free base by predissolved polymers in SIF buffer pH 6.8*

Four polymers (Eudragit E, Eudragit L100-55, HPMC-AS and HPMC-P) increased significantly the equilibrium solubility of Compound A (**Figure 37A**). Such solubilization is unusual as typically polymers are poor solubilizers. The methacrylates and HPMC derivatives were strong solubilizers of Compound A with a 532 fold improvement with Eudragit E, 274 fold with Eudragit L100-55, 373 fold with HPMC-AS and 675 fold with HPMC-P over the equilibrium solubility of Compound A. In contrast, PVPVA64 and HPMC had almost no solubilization effect. This suggested a strong affinity of Compound A with the Eudragits and HPMC derivatives, and these polymers were selected for the precipitation inhibition experiment.
The two methacrylates were also good precipitation inhibitors and slowed down precipitation to a significant level, while HPMC-AS and HPMC-P were less effective precipitation inhibitors (**Figure 37B**).

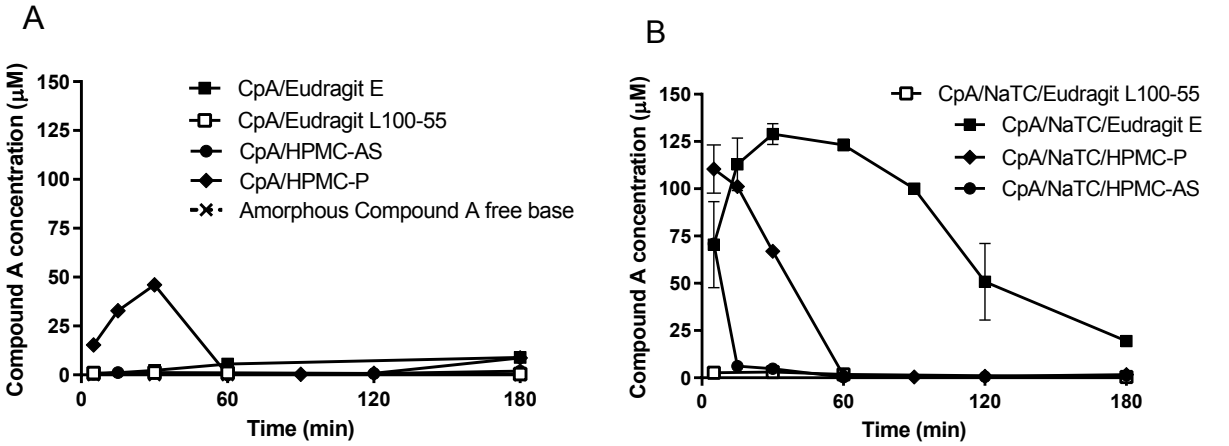

Figure 38. *Dissolution of binary (A) or ternary (B) amorphous solid dispersions (ASDs) of Compound A (CpA) in SIF buffer pH 6.8. The drug load was 10%. In the ternary ASDs the mass ratio NaTC:polymer was 1:3 (w/w). The ASDs were prepared with Compound A free base.*

The release of the Compound A from binary ASDs containing Compound A and polymers in SIF buffer was very low for all systems (**Figure 38A**). The HPMC-P ASD generated concentrations that were 1'250 x higher than the equilibrium solubility of Compound A free base in SIF buffer but dissolved molecules rapidly precipitated after 30 min. The release from the other systems was extremely slow and only reached a few percent after 3 h. The pure amorphous material did not dissolve. Reasons for a low release/dissolution could be a low solubility of the amorphous form of Compound A, a poor wettability of the freeze-dried powders, and/or recrystallization of the API at the dissolving surface or swelling and gelling of the polymer matrix.

In an attempt to improve release from the ASDs, NaTC was added into the ASD matrix to form ternary systems. This led to a strong improvement in Compound A release from all ASDs, except from the Eudragit L100-55 one (**Figure 38B**). The HMPC derivatives (HPMC-AS and HPMC-P) could sustain high concentrations for a few minutes only, whereas Eudragit E provided an excellent parachute, which is in line with the results from the precipitation inhibition assay (**Figure 37B**). The mechanism by which NaTC enhanced Compound A release has not been fully elucidated, but it could come from a wettability effect or a solubilization effect, as it was discussed in Chapter 2. Based on these results, HPMC-P and Eudragit E were selected as lead systems.

The dissolution of ASDs and crystalline Compound A free base and hydrochloride (as references) was further investigated with a pH shift from 2 to 6.5 after 60 min to mimic the transfer of from the stomach to the intestine. Both forms of Compound A (free base and HCl salt) were well soluble at low pH (**Figure 39A**), however the bioavailability of a pH 1.2 acidic solution is only 50% (internal data). Thus, precipitation

upon transfer to the small intestine likely occurs *in vivo* and might impact absorption. Therefore it was of interest to evaluate whether the polymers and NaTC present in the ASDs could mitigate this precipitation.

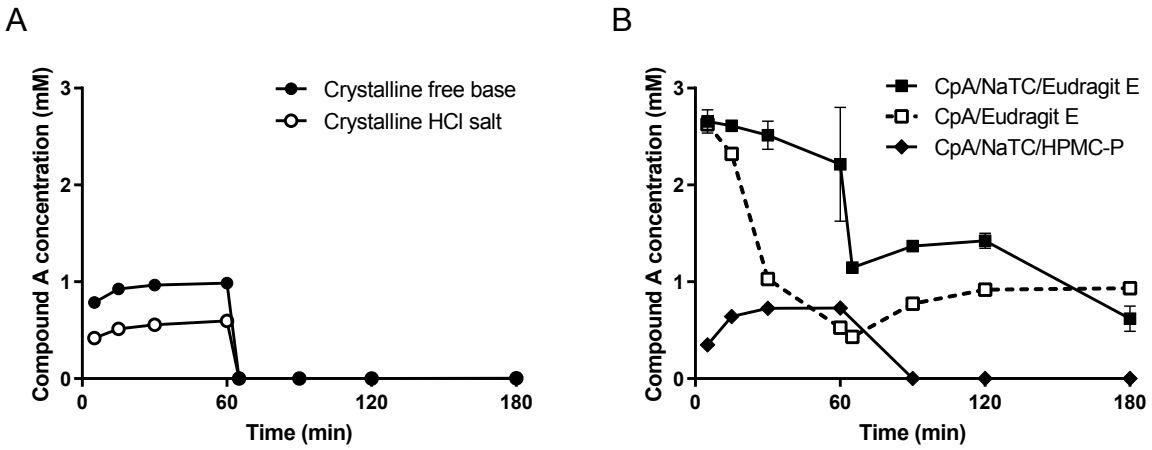

Figure 39. *Dissolution of (A) crystalline Compound A (CpA) and (B) ASDs with a pH shift from 2 to 6.5 after 60 min. In the ASDs, the drug load was 10%, and in ternary ASDs the mass ratio NaTC:polymer was 1:3 (w/w). The ASDs were prepared with Compound A free base.*

Eudragit E is a basic polymer and dissolves at low pH. Combination of Eudragit E with NaTC enabled a fast release and the maintenance of high concentrations during the first part of the experiment at low pH (**Figure 39B**). In contrast, the binary Eudragit E ASD was less stable at pH 2 and Compound A started to precipitate at pH 2, eventually resulting in lower concentrations at pH 6.8. Hence NaTC has already some solubilization or precipitation inhibition effect at pH 2. HPMC-P is an acidic polymer which dissolves above pH 5.5, thus release of Compound A was limited at pH 2.

Generally, the change of pH from 2 to 6.5 induced rapid precipitation of all systems (**Figure 39**). Nevertheless, while the crystalline forms (Compound A free base and the hydrochloride salt) immediately precipitated to very low concentrations (< 0.02 µg/ml, the limit of detection by UPLC-UV), presence of polymers and NaTC in the ASDs slowed down precipitation to a significant level (**Figure 39B**). In addition, redissolution after the pH shift was observed with the Eudragit E ASDs, and very high concentrations (30'000 fold higher than the equilibrium solubility of Compound A) were maintained for 2 h. Prolonged maintenance of high concentrations could indicate a synergistic solubilization effect of Eudragit E and NaTC on Compound A, or a precipitation inhibition effect. Unfortunately, due to the low solubility of Compound A and overall low concentrations generated in these assays it was not possible to study any interactions between the API, the polymer and the bile salt by NMR techniques.

Solid State Characterization of Ternary Amorphous Solid Dispersion

The ternary ASDs prepared with Compound A HCl and Eudragit E, HPMC-P and NaTC by freeze-drying were amorphous as indicated by XRPD analysis (**Figure 40**).

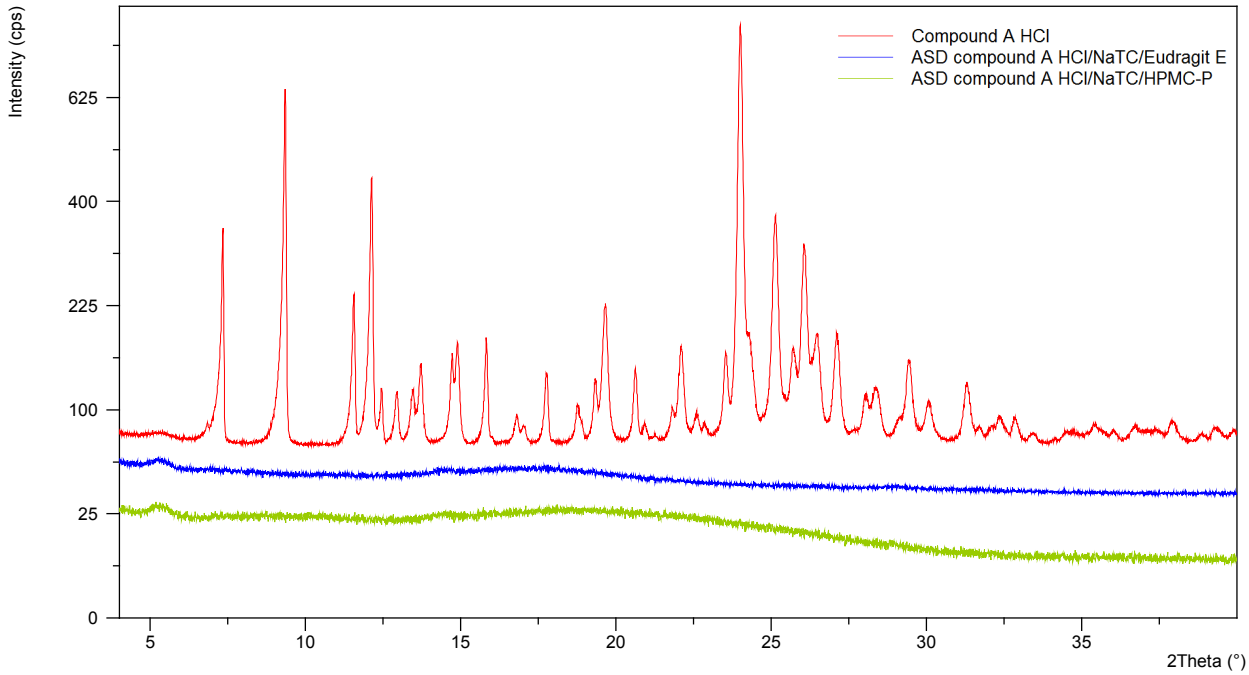

Figure 40. *XRPD diffractograms of ternary ASDs of Compound A HCl prepared by freeze drying and the crystalline reference*

No recrystallization or melting events from the ternary ASDs were detected by thermal analysis (DSC; **Figure 41 and Figure 42**). The glass tansition (T_g) of the Eudragit E ASD was 93.4°C which is in between that of individual components (T_g Eudragit E: 45°C, T_g NaTC: 153.7°C and T_g amorphous Compound A HCl: 139.5°C. Data not shown). Two glass transitions (T_g) were observed in the HPMC-P ASD; 135.5°C and 160.9°C. The first T_g could reflect a Compound A/HPMC-P rich phase (T_g HPMC-P; 133°C [96]) while the second T_g a Compound A/NaTC rich phase. Compound A probably did not phase separated on its own as no T_g around 140°C was observed. Phase separation might have as well occurred upon heating during the first heating cycle, and thus might not be relevant for stability.

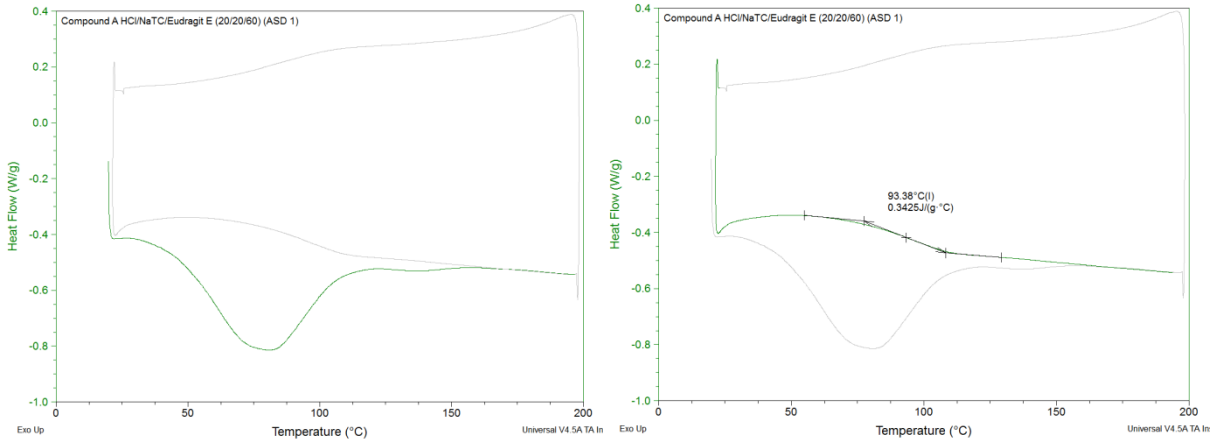

Figure 41. *DSC thermograms of ASD 1 (Compound A HCl/NaTC/Eudragit E (20/20/60)). Left: first heating cycle highlighted. Right: Second heating cycle highlighted*

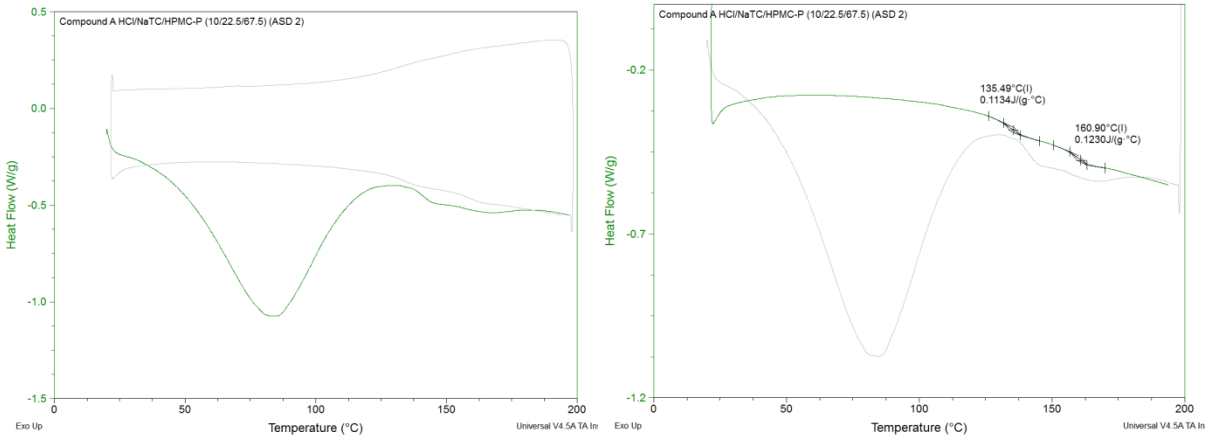

Figure 42. *DSC thermograms of ASD 2 (Compound A HCl/NaTC/HPMC-P (10/22.5/67.5)). Left: first heating cycle highlighted. Right: Second heating cycle highlighted*

Stability study of Amorphous Compound A

The solid state stability of pure amorphous substances (Compound A free base and Compound A HCl) was investigated under stress conditions. The storage temperature was chosen to be close to the Tg of Compound A (105°C for Compound A free base and 139.5°C for Compound A HCl. Data not shown) and the influence of humidity was investigated. Samples were stored at 80°C with desiccant and at 80°C /75% to allow sufficient mobility.

XRPD analysis at time 0 confirmed the amorphous nature of the freeze-dried samples (**Figure 43).** After 3 days at 80°C/75%RH both forms had recrystallized. The free base recrystallized as the same initial polymorph while the hydrochloride salt recrystallized as a different form. When stored under dry

conditions, the free base recrystallized within one month while the hydrochloride salt remained amorphous. Consequently, the amorphous form of the hydrochloride salt was more stable than the amorphous form of the free base.

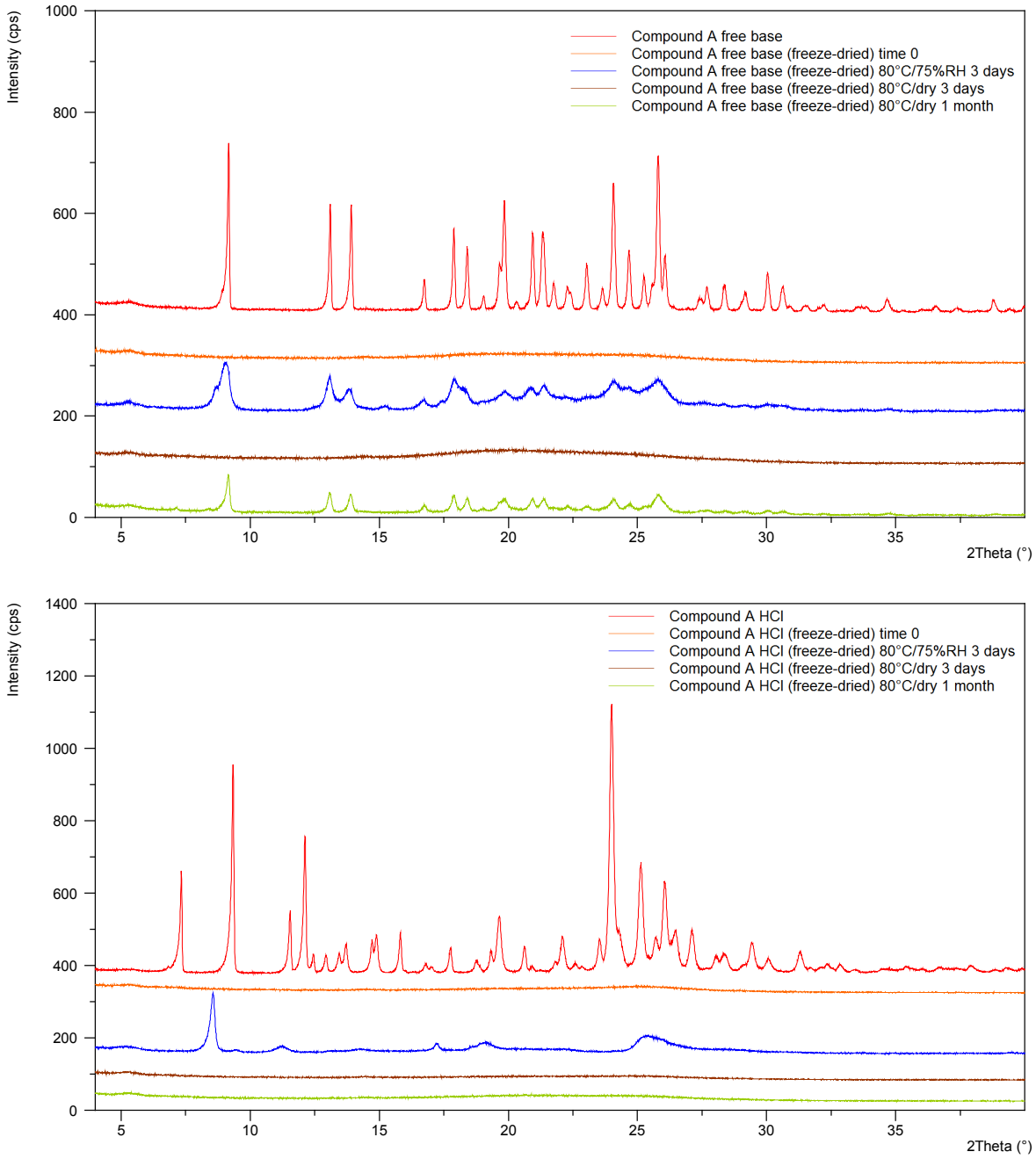

Figure 43. *(Upper) XRPD diffractograms of pure Compound A free base freeze-dried at time 0 and after storage under different conditions and crystalline reference. (Lower) XRPD diffractograms of pure Compound A hydrochloride salt freeze-dried at time 0 and after storage under different conditions with crystalline reference*

5.3.3 Capsule development for *in vivo* evaluation

The aim of the *in vivo* study was to test whether the new formulation principles could achieve a similar exposure in the fasted state than that of the reference formulation in the fed state. Selected formulations were tested in four fasted dogs, and the exposure was compared with the reference formulation in the fed state (internal data).

Two different strategies were explored. The first strategy was to release Compound A in the stomach by using a basic polymer, Eudragit E. This would allow a high concentration of Compound A to be transferred from the stomach into the duodenum, and the parachute effect of the formulation was expected to sustain absorption. The second strategy was to bypass dissolution in the stomach by targeting the release of Compound A in the duodenum. The latter approach prevents portioning from the stomach and could potentially result in higher concentrations at the site of absorption. A dramatic precipitation upon transfer from the stomach to the duodenum would also be avoided. Bypassing dissolution in the stomach typically requires the use of enteric coating which, given time constraints, could not be developed for the present study. Instead, it was decided to treat the dogs with ranitidine to increase stomach pH to a neutral value.[97]

Selection of the Solid Form

The solid form (free base vs. hydrochloride salt) to be used in the ASD was selected according to two criteria: solid state stability and dissolution performance. Compound A HCl is physically more stable in the amorphous state than the free base (see Stability study of pure Compound A above).

The dissolution performance was similar between the two forms (**Figure 44**), thus the hydrochloride was selected.

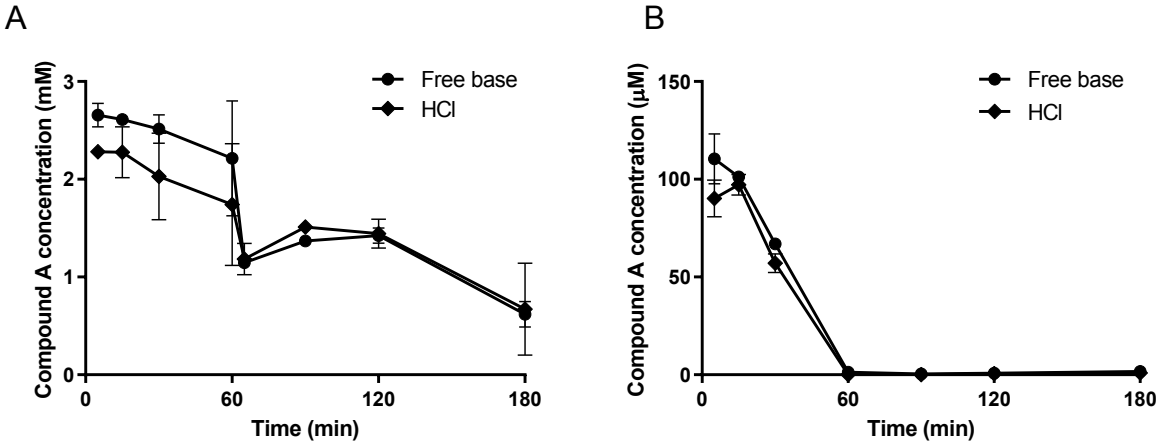

Figure 44. *Dissolution profiles of (A) CpA/NaTC/Eudragit E and (B) CpA/NaTC/HPMC-P ternary ASDs containing either Compound A free base or Compound A HCl. Experiment in (A) was performed with a pH*

shift from 2 to 6.5 after 60 min. Experiments in (B) was performed in SIF buffer at pH 6.8. The drug load was 10% and the ratio NaTC:polymer was 1:3 (w/w).

Selection of the Drug Load

The daily dose of Compound A in humans translates into a 50 mg dog for a 10 kg dog. The drug load could be increased to 20 % for the Eudragit E/NaTC ASD, as the performance was not negatively impacted. Instead, increasing the drug load of the HPMC-P/NaTC ASD resulted in a slower release (data not shown), thus it was kept at 10 %. The composition of the two selected ASDs is shown in **Table 5**.

Table 5. *Overview of the two ASDs selected for the in vivo study.*

ASD	Compound A HCl (wt.%)	NaTC (wt.%)	Eudragit E (wt.%)	HPMC-P (wt.%)
1	20	20	60	0
2	10	22.5	0	67.5

Solid State Analysis and Short Stability Study

The solid state stability of ternary ASDs selected for the *in vivo* study was investigated at 25°C/60%RH, 40°C/75%RH, and 40°C and 60°C with desiccant. After one month, samples stored at 40°C/75% started to recrystallize while all other samples were still amorphous (**Figure 45**). One single peak at 32° was observed at 25°C/60%RH, 40°C and 60°C for ASD 1. This peak might be an artefact as it did not correspond to any peak of the recrystallizing form, nor of the starting Compound A hydrochloride polymorph.

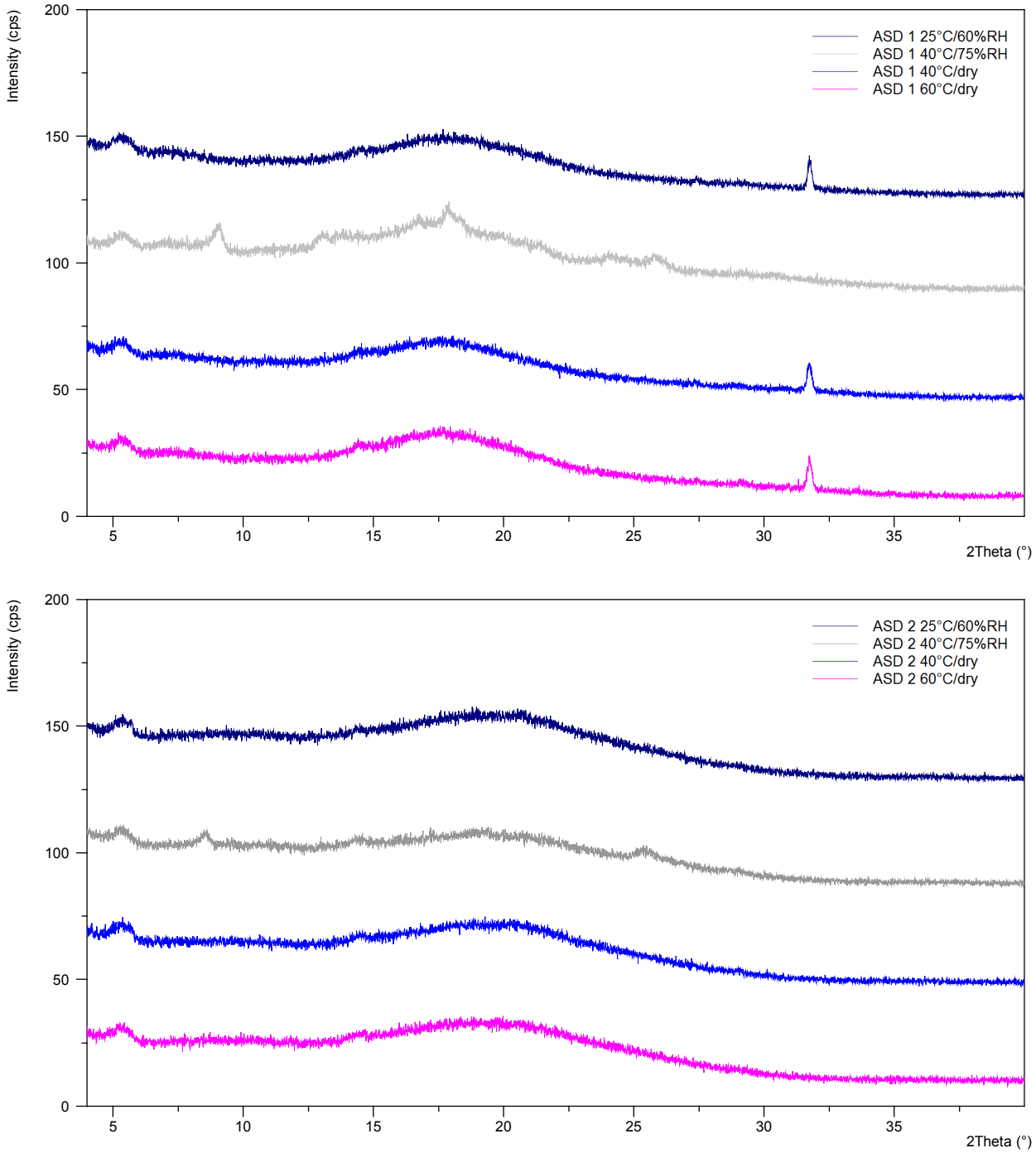

Figure 45. *XRPD diffractograms of (upper) Compound A HCl/NaTC/Eudragit E (20/20/60) ASD (ASD n°1), and (lower) Compound A HCl/NaTC/HPMC-P (10/22.5/67.5) ASD (ASD n°2) after one month at different storage conditions.*

Optimization of Disintegration and Dissolution of the Capsules

Capsules hand-filled with freeze-dried powders showed very poor disintegration. Formation of a gel layer around the dissolving content of the capsules was observed and is probably due to the high percentage of polymer in the matrix (60% in ASD 1 and 67.5% in ASD 2). Upon contact with water the polymer seemed to swell and get sticky. Different approaches were investigated to improve disintegration: blending the ASD matrix with a soluble phase (mannitol) to introduce a spacer and prevent gelling, addition of a superdisintegrant (crospovidone; PVP XL) or modification of the powder properties. The different trials and their results are summarized in **Table 6** and **Table 7**.

Table 6. *Overview of the trials to improve disintegration of capsules containing ASD 1 at pH 2.*

Trial	Method	Disintegration time (min)
1	Freeze-dried material blended with mannitol (1:1 ratio)	>15
2	Freeze-dried material blended with PVP XL (1:1 ratio)	>15
3	Freeze-dried material blended with mannitol (1:1 ratio) and 20% PVP XL	>15
4	Freeze-dried material compressed and milled 0-1000 µm fraction	5
5	Freeze-dried material compressed and milled 250-500 µm fraction	3
6	Freeze-dried material compressed and milled 0-500 µm fraction	>15

Table 7. *Overview of the trials to improve disintegration of capsules containing ASD 2 at pH 6.8.*

Trial	Method	Disintegration time (min)
1	Freeze-dried material	>15
2	Freeze-dried material blended with mannitol (1:1 ratio)	5
3	Freeze-dried material compressed and milled 0-1000 µm fraction	10

Addition of mannitol as an external phase did not improve the disintegration of ASD 1. It did improve the disintegration of ASD 2 but such an increase in mass was not feasible given the low drug load of this ASD (it would result in a too high number of capsules to be dosed in dogs). The PVP XL superdisintegrant was

ineffective. Probably some level of compression is needed for its action. Powder densification (by compression) followed by a milling step led to a significant improvement of the disintegration time. In addition, it was observed that particle size distribution had a strong impact on disintegration; the finer fraction (< 250 µm) led to an increase in disintegration time. Formation of the polymer plug appeared to depend on the material properties. The high porosity and surface area of the freeze-dried material and the high surface area of the fines obtained after milling systematically led to a formation a of polymer-gel layer around the dosage form. Probably, as water entered the pores it dissolved polymer which then blocked the pores and prevented further water ingression and disintegration. In addition when swelling the polymer does not dissolve away and sticks to the surface which leads to particle agglomeration and hamper disintegration.

Dissolution of the capsules was performed in a paddle USP 2 apparatus at pH 1 for ASD 1 and pH 6.8 for ASD 2 (**Figure 46**).

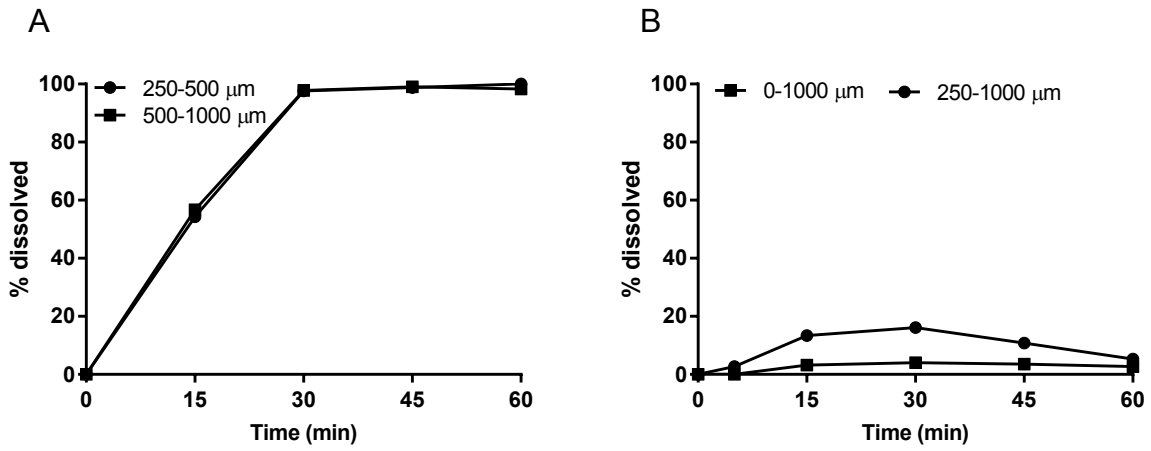

Figure 46. *Dissolution of capsules filled with different sieved fractions of milled freeze-dried amorphous solid dispersions (ASDs) in the USP 2 apparatus. (A) ASD 1 at pH 1 and (B) ASD 2 at pH 6.8.*

Complete dissolution of capsules filled with ASD 1 was achieved within 30 min at pH 1 (**Figure 46A**). Dissolution of capsules filled with ASD 2 at pH 6.8 was limited and precipitation was observed (**Figure 46B**). The dissolution of ASD 2 was dependent on powder properties: inclusion of the fines (0-250 µm fraction) induced polymer gelling and retarded dissolution.
Thus, capsules for the study were filled with the 250-1000 µm fraction of milled material. 131.5 mg of powder was filled per size 00 capsules, which resulted in a total of two capsules for ASD 1 and four capsules for ASD 2 to achieve a 50 mg dose.

Compression and milling did not affect the physical state of the ASDs, i.e. they remained amorphous (**Figure 47**).

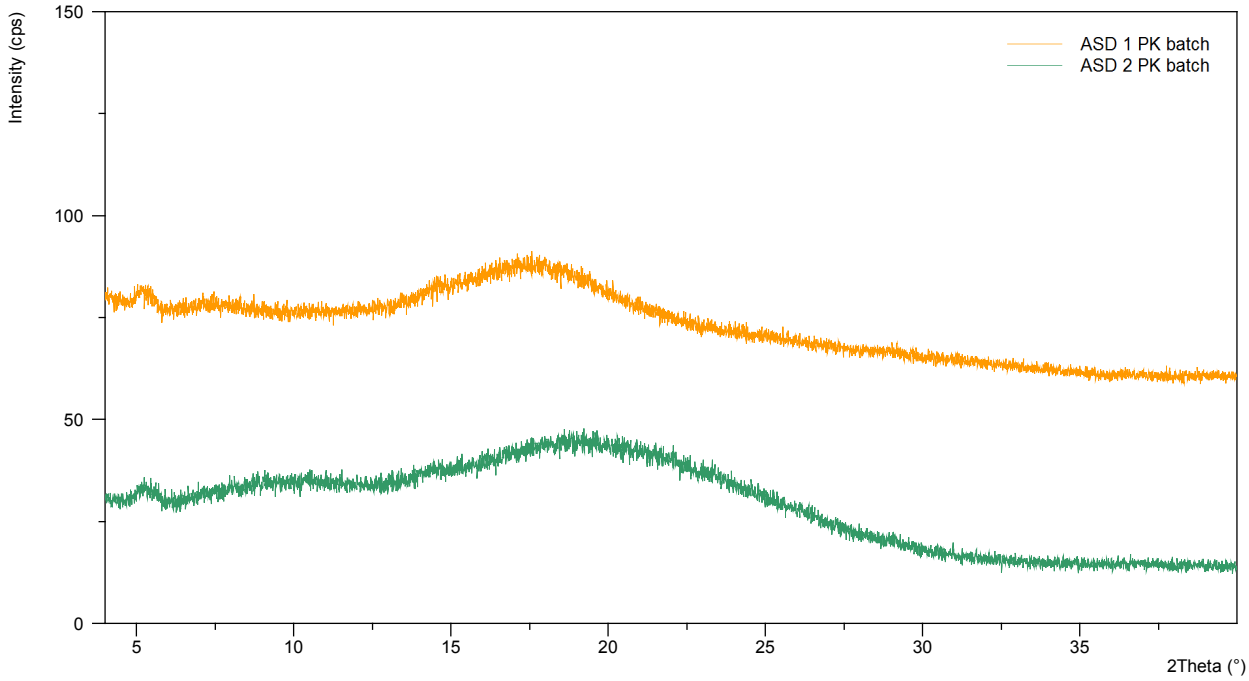

Figure 47. *XRPD diffractograms of the freeze-dried ASDs after compression and milling. These batches were used for the in vivo pharmacokinetics (PK) study*

5.3.4 *In vivo* pharmacokinetics study in dogs

Concentrations and derived pharmacokinetic parameters for Compound A after administration of ASDs in capsules to fasted dogs are presented in **Table 8** and **Figure 48** together with historical data on the reference formulation which is a standard blend with excipients in a capsule.

Table 8. *Overview of the pharmacokinetic parameters after oral administration of ASD 1, ASD 2 and comparison with the reference formulation (historical data)*

	ASD 1 (fasted)	**ASD 2 (fasted)**	**Reference Formulation (fasted)**	**Reference Formulation (fed)**
C_{max} (ng/mL)	293 ± 184	520 ± 382	587	755
$T_{max0-12h}$ (h)	13 [2-24]	1.5 [1-2]	1.5 [1-1.5]	3 [1.5-4.0]
AUC_{last} (h*ng/mL)	3280 ± 2890	4430 ± 3430	1940 ± 276	3360 ± 772
AUC_{0-12h} (h*ng/mL)	1200 ± 1320	2770 ± 2600	1940 ± 276	3360 ± 772

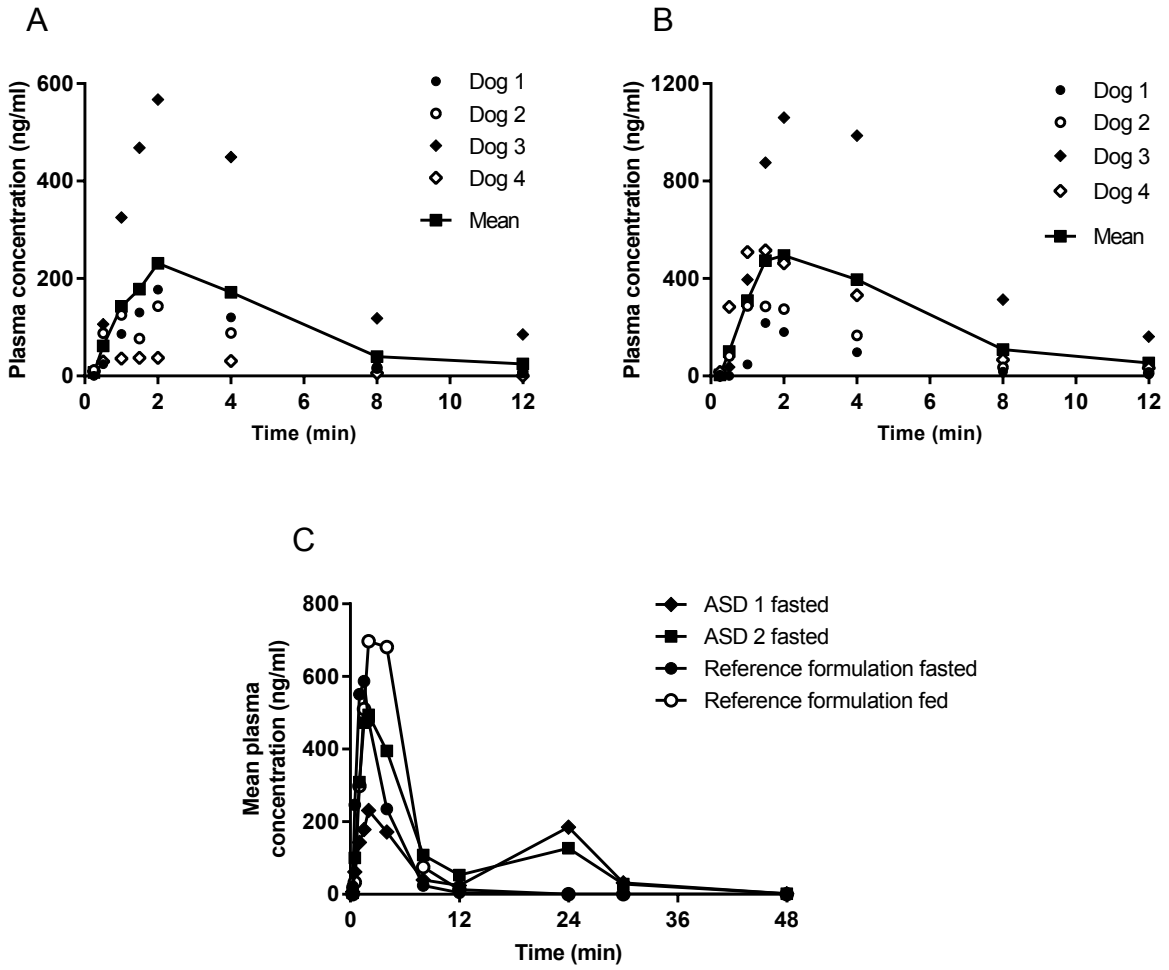

Figure 48. *Individual and mean plasma concentrations in dogs after oral dosing of capsules containing (A) ASD 1 (B) ASD 2 and (C) ASD 1 and 2 in comparison to the reference formulation under fasted and fed conditions.*

The $AUC_{0\text{-}12h}$ with ASD 2 was close to that of the reference formulation under fed conditions (2770 vs. 3360 h*ng/ml; **Table 8**). More interestingly deconvoluted data of the input function showed a delivery lasting up to 6 hours as compared to 3 h for the reference formulation in the fasted state (**Figure 49**). This demonstrated that ASD 2 could be superior to the reference formulation in terms of delivery.

Improving delivery in the fasted state might go along a reduction of the food effect which was the aim of this investigation. To enable a proper evaluation of the food effect, ASD 2 would need to be administered to dogs in the fed state as well, which could not been done in the present investigation.

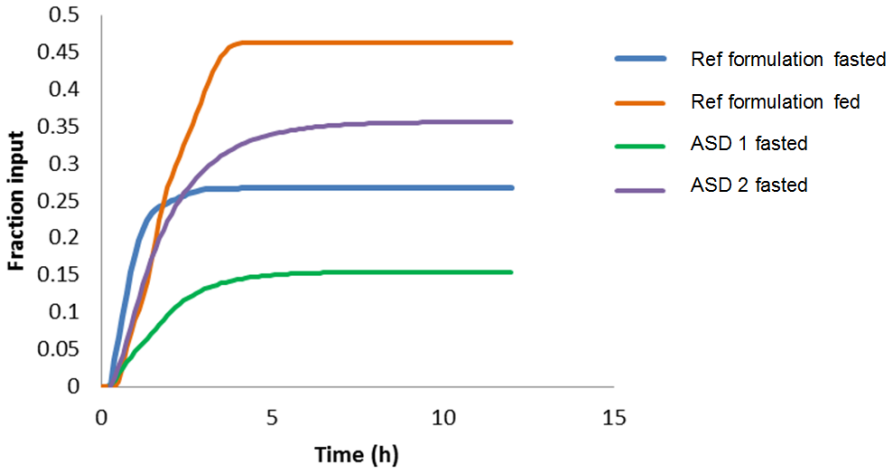

Figure 49. *Deconvolution of mean fraction absorbed values*

Surprisingly, ASD 1 yielded a much lower exposure than ASD 2. In fact, the exposure was even lower than that of the reference formulation in the fasted state. There was no relationship between *in vitro* profiles and *in vivo* bioavailability, as the best performing system *in vitro* (ASD 1) gave the lower exposure *in vivo*.

One hypothesis could be that the two ASDs generated different types of solutions. The solutions generated by ASD 2 were highly unstable (**Figures 44B and 46B**) and precipitation occurred rapidly. This could reflect a high level of supersaturation. Supersaturation increases the free drug fraction in solution which drives diffusion through enterocytes' membrane. In contrast, solutions generated from ASD 1 were more stable over time (**Figure 44A**). This could relate to some solubilization of Compound A in colloidal micelles or aggregates formed by an interaction with Eudragit E and/or NaTC. Particularly, nano-colloids are known to increase the apparent solubility while the drug is not freely available, i.e. the free drug fraction is not increased and diffusion through membranes might not be as high as from supersaturated solutions.

Another explanation could come from the drug load: in ASD 2 the drug load was only 10% which translated into a NaTC and polymer amount twice higher than in ASD 1. This could critically impact dissolution and supersaturation as the solubilization effect of NaTC depends on its concentration (**Figure 36B**).

The third hypothesis could come from the different pH environments between the two arms. Since the stomach pH of the dogs in the second arm was increased by administration of ranitidine, ASD 2 was not in contact with a low pH environment. This might have had an impact on precipitation in the duodenum (i.e. less drastic), although some precipitation was still expected based on in vitro data (**Figure 46B**).

Inter-subject variability was high for both ASDs, with C_{max} coefficient of variation (CV) of 62.8 and 73.5%, and AUC_{last} CV of 88.1 and 77.4%, respectively for ASD 1 and ASD 2. The high number of capsules administered and their poor disintegration could partially account for the variability, as it cannot be excluded that one or several of the capsules did not disintegrate properly, leading to different expositions.

The double peak observed at 24 h is assumed to originate from differences in the protocol between the present study and the reference study. These studies were not conducted at the same site, and known differences exist between the two sites. In particular the food given to dogs differs and is believed to lead to such differences, thus this should not be considered in the interpretation of the data.

Although *in vitro* data cannot fully explain *in vivo* observations, results of this study demonstrated the value of bile salts in formulating poorly water-soluble APIs. While the solubilization capacity of bile salts and mixed micelles is since long recognized and despite their tremendous efficacy in solubilizing liposolubles vitamins and other lipophilic food components,[98] few efforts have been made to exploit them within drug products. This stems in part from a lack of understanding of the interactions between APIs and the dynamic bile salt-lecithin micellar environment at the molecular level. Recent reports using NMR techniques started to shed light on these interactions and revealed a strong affinity of some APIs with bile salts. APIs are able to displace NaTC molecules from pure NaTC micelles to form mixed API-NaTC micelles, while other APIs are incorporated within the core of simple and mixed micelles in a concentration-dependent behaviour.[32] The API specificities favoring interactions with bile salts remain elusive, but some level of amphiphilicity seems to be required.
At this point a plethora of questions arise: how can the interaction of APIs with bile salts be modelled and exploited in the delivery of poorly water-soluble APIs? How is the interaction in presence of polymers and other excipients? What is the role of lecithin in this highly dynamic system? Are bile salts safe to administer orally?

5.4 Conclusion

The aim of this investigation was to develop a formulation principle of Compound A that would be less prone to food effect, in order to increase the safety of the drug product and simplify the posology. Exploring the root cause of the positive food effect revealed a significant impact from a bile salt, NaTC. Incorporation of NaTC in polymeric ASDs led to a significant improvement of the spring phase in aqueous environment, as compared to binary polymeric ASDs. Stable ASDs were developed and administered to Beagle dogs. Despite a large variability, the *in vivo* results pointed towards a superior performance of the newly developed HPMC-P/NaTC ASD over the reference formulation in terms of release in the fasted state. This could be ascribed to an improved wetting and solubilization of Compound A in presence of bile

salts and polymers, and to the generation of supersaturated states. Increased exposure with ASD 2 in the fasted state as compared to the reference formulation could go along with a reduction of the food effect provided that ASD 2 exposure in the fed state is similar to that of the reference formulation, which remains to be investigated. This work opens the door to fascinating field of research to unveil interactions of APIs with the unique solubilizing bile salts system and to find new ways to exploit it to overcome low solubility challenges.

6 Outlook: *in vivo* biorelevance of *in vitro* dissolution profiles

The work presented in this thesis explored different strategies to achieve and maintain high concentrations of poorly water-soluble APIs in aqueous media. Different parts focused on different aspects; co-crystals with hydrotropic coformers enabled association in solution which prevented nucleation of the most stable hydrate form once in solution, thus maintaining high concentrations for several hours. Addition of hydrotropic agents and bile salts in polymeric matrices of ASDs enhanced release and dissolution of the APIs. Besides, it was observed that bile salt-rich medium extended the parachute of ASDs to a significant extent.

The *in vivo* translation of these *in vitro* profiles remains largely unknown due to the complex interplay of physiological and physicochemical factors influencing oral absorption, and due to our limited understanding of the absorption process(es). While it is established that higher concentrations in the duodenum and jejunum correlate with higher plasma levels,[99] relationships between the kinetics of dissolution and precipitation, and the dynamics of absorption remain speculative and key questions related to dissolution and precipitation are yet to be answered. Studies comparing *in vitro* and *in vivo* data, and in particular studies collecting aspirates from the different compartments of the gastrointestinal tract in humans started to provide responses.

Concentrations higher than the equilibrium solubility of a basic API can be achieved by means of supersaturation. Weak bases are predominantly ionized in the acidic environment of the stomach and often have a good solubility in this environment, thus, transfer from the stomach to the duodenum may induce supersaturation of the un-ionized form. In addition, supersaturation can be achieved from the dissolution of a salt, a co-crystal, an ASD or any other supersaturating drug delivery system.

The prerequisite to achieve supersaturation is dissolution, and two important questions are:
(1) Where should dissolution take place?
(2) What is the optimal dissolution rate?
in order to maximize bioavailability from enabling formulations of poorly water-soluble APIs.

Formulations can be designed to release the API in the stomach or in the duodenum (delivery to more distal part of the intestine is also possible). Although the gastric environment is the compartment of the gastrointestinal tract that provides the highest solubility for weak bases, the rate and extent of dissolution of a dosage form in the stomach is strongly influenced by physiological factors like the gastric pH, volume, and residence time. Besides, the rate of gastric emptying and dilution by ongoing intestinal

secretions will affect the resulting supersaturation levels achieved in the duodenum. An *in vivo* study by Rubbens et al. illustrated the influence of the stomach pH on bioavailability.[100] Stomach and duodenal aspirates collected after oral administration of indinavir sulphate capsules to healthy volunteers showed that concomitant proton pump inhibitor intake (associated with an increased stomach pH) resulted into a lower dissolution in the stomach and lower supersaturation ratios in the duodenum which explained the substantial decrease in exposure observed.[101] Similar observations were made by Walravens et al.[102] Administration of a posaconazole suspension in an increased stomach pH due to concomitant esomeprazole intake led to lower gastric concentrations, lower intestinal concentrations and a lower systemic exposure in healthy volunteers. In contrast, co-administration with Coca-Cola, a medium increasing the solubility of posaconazole, resulted in higher gastric concentrations, higher intestinal concentrations and a higher systemic exposure, without any change of the gastric pH. In addition to concentrations, supersaturation levels are important to understand the thermodynamic state of dissolved molecules. Hens et al. measured supersaturation levels in duodenal fluids of healthy volunteers after intragastric administration of either a solution (20 mg) at pH 1.6, a suspension (40 mg) at pH 1.6 or a suspension (40 mg) at pH 7.1.[103] The gastric pH was transiently increased to pH 4 after administration of the neutral suspension whereas it remained around 2.5 for the acidified one, resulting in higher gastric concentrations in the latter case. Posaconazole from the neutral suspension did not induce supersaturation in the duodenum, while the acidic suspension and solution induced supersaturation. Despite significant precipitation upon transfer from the stomach to the duodenum, a twofold increase in the plasma AUC was obtained after administration of the acidified suspension as compared to the neutral suspension.

Learnings from these pieces of work highlight the importance of the gastric environment on the bioavailability of weak bases when dissolution takes place in the stomach. Since gastric conditions may largely differ between patients (baseline physiological differences, physio pathological factors or co-medication), different rates and extents of dissolution in the stomach may result in variable exposure. In addition, supersaturation stability in the gastric environment has been reported to be inferior to that in the intestinal environment which bears the risk that an API released from supersaturating drug delivery systems in the stomach might precipitate before transfer to the small intestine.[104]

Targeting release and dissolution processes from the formulation in the duodenum by use of an enteric matrix or coating could be an alternative to reduce the influence of gastric factors on intestinal concentrations. This strategy was pursued with posaconazole in order to develop a formulation whose performance would not be impacted by changes in gastric pH, motility and food intake. Gastric, duodenal and intestinal aspirates sampled after administration of a HPMC-AS ASD of posaconazole confirmed that dissolution occurred mainly in the duodenum and led to supersaturation in the jejunum independently of the prandial conditions.[105] Pharmacokinetics studies in humans confirmed that neither food intake, neither

concomitant administration of gastric pH-modifying agents nor motility influencing agents resulted in clinically relevant changes in bioavailability.[106, 107] In addition, targeting release in the duodenum could prevent intestinal dilution accompanying gastric emptying. Indeed transfer of liquids from the stomach to the duodenum typically happens by portions and magnetic resonance imaging studies have evidenced that "the liquid in the small intestine exists in discrete liquid pockets".[108] This implies that the dose, if dissolved it the stomach, will be portioned and diluted within the different liquid pockets. This portioning might reduce API concentrations in the intestinal lumen.

The second question regarding dissolution is the rate of release and dissolution of the API from enabling formulations. While it is well established that the energy barrier to nucleation decreases as the degree of supersaturation increases, the influence of the rate of supersaturation generation (i.e. the rate of API release and dissolution) on the precipitation kinetics remains unclear. Sun et al. claimed that the maximum level of supersaturation depends on the rate of supersaturation generation".[109] This implies that a faster dissolution, by generating higher levels of supersaturation, would hasten precipitation. However, only a few studies did show that drug release rate influenced absorption, and that a slower release was beneficial. Van Speybroeck et al. observed that *in vitro* supersaturation generated by a slower release of fenofibrate from ordered mesoporous silica was maintained for a longer period of time as compared to a faster release, in FaSSIF.[110] Subsequently, in rats, the slower releasing formulation had a superior biopharmaceutical performance. In another study, Six et al. found a correlation between the dissolution rate of different ASDs in simulated gastric fluid under sink conditions and the exposure in humans.[111] However, in the latter study *in vitro* dissolution under non-sink conditions was not performed, thus the different precipitation inhibition effect of the different polymers were unknown and could account as well for the different exposures in humans.
Besides, one has to consider that if API release and dissolution from supersaturating drug delivery systems occur in the stomach, the supersaturation levels in the duodenum will eventually be largely dictated by gastric motility and gastric emptying, rather than by the formulation design. Thus, the impact of dissolution rate on precipitation kinetics might be only relevant for absorption if dissolution happens in the upper part of the small intestine, at the site of absorption. In addition, its relevance most likely depends on the crystallization propensity and the absorption of the API.

The second step to achieve high API concentrations in the intestinal lumen is to maintain supersaturation by preventing precipitation of the drug from supersaturated states. During the development of supersaturating drug delivery systems, a strong focus is placed on the parachute effect of the formulation, and high amounts of polymers or other precipitation inhibitors are often included in the formulation to mitigate precipitation during *in vitro* dissolution testing. Nevertheless, *in vitro* dissolution assays often lack biorelevance (hydrodynamics, media composition etc.) and do not have any absorption compartment. As a result, the occurrence, extent and very relevance of precipitation *in vivo* is challenging to predict from *in*

vitro experiments. Indeed, on-going absorption by continuously removing dissolved drug molecules from the intestinal lumen decreases supersaturation levels. The presence of bioendogenous solubilizers and precipitation inhibitors such as bile salts, lecithin and food components also have an effect on drug supersaturation and precipitation. Thus, it is reasonable to speculate that precipitation *in vivo* is most likely less drastic than observed during *in vitro* dissolution testing.[112]

This has been observed on several instances. Lohani et al. dosed suspensions of either co-crystals (maleic and benzoic acid) or a HPMC-P ASD of a BCS class II weak base to rats.[113] Although during biorelevant two steps *in vitro* dissolution assays the co-crystals rapidly dissociated and precipitated while the ASD maintained supersaturation, *in vivo* the bioavailability was not different between the three formulations. Similar observations have been made with salts. Salts commonly dissociate in solution and might rapidly precipitate upon dissolution or upon a change in pH. *In vivo*, a fast absorption in the duodenum can circumvent precipitation and many salts do have a higher bioavailability than their free forms. Suspensions of either the free base or the hydrochloride salt of pioglitazone were intragastrically administered to rats and analysis of gastrointestinal fluids revealed that, although precipitation occurred upon transfer to the duodenum, the solid fraction did not increase while the dissolved fraction largely decreased reflecting a decrease in the driving force for precipitation by active removal of dissolved API from the lumen.[114] Despite precipitation, absorption from the HCl salt was four times higher than from the free form. In another study in humans, Carlert et al. evaluated the *in vitro-in vivo* relationship of aqueous co-solvent solutions and mesylate tablets of a BCS class II weak base.[115] *In vitro*, rapid precipitation was systematically observed with all formulations, while in humans dose proportionality was observed until doses that would certainly produce supersaturation in the upper small intestine. The authors concluded that *in vivo* either precipitation did not occur, either it occurred into a precipitate that sustained absorption.

Indeed, if precipitation does occur, the resulting precipitate is an important determinant for further absorption. Dissolved molecules in supersaturated solutions may go through different paths to phase separate into a solid phase. Drug molecules can directly recrystallize as a crystalline form, or they may precipitate as an amorphous solid. Other systems first undergo liquid-liquid phase separation when the amorphous solubility of the API has been exceeded resulting into a dispersed, colloidal drug-rich phase. Such states have been described to sustain a high flux for permeation through intestinal membranes due to the high thermodynamic activity of dissolved drug molecules in the continuous solution phase while the phase separated drug-rich phase acts as a reservoir to replenish the solution phase as absorption takes place.[116] The physical state and the polymorphic form of the solid precipitate also influence the rate of re-dissolution and availability for absorption. For instance, the hydrochloride salt of FTI-2600, a BCS class II weak base, precipitated as a metastable amorphous free base which contributed to the improved bioavailability as compared to the free form in dogs.[117] Particle size distribution is also important, and for drugs which recrystallize as fine precipitates, redissolution of the fine precipitate is able to sustain

absorption. Due to its moderate permeability, cinnarizine is most likely to precipitate in the duodenum. Indeed, rats' duodenal aspirates indicated a rapid precipitation of cinnarizine upon transfer to the small intestine after administration of the HCl salt.[118] However, redissolution of the precipitate, which was much finer than the original material (0.5 µm vs. 40.5 µm) sustained absorption and resulted in plasma concentrations higher than the free form. ASDs have even been reported to even form nanoparticles upon dispersion in aqueous environment.[119]

On the other hand, several studies reported a correlation between the *in vitro* parachute effect and *in vivo* bioavailability. Liu et al. prepared tablets of physical mixtures of Sorafenib with either PVPVA64 alone, SLS alone or a combination thereof.[120] *In vitro* the formulation with both PVPVA64 and SLS precipitated faster than PVPVA64 alone and this was rationalized by competing interactions between SLS and Sorafenib with PVPVA64. *In vivo* exposure in dogs correlated with *in vitro* ranking and the formulation with PVPVA64 having the more prolonged parachute effect *in vitro* gave the higher exposure. Similar observations were made with posaconazole HPMC-AS ASDs where the presence of SLS negated the crystallization inhibition effect of HPMC-AS by competing interactions, resulting in a lower exposure *in vivo*.[121] Data from a study with aspirates from healthy volunteers evidenced slightly higher duodenal supersaturation in presence of HPMC after administration of an albendazole suspension.[122]

In addition to dissolution and supersaturation/precipitation, other solution phenomena such as aggregation and solubilization might have an influence on absorption. For instance, aggregation might prevent precipitation. Narang et al. observed that the aggregation of Brivanib alanilate at low pH was linked to its tendency to supersaturate upon pH shift.[13] The size of aggregates could influence the region for absorption as certain types of aggregates might only be absorbable under a given size which could be obtained only after sufficient dilution along the gastrointestinal tract.[16]

The solubility-permeability tradeoff reflects a decrease in diffusion through biological membranes when solubility is increased by solubilization techniques, as only the free faction of dissolved drug molecules is available for diffusion. Solubilization via micellization or complexation reduces the free faction of the API, which translates into a lower effective concentration gradient hence a lower effective thermodynamic driving force for permeation.[123] A recent study by Berben et al. evidenced the consequence of this interplay on oral exposure of itraconazole in healthy volunteers.[124] A solution of itraconazole in hydroxypropyl-β-cyclodextrin was administration with or without a glass of water and concentrations were monitored in gastric and duodenal aspirates and in plasma. More pronounced precipitation occurred in the duodenum with concomitant intake of water due to dilution effects on the cyclodextrin system. However, there was no difference in plasma concentration-time profiles between the two conditions. Further *in vitro* permeability experiments with the freshly aspirated intestinal fluids confirmed that higher duodenal itraconazole concentrations did not increase diffusion through cellular membranes, presumably

because the free fraction of the drug was not increased. Thus, the solubility-permeability interplay has to be considered during the development of supersaturating drug delivery systems that are based on solubilization, e.g. like the bile salt systems.

To conclude, the interplay between dissolution, supersaturation, precipitation and absorption, and the impact of physiological factors, API physicochemical factors and formulation attributes are far from being understood. While more strategies have been discovered to tailor the performance of enabling formulations, *in vivo* translation will only go along with a better understanding of the different processes involved in oral absorption.

7 Summary

The number of active pharmaceutical ingredients (APIs) exhibiting a low solubility in aqueous media or a slow dissolution rate kept rising over the past years urging formulation scientists to explore new ways to tackle poor solubility and to enable oral absorption from such compounds. Bioavailability of poorly water-soluble compounds can be improved by increasing the dissolution rate and/or by increasing the gastro intestinal concentration through transient supersaturation. The dissolution rate of the API can be typically modified by the choice of the physical form, the polymorphic form, the powder surface area, and the local pH, while a transient supersaturation can be extended mainly by nucleation or crystallization inhibiting effects. In the present thesis, three strategies were explored to tailor the dissolution rate, the supersaturation and the hydrotropic solubilization of basic APIs.

The first part of this thesis followed a bioinspired approach to extend the kinetic solubility of salts and co-crystals. API salts and co-crystals are high energy forms that can generate supersaturated solutions with respect to any more stable form, typically the most stable API form in the physiological environment. The transient kinetic stabilization of supersaturated states, also termed “parachute effect”, is considered to improve bioavailability and is one aspect of the formulation that can be tailored. Inspiration from plants, which store high concentrations of aromatic bases in their vacuoles via complexation with polyphenols, sparked the evaluation to use hydroxybenzoic acid derivatives for salt and co-crystal engineering. Imatinib was chosen as the model compound for this investigation as its aromaticity and flat molecular architecture could favor interactions with hydroxybenzoic acid derivatives. One 1:1 Imatinib syringate co-crystal (I-SYA (1:1)) and one 1:2 Imatinib syringate co-crystal salt (I-SYA (1:2)) were obtained. Their dissolution assays in simulated intestinal fluid (SIF; a 50 mM phosphate buffer of pH 6.8) revealed that they formed stable solutions for several hours and days, respectively, in contrast to the marketed Imatinib mesylate salt (approx. 1h). This kinetic stability in solution was linked to the nucleation inhibition of the less soluble Imatinib hydrate by syringic acid (SYA). In solution ^{1}H-NMR studies evidenced the aggregation of Imatinib and SYA. The amphiphilic nature of both Imatinib and SYA is considered to drive their association in solution, additionally, multiple intermolecular interactions such as hydrogen bonds and π-π stacking are likely to contribute. The association in solution enabled a phase of extended supersaturation, i.e., a parachute against desupersaturation, while no negative impact of aggregation on the diffusion of both Imatinib and SYA through cellular membranes was observed.

A prerequisite to reach supersaturation is a rapid release and dissolution of the API from the formulation. Accordingly, the second and third part of this thesis focused on the so-called “spring effect” of amorphous solid dispersions (ASDs). The addition of a hydrotropic agent, meaning a molecule that can solubilize poorly water-soluble APIs in aqueous solutions (well-known examples of hydrotropes are benzoic acid and nicotinamide) into an amorphous Ciprofloxacin-polymer matrix led to ternary systems with a

significantly faster release and higher concentration of the API in SIF as compared to binary ASDs consisting of Ciprofloxacin (CPX) and polymer only. The stronger spring could be rationalized by an improved wetting of the ASD, or/and by a hydrotropic solubilization effect, although these hypotheses need further investigation. Marked differences in the dissolution profiles of binary ASDs were observed in biorelevant fasted simulated intestinal fluid (FaSSIF; a medium containing sodium taurocholate (NaTC; 3 mM) and lecithin (0.75 mM) at pH 6.5) as compared to SIF. In FaSSIF, API release from binary polymeric ASDs was largely improved, and the duration of supersaturation was extended. This suggests that the bile salt NaTC and lecithin present in FaSSIF do improve both dissolution rate and supersaturation of ASDs, the two pillars of ASDs as oral enabling formulations. Indeed, bile salts are endogenous surfactants which, together with phospholipids, play an important role in the wetting, solubilization, and absorption of lipophilic compounds.

The aim of the third part of the present thesis was to study ASDs as formulation principles reducing the strong positive food effect of Compound A. By inclusion of NaTC within the matrix of polymeric ASDs a significant improvement of the dissolution rate and the kinetic solubility in SIF were achieved. Transient supersaturated states of up to four orders of magnitude over the equilibrium solubility were obtained. Two ASDs were selected for further *in vivo* evaluation in dog. The first was a NaTC/Eudragit E based ASD meant to dissolve and release Compound A in the acidic environment of the stomach, where its solubility is the highest. The second relied on the release of Compound A in the neutral environment of the duodenum and jejunum by using an enterically dissolving polymer, HPMC-P. Releasing the API at the site of its putative absorption was an attempt to control supersaturation levels in the duodenum and to prevent portioning and thus dilution effects during transfer from the stomach. In fasted dogs, exposure from the NaTC/HPMC-P ASD was close to that of the reference Compound A formulation under fed conditions, which suggests an improved dissolution rate and kinetic solubility under fasted conditions. The exposure from the NaTC/Eudragit E ASD was twice as low as from the NaTC/HPMC-P ASD, and also lower compared to Compound A reference formulation, whereas *in vitro* the parachute effect of the NaTC/Eudragit E ASD was largely superior to that of the NaTC/HPMC-P ASD. A difference in the extend of the parachute could be related to differences in the thermodynamic activity of dissolved molecules from the two ASDs. Indeed, the high instability of the NaTC/HPMC-P ASD could stem from a high thermodynamic activity driving diffusion through membranes, whereas less instable solutions of NaTC/Eudragit E could indicate solubilization effects which often translate into a lower flux through the biological membrane as the free drug concentration is typically not increased. Additionally, the pH of the environment where dissolution takes place might be an important factor for absorption, and could also account for the difference in exposure from the two ASDs.

The aim of this thesis was to explore how the intimate environment of weak, poorly soluble bases could be functionalized to improve dissolution rate and kinetic solubility. The investigations highlighted that the

performance of enabling oral delivery formulations of weak bases in aqueous media can be enhanced at different levels. At one end initial dissolution rate of ASDs can be tailored by introducing hydrotropes or/and bile salts within the polymeric matrix of ASDs. Bile salts, when combined with appropriate polymers, had also a precipitation inhibition effect enabling the maintenance of supersaturation for a bio-relevant period of time. These results set the ground for further investigations to comprehend specific interactions between bile salts and APIs, and potentially polymers at the molecular level. It will be interesting to explore how such complex systems can be exploited in the formulation design of poorly water-soluble APIs. In addition, it was observed that the duration of supersaturation generated by salts/co-crystals can be extended by the pertinent selection of counterions or coformers. The *in vivo* relevance of these tunings remains to be evaluated, as translation from closed, *in vitro* systems to the highly dynamic gastrointestinal environment is not straightforward. A better understanding of the contribution of each kinetic stage (dissolution, supersaturation, and precipitation) and their interplay with physiological factors impacting absorption is essential to facilitate the design of formulations with improved pharmacokinetics.

8 Zusammenfassung

Die Anzahl chemischer Wirkstoffe, welche sich schlecht oder langsam auflösen, hat in den vergangenen Jahren stetig zugenommen. Aus diesem Grunde müssen Entwickler neuer Formulierungen Wege finden, um die Löslichkeit und damit die Absorbtion dieser Wirkstoffe zu verbessern. Grundsätzlich kann die Bioverfügbarkeit schlecht wasserlöslicher Wirkstoffe verbessert werden, wenn die Auflöserate verbessert wird und/oder durch höhere Konzentrationen der Wirkstoffe am Resorptionsort, beispielsweise durch kontrollierte Übersättigungen. Die Auflösungsrate eines Wirkstoffes kann durch die Wahl der physikalischen Form (Salz und Polymorph), Modifikation der spezifischen Oberfläche (Mahlen) und lokalem pH Wert (Ionisierungszustand) maßgeblich beeinflusst werden. Im Falle von kontrollierten Übersättigungen, kann die Verlängerung der Dauer der Übersättigung durch die Unterdrückung der Bildung von Kristallisationskeimen erreicht werden. In der vorliegenden Promotionsarbeit wurden neue Strategien entlang dieser Herausforderungen für schwach basische Wirkstoffe untersucht und entwickelt.

Im ersten Teil der Arbeit wurden biomimetische Strategien angewandt, um die physikalischen und biopharmazeutischen Eigenschaften basischer Wirkstoffe zu verbessern. Dieses erfolgte mit der Absicht, durch strukturelles Design von Salzen oder Co-Kristallen das Ausfallen des Wirkstoffes aus Lösungen hinauszögern und eine Aufklärung der zugrundeliegenden Mechanismen vorzunehmen. Dabei konnten mit ausgesuchten Wirkstoff-Salzen oder Co-Kristallen Lösungen erzeugt werden, welche zu Übersättigungen führten. Diese thermodynamisch instabilen allerdings (vorübergehend) kinetisch gehemmt vorliegenden Zustände sind mit dem Begriff „Fallschirm Effekt“ in der Literatur verknüpft, womit die Verlängerung der Übersättigungen durch geeignete Salz-/Cokristallbildung metaphorisch umschrieben ist. Diese kinetisch gehemmten und somit langanhaltend vorliegenden Übersättigungen sind entscheidend für die Verbesserung der Bioverfügbarkeit. Pflanzen nutzen diese Effekte ebenfalls aus. So können Pflanzen aromatische und schlecht wasserlösliche Basen in übersättigten Lösungen kinetisch „stabilisieren“, in dem diese an Polyphenol-Komplexe in den Vacuolen ihrer Zellen komplexiert vorliegen. Hier wurden diese bei Pflanzen beobachteten Effekte für Hydroxybenzoesäure-Derivate übernommen untersucht und zur pharmazeutischen Verbesserung des Wirkstoffes Imatinib angewandt. Das aromatische Imatinib hat eine flache molekulare Struktur, die mit Hydroxybenzoesäure-Derivaten interagieren sollte. Es wurde ein 1:1 Imatinib-Syringat Co-Kristall (I-SYA (1:1)) sowie ein 1:2 Imatinib-Syringat Co-Kristall Salz (I-SYA (1:2)) hergestellt. Mittels dieser Salze konnten beeindruckende kinetisch „stabilisierte“ und übersättigte Lösungen des Imatinib realisiert werden, die beispielsweise in künstlicher Darmflüssigkeit (SIF) über Stunden beziehungsweise Tage vorlagen. Dieses steht im Gegensatz zum handelsüblichen Imatinib-Mesylat (Dauer der Übersättigung ca. 1 Stunde). Die kinetische „Stabilisierung“ der Lösung wurde mechanistisch mittels 1H-NMR Studien auf eine Unterdrückung/Verzögerung der Kristallkeimbildung des weniger löslichen Imatinib Hydrates durch Anwesenheit der Polyphenolsäure

(Syringasäure) zurückgeführt. In-vitro Transportstudien durch biologische Barrieren zeigten, dass die Syringasäure die Permeabilität des Imatinib nicht nachteilig beeinflusste.

Während in diesem Kapitel die Verlängerung von Übersättigungszuständen das Ziel war (Fallschirm Effekt; „parachute"), ist die Optimierung des Ausmaßes der Übersättigung das Ziel der folgenden Kapitel, welches in der Literatur als „Feder-Effekt" („spring") bekannt geworden ist. Eine Voraussetzung zum Erreichen von Übersättigung ist die rasche Auflösung und Freisetzung des Wirkstoffes aus der Formulierung. Diesen „Feder-Effekt" wurde hier in amorphen Feststoffdispersionen (ASDs) erreicht. Zielführend war die Anwendung hydrotroper Moleküle, welche in wässerigen Lösungen lösungsvermittelnd auf schlecht wasserlösliche Substanzen wirken. Diese Formulierungen führten bei amorphen Wirkstoff-Polymer Gemischen zu ternären Systemen mit deutlich schnellerer Wirkstofffreisetzung und es konnten deutlich höhere Konzentration an gelöstem Wirkstoff in simulierten gastrointestinalen Flüssigkeiten erreicht werden, als dieses im Vergleich zu binären ASDs der Fall war, die lediglich aus Wirkstoff und Polymer zusammengesetzt waren. Im Übrigen konnte gezeigt werden, dass sich die Auflösungsprofile der ASDs in verschiedenen Medien unterschieden. Durch diesen Vergleich in unterschiedlichen Medien konnte die Bedeutung des Taurocholats und des Lezithins (beide Moleküle sind Bestandteil der Gallenflüssigkeit) für die Verbesserung der Auflösungsrate von ASDs gezeigt werden. Gallensalze können in diesem Sinne als „endogene Tenside" verstanden werden, die zusammen mit Phospholipiden eine wichtige Rolle in der Lösungsvermittlung und Absorption von lipophilen Substanzen haben.

Während im vorhergehenden Teil die Bedeutung von Gallensalzen für Auflösungsphänomene aus ASDs im Zentrum des Interesses lag, wurde nun eine andere Herausforderung pharmazeutischer Entwicklungen adressiert, der sogenannte „Food effect". Dieser Effekt meint die nahrungsbedingte Änderung der Bioverfügbarkeit von Wirkstoffen. In diesen Arbeiten führte der Zusatz von Natriumtaurocholat in eine ASD Matrix zu einer Verbesserung der Auflösungsrate und der kinetischen Löslichkeit in simulierten intestinalen Flüssigkeiten mit der bemerkenswerten Verbesserung der kinetischen Löslichkeit um bis zu vier log Einheiten im Vergleich zur thermodynamischen Löslichkeit. Zwei ASD Formulierungen wurden für eine Studie am Hund ausgewählt, die eine bestehend aus Natriumtaurocholat/Eudragit E (Eudragit E löst sich in der sauren Umgebung des Magens auf) und die andere aus Natriumtaurocholat/HPMC-P (HPMC-P setzt Wirkstoffe in der pH-neutraler Umgebung des Dünndarms frei). Unerwartet waren die resultierenden Wirkstoff-Blutspiegel. Die Blutspiegel nach Verabreichung der NaTC/Eudragit E ASD waren nur etwa halb so hoch als jene von NaTC/HPMC-P, was im Gegensatz zu den *in-vitro* Konzentrationsprofilen steht. Eine mögliche Erklärung ist, dass instabile Lösungen, wie sie für die Natriumtaurocholat/HPMC-P ASD *in vitro* beobachtet wurden, die Diffusion durch die biologische Membran antreiben, wogegen dieser Effekt umso geringer ausfällt, je stabiler die erzeugte Lösung ist, wie das im Falle der Natriumtaurocholat/Eudragit E ASD *in vitro* der Fall war. Ein

anderer Faktor, der in diesem Zusammenhang zu diskutieren ist, ist der unterschiedliche pH–Wert am Ort, an dem beide ASD den Wirkstoff freisetzen.

Übergreifendes Ziel der Promotionsarbeit war die Optimierung der unmittelbaren Umgebung von schwachen, schlecht löslichen Basen, um die Auflösungsgeschwindigkeit und kinetische Löslichkeit der Wirkstoffe zu verbessern. Einerseits lässt sich die Auflösungsrate durch den Zusatz von hydrotropen Substanzen und/oder Gallensalzen zur Polymermatrix von ASDs steigern. Die Kombination von Gallensalzen mit geeigneten Polymeren konnte effektiv das Ausfallen des Wirkstoffes begrenzen und die Dauer von Übersättigungen deutlich verbessern. Diese interessanten Kombinationen sollten für andere Polymere zukünftig untersucht werden, so dass die spezifischen Wechselwirkungen zwischen Gallensalzen und Wirkstoff, gegebenenfalls auch mit Polymeren, auf molekularer Ebene besser verstanden werden können. In einem Teil der Promotionsarbeit wurde auch gezeigt, dass die Dauer der Übersättigung durch eine gezielte Auswahl von Gegenionen oder von Co-Kristallbildnern verlängert werden kann. Die *in vivo* Relevanz dieser Ansätze, sind vor dem Hintergrund der sehr dynamischen Verhältnisse im Magen-Darm-Trakt zu bewerten. Darüber hinaus ist ein besseres Verständnis des Zusammenspiels der kinetischen Phasen der Freisetzung (Auflösung, Übersättigung und Ausfällung) mit physiologischen Einflussgrößen zu erarbeiten, um zuverlässig Darreichungsformen mit besseren pharmazeutischen Eigenschaften zu entwickeln.

9 Acknowledgements

I would like to thank Prof. Dr. Dr. Lorenz Meinel for giving me the opportunity to complete this thesis in collaboration with the University of Würzburg, and for his support. From the University of Würzburg, I would like to give a special thank to Dr. Johannes Wiest for the enriching collaboration. His scientific expertise and the discussions were very valuable and fruitful.

At Novartis I would like to extend my sincere thanks to Dr. Frank Schäfer for embedding this PhD work in the daily business of his team and for providing valuable support throughout this time and beyond.
Acknowledgements go to several colleagues from the Particle Engineering Network group for their help with various aspects of my thesis; Evgenia Rousaki with salt and co-crystal screening, Sara Rossi for her help to grow crystals, and Ute Wieckhusen, Christian Kirchhoffer and Mario Rentsch for their support in the lab.
To colleagues from the Chemical and Pharmaceutical Profiling group for sharing their equipments, in particular special thanks go to Agnese Vit, and to Dr. Toni Widmer.
To colleagues from the Global Discovery Chemistry group for their numerous attempts to eventually elucidate the single crystal X-Ray structure of the tiny Imatinib syringate co-crystals. In particular, special thanks go to Philippe Piechon for his expertise.
To Stephane Rodde and Dr. Bernard Faller from the Global Discovery Chemistry group for their interest in my work, the great discussions, and their support with various analytical techniques. Special thanks to Norbert Lange who performed the LE-MDCK permeability assays.
To colleagues from Pharmacokinetics Sciences group for supporting the *in vivo* studies.

I am extremely thankful to Dr. Cornelius Harlacher for his supervision. His scientific approach and thinking taught me a lot.

I would like to express my gratitude towards Dr. Bruno Galli for his guidance. I have truly appreciated working with him during these years. His vision, ingenuity and authenticity have deeply influenced my scientific thinking and personal growth.

I am extremely thankful to my family and friends, and in particular to my husband for his unconditional love and encouragement.

10 List of abbreviations

Abbreviation	Description
API	Active Pharmaceutical Ingredient
ASD	Amorphous Solid Dispersions
AUC	Area Under the plasma drug concentration-time Curve
BCS	Biopharmaceutical Classification System
BEH	Ethylene Bridged Hybrid
BSA	Albumin Bovine Serum
CAC	Criticial Aggregation Concentration
CI	Counterion
C_{max}	Maximum serum/plasma concentration after administration
CpA	Compound A
CPX	Ciprofloxacin
CV	Coefficient of Variation
DMEM	Dulbecco's Modified Eagle Medium
DMSO-d6	Deuterated Dimethyl Sulfoxide
DSC	Differential Scanning Calorimetry
DT	Disintegration Time (min)
ESI	Electrospray Ionization
FaSSIF	Fasted Simulated Intestinal Fluid
FeSSIF	Fed Simulated Intestinal Fluid
GIT	Gastrointestinal Tract
HBSS	Hank's balanced salt solution
HCl	Hydrochloric acid
HEPES	Hydroxyethyl piperazineethanesulfonic acid
HESI-II	Heated Electrospray Ionization
HPMC	Hydroxypropylmethylcellulose
HPMC-AS	Hydroxypropylmethylcellulose accetate succinate
HPMC-P	Hydroxypropylmethylcellulose phthalate
IFB	Imatinib Free Base
IH	Imatinib Hydrate
IM	Imatinib Mesylate
I-SYA (1:1)	Imatinib Syringate co-crystal
I-SYA (1:2)	Imatinib Syringate co-crystal salt
LC-MS/MS	Liquid Chromatography-tandem Mass Spectrometry

LE-MDCK	Low Efflux Madin-Darby Canine Kidney cells
LLPS	Liquid-Liquid Phase Separation
M	Molar (moles/L)
NaCl	Sodium Chloride
NaOH	Sodium Hydroxide
NaTC	Sodium Taurocholate
NMR	Nuclear Magnetic Resonance
P_{app}	Apparent Permeability
PES	Polyethersulfone
PET	Polyethylene Terephthalate
PK	Pharmacokinetics
PVDF	Polyvinylidene fluoride
PVP VA 64	Poly(vinylpyrrolidone-co-vinyl-acetate)
PVP XL	Crospovidone
RH	Relative Humidity
ROESY	Rotational Nuclear Overhauser Effect Spectroscopy
SD	Solid Dispersion
SIF	Simulated Intestinal Fluid
SYA	Syringic Acid
T_g	Glass Transition Temperature
TGA	Thermal Gravimetric Analysis
T_{max}	Time at which C_{max} is observed
TOCSY	Total Correlated Spectroscopy
UPLC	Ultra Performance Liquid Chromatography
USP	United States Pharmacopeia
VAN	Vanillic Acid
XRPD	X-Ray Powder Diffraction

11 Bibliography

1. Ran, Y.; Yalkowsky, S. H. Prediction of drug solubility by the General Solubility Equation (GSE). *J Chem Inf Comput Sci* **2001,** *41*, 354-57.
2. Jain, N.; Yalkowsky, S. H. Estimation of the aqueous solubility I: Application to organic nonelectrolytes. *J Pharm Sci* **2001,** *90*, (2), 234-52.
3. McNaught, A. D., Wilkinson, A. , *IUPAC. Compendium of Chemical Terminology ("the Gold Book")*. 2 ed.; Oxford, **1997**.
4. Siepmann, J.; Siepmann, F. Mathematical modeling of drug dissolution. *Int J Pharm* **2013,** *453*, (1), 12-24.
5. Noyes, A. A.; Whitey, W. R. The rate of solution of solid substances in their own solutions. **1897**, 930-34.
6. Nernst, W. Theorie der Reaktiongeschwindigkeit in heterogenen Systemen. **1903**, 52-55.
7. Smith, D.; Artursson, P.; Avdeef, A.; Di, L.; Ecker, G. F.; Faller, B.; Houston, J. B.; Kansy, M.; Kerns, E. H.; Kramer, S. D.; Lennernas, H.; van de Waterbeemd, H.; Sugano, K.; Testa, B. Passive lipoidal diffusion and carrier-mediated cell uptake are both important mechanisms of membrane permeation in drug disposition. *Mol Pharm* **2014,** *11*, (6), 1727-38.
8. Wohnsland, F.; Faller, B. High-throughput permeability pH profile and high-throughput alkane-water log P with artificial membranes. *J Med Chem* **2001,** *44*, 923-30.
9. Kulkarni, A.; Han, Y.; Hopfinger, A. J. Predicting Caco-2 Cell Permeation Coefficients of Organic Molecules Using Membrane-Interaction QSAR Analysis. *J Chem Inf Comput Sci* **2002,** *42*, 331-42.
10. Borbas, E.; Sinko, B.; Tsinman, O.; Tsinman, K.; Kiserdei, E.; Demuth, B.; Balogh, A.; Bodak, B.; Domokos, A.; Dargo, G.; Balogh, G. T.; Nagy, Z. K. Investigation and Mathematical Description of the Real Driving Force of Passive Transport of Drug Molecules from Supersaturated Solutions. *Mol Pharm* **2016,** *13*, (11), 3816-26.
11. Raina, S. A.; Zhang, G. G.; Alonzo, D. E.; Wu, J.; Zhu, D.; Catron, N. D.; Gao, Y.; Taylor, L. S. Impact of Solubilizing Additives on Supersaturation and Membrane Transport of Drugs. *Pharm Res* **2015,** *32*, (10), 3350-64.
12. Doak, A. K.; Wille, H.; Prusiner, S. B.; Shoichet, B. K. Colloid formation by drugs in simulated intestinal fluid. *J Med Chem* **2010,** *53*, (10), 4259-65.
13. Narang, A. S.; Badawy, S.; Ye, Q.; Patel, D.; Vincent, M.; Raghavan, K.; Huang, Y.; Yamniuk, A.; Vig, B.; Crison, J.; Derbin, G.; Xu, Y.; Ramirez, A.; Galella, M.; Rinaldi, F. A. Role of Self-Association and Supersaturation in Oral Absorption of a Poorly Soluble Weakly Basic Drug. *Pharm Res* **2015,** *32*, (8), 2579-94.
14. Usman, M.; Cheema, M. A.; Khan, A.; Farooqi, Z. H.; Mosquera, V.; Siddiq, M. A comparative study of thermodynamic properties of structurally related phenothiazine drugs in aqueous solution. *J Chil Chem Soc* **2013,** *58*, (3), 1842-45.
15. Schreier, S.; Malheiros, S. V. P.; de Paula, E. Surface active drugs. Self-association and interaction with membranes and surfactants. Physicochemical and biological aspects. *Biochimica et Biophysica Acta* **2000**, 210-34.
16. Frenkel, Y. V.; Clark, A. D.; Das, K.; Wang, Y.-H.; Lewi, P. J.; Janssen, P. A. J.; Arnold, E. Concentration and pH dependent aggregation of hydrophobic drug molecules and relevance to oral BAV. *J Med Chem* **2005,** *48*, 1974-83.
17. Owen, S. C.; Doak, A. K.; Wassam, P.; Shoichet, M. S.; Shoichet, B. K. Colloidal aggregation affects the efficacy of anticancer drugs in cell culture. *ACS Chem Biol* **2012,** *7*, (8), 1429-35.
18. Neuberg, C. Hydrotropy. *Biochem Z* **1916**, (76), 107-76.
19. Higuchi T, B. S. The solubility and complexing properties of oxytetracycline and tetracycline. III. Interactionc in aqueous solution with model compounds, biochemicals, metals, chelates and hexametaphosphate. *J Am Pharm Assoc* **1959**, (48), 557-64.
20. Sanghvi, R.; Evans, D.; Yalkowsky, S. H. Stacking complexation by nicotinamide: a useful way of enhancing drug solubility. *Int J Pharm* **2007,** *336*, (1), 35-41.
21. Hussain, M. A.; DiLuccion, R. C.; Maurin, M. B. Complexation of moricizine with nicotinamide and evaluation of the complexation constants by various methods. *J Pharm Sci* **1992,** *82*, (1), 77-79.

22. Booth, J. J.; Omar, M.; Abbott, S.; Shimizu, S. Hydrotrope accumulation around the drug: the driving force for solubilization and minimum hydrotrope concentration for nicotinamide and urea. *Phys Chem Chem Phys* **2015,** *17*, (12), 8028-37.
23. Das, S.; Paul, S. Computer Simulation Studies of the Mechanism of Hydrotrope-Assisted Solubilization of a Sparingly Soluble Drug Molecule. *J Phys Chem B* **2016,** *120*, (14), 3540-50.
24. Ferreira, G. S. S.; Périgo, D. M.; Politi, M. J.; Schreier, S. Effect of anions from the Hofmeister series and urea on the binding of the charged and uncharged forms of the local anesthetic tetracaine to zwitterionic micelles. *Photochem Photobiol* **1996,** *63*, (6), 755-61.
25. Hofmann, A. F.; Hagey, L. R. Bile acid chemistry, biology and therapeutics during the last 80 years: historical aspects. *J Lipid Res* **2014,** *55*, 1553-95.
26. Mukerjee, P.; Cardinal, J. R. Solubilization as a method for studying self-association: Solubility of naphthalene in the bile salt sodium cholate and the complex pattern of its aggregation. *Journal of Pharmaceutical Sciences* **1976,** *65*, (6), 882-86.
27. Riethorst, D.; Baatsen, P.; Remijn, C.; Mitra, A.; Tack, J.; Brouwers, J.; Augustijns, P. An In-Depth View into Human Intestinal Fluid Colloids: Intersubject Variability in Relation to Composition. *Mol Pharm* **2016,** *13*, (10), 3484-93.
28. Elvang, P. A.; Hinna, A. H.; Brouwers, J.; Hens, B.; Augustijns, P.; Brandl, M. Bile Salt Micelles and Phospholipid Vesicles Present in Simulated and Human Intestinal Fluids: Structural Analysis by Flow Field-Flow Fractionation/Multiangle Laser Light Scattering. *J Pharm Sci* **2016,** *105*, (9), 2832-9.
29. van Hasselt, P. M.; Janssens, G. E.; Slot, T. K.; van der Ham, M.; Minderhoud, T. C.; Talelli, M.; Akkermans, L. M.; Rijcken, C. J.; van Nostrum, C. F. The influence of bile acids on the oral bioavailability of vitamin K encapsulated in polymeric micelles. *J Control Release* **2009,** *133*, (2), 161-8.
30. Woollett, L. A.; Wang, Y.; Buckley, D. D.; Yao, L.; Chin, S.; Granholm, N.; Jones, P. J.; Setchell, K. D.; Tso, P.; Heubi, J. E. Micellar solubilisation of cholesterol is essential for absorption in humans. *Gut* **2006,** *55*, (2), 197-204.
31. Lindholm, A.; Henricsson, S.; Dahlqvist, R. The effect of food and bile acid administration on the relative bioavailability of cyclosporin. *Br J Clin Pharmac* **1990,** *29*, 541-48.
32. Vogtherr, M.; Marx, A.; Mieden, A. C.; Saal, C. Investigation of solubilising effects of bile salts on an active pharmaceutical ingredient with unusual pH dependent solubility by NMR spectroscopy. *Eur J Pharm Biopharm* **2015,** *92*, 32-41.
33. Yeap, Y. Y.; Trevaskis, N. L.; Quach, T.; Tso, P.; Charman, W. N.; Porter, C. J. Intestinal bile secretion promotes drug absorption from lipid colloidal phases via induction of supersaturation. *Mol Pharm* **2013,** *10*, (5), 1874-89.
34. Yeap, Y. Y.; Trevaskis, N. L.; Porter, C. J. The potential for drug supersaturation during intestinal processing of lipid-based formulations may be enhanced for basic drugs. *Mol Pharm* **2013,** *10*, (7), 2601-15.
35. Chen, J.; Mosquera-Giraldo, L. I.; Ormes, J. D.; Higgins, J. D.; Taylor, L. S. Bile Salts as Crystallization Inhibitors of Supersaturated Solutions of Poorly Water-Soluble Compounds. *Crystal Growth & Design* **2015,** *15*, (6), 2593-97.
36. Li, N.; Mosquera-Giraldo, L. I.; Borca, C. H.; Ormes, J. D.; Lowinger, M.; Higgins, J. D.; Slipchenko, L. V.; Taylor, L. S. A Comparison of the Crystallization Inhibition Properties of Bile Salts. *Crystal Growth & Design* **2016,** *16*, (12), 7286-7300.
37. Lu, J.; Ormes, J. D.; Lowinger, M.; Mann, A. K. P.; Xu, W.; Patel, S.; Litster, J. D.; Taylor, L. S. Impact of Bile Salts on Solution Crystal Growth Rate and Residual Supersaturation of an Active Pharmaceutical Ingredient. *Crystal Growth & Design* **2017,** *17*, (6), 3528-37.
38. Lu, J.; Ormes, J. D.; Lowinger, M.; Mann, A. K. P.; Xu, W.; Litster, J. D.; Taylor, L. S. Maintaining Supersaturation of Active Pharmaceutical Ingredient Solutions with Biologically Relevant Bile Salts. *Crystal Growth & Design* **2017,** *17*, (5), 2782-91.
39. P. Heinrich Stahl, C. G. W., *Handbook of Pharmaceutical Salts. Properties, Selection, and Use*. Zürich Switzerland, 2002.
40. Li, S.; Wong, S.; Sethia, S.; Almoazen, H.; Joshi, Y. M.; M., S. A. T. Investigation of Solubility and Dissolution of a Free Base and Two Different Salt Forms as a Function of pH. *Pharm Res* **2005,** *22*, (4), 628-35.
41. Aitipamula, S.; Banerjee, R.; Bansal, A. K.; Biradha, K.; Cheney, M. L.; Choudhury, A. R.; Desiraju, G. R.; Dikundwar, A. G.; Dubey, R.; Duggirala, N.; Ghogale, P. P.; Ghosh, S.; Goswami, P. K.; Goud, N. R.; Jetti, R. R. K. R.; Karpinski, P.; Kaushik, P.; Kumar, D.; Kumar, V.; Moulton, B.; Mukherjee,

A.; Mukherjee, G.; Myerson, A. S.; Puri, V.; Ramanan, A.; Rajamannar, T.; Reddy, C. M.; Rodriguez-Hornedo, N.; Rogers, R. D.; Row, T. N. G.; Sanphui, P.; Shan, N.; Shete, G.; Singh, A.; Sun, C. C.; Swift, J. A.; Thaimattam, R.; Thakur, T. S.; Kumar Thaper, R.; Thomas, S. P.; Tothadi, S.; Vangala, V. R.; Variankaval, N.; Vishweshwar, P.; Weyna, D. R.; Zaworotko, M. J. Polymorphs, Salts, and Cocrystals: What's in a Name? *Crystal Growth & Design* **2012,** *12*, (5), 2147-52.
42. Prasad, D.; Chauhan, H.; Atef, E. Role of Molecular Interactions for Synergistic Precipitation Inhibition of Poorly Soluble Drug in Supersaturated Drug-Polymer-Polymer Ternary Solution. *Mol Pharm* **2016,** *13*, (3), 756-65.
43. Edueng, K.; Mahlin, D.; Bergstrom, C. A. S. The Need for Restructuring the Disordered Science of Amorphous Drug Formulations. *Pharm Res* **2017,** *34*, (9), 1754-72.
44. Wiest, J.; Saedtler, M.; Balk, A.; Merget, B.; Widmer, T.; Bruhn, H.; Raccuglia, M.; Walid, E.; Picard, F.; Stopper, H.; Dekant, W.; Luhmann, T.; Sotriffer, C.; Galli, B.; Holzgrabe, U.; Meinel, L. Mapping the pharmaceutical design space by amorphous ionic liquid strategies. *J Control Release* **2017,** *268*, 314-22.
45. Hauser, M. T. W., M. Uptake of alkaloids by latex vesicles and isolated mesophyll vacuoles of chelidonium majus (Papaveraceae). *Z. Naturforsch* **1990**, (45c), 949-957.
46. Mösli Waldhauser, S. S.; Baumann, T. W. Compartmentation of caffein and related purine alkaloids depends exclusively on the physical chemistry of their vacuolar complex formation with chlorogenic acid. *Phytochemistry* **1996,** *42*, (4), 985-96.
47. Gorter, K. Beiträge zur Kenntniss des Kaffees. *Justus Liebigs Annalen der Chemie* **1907,** *359*, 217-44.
48. D'Amelio, N. P., G.; Dreyer, J.; Carloni, P.; Navarini, L. NMR Studies of Hetero-Association of Caffeine with di-O-Caffeoylquinic Acid Isomers in Aqueous Solution. *Food Biophysics* **2015,** *10*, 235-43.
49. Torre, J. C.; Schmidt, G. W.; Paetz, C.; Reichelt, M.; Schneider, B.; Gershenzon, J.; D'Auria, J. C. The biosynthesis of hydroxycinnamoyl quinate esters and their role in the storage of cocaine in Erythroxylum coca. *Phytochemistry* **2013,** *91*, 177-86.
50. Pasic, I.; Lipton, J. H. Current approach to the treatment of chronic myeloid leukaemia. *Leuk Res* **2017,** *55*, 65-78.
51. Pacheco-Palencia, L. A. M.-T., S.; Talcott, S.T. Chemical composition, antioxidant properties, and thermal stability of a phytochemical enriched oil from açai (Euterpe oleacea Mart.). *Journal of agricultural and food chemistry* **2008,** *56*, (12), 4631-36.
52. Russell, W. R.; Scobbie, L.; Labat, A.; Duthie, G. G. Selective bio-availability of phenolic acids from Scottish strawberries. *Mol Nutr Food Res* **2009,** *53 Suppl 1*, S85-91.
53. Ragusa, A.; Centonze, C.; Grasso, M. E.; Latronico, M. F.; Mastrangelo, P. F.; Sparascio, F.; Fanizzi, F. P.; Maffia, M. A Comparative Study of Phenols in Apulian Italian Wines. *Foods* **2017,** *6*, (4).
54. Pandey, M. M.; Katara, A.; Pandey, G.; Rastogi, S.; Rawat, A. K. An important Indian traditional drug of ayurveda jatamansi and its substitute bhootkeshi: chemical profiling and antioxidant activity. *Evid Based Complement Alternat Med* **2013.**
55. Wei, X.; Chen, D.; Yi, Y.; Qi, H.; Gao, X.; Fang, H.; Gu, Q.; Wang, L.; Gu, L. Syringic Acid Extracted from Herba dendrobii Prevents Diabetic Cataract Pathogenesis by Inhibiting Aldose Reductase Activity. *Evid Based Complement Alternat Med* **2012**.
56. Srinivasan, S.; Muthukumaran, J.; Muruganathan, U.; Venkatesan, R. S.; Jalaludeen, A. M. Antihyperglycemic effect of syringic acid on attenuating the key enzymes of carbohydrate metabolism in experimental diabetic rats. *Biomedicine & Preventive Nutrition* **2014,** *4*, (4), 595-602.
57. Itoh, A. I., K.; Kondoh, M.; Kawase, M.; Watari, A.; Kobayashi, M.; Tamesada, M.; Yagi, K. Hepatoprotective effect of syringic and vanillic acid on CCl_4-induced liver injury. *Biol. Pharm. Bull.* **2010,** *33*, (6), 983-87.
58. Dalmagro, A. P.; Camargo, A.; Zeni, A. L. B. Morus nigra and its major phenolic, syringic acid, have antidepressant-like and neuroprotective effects in mice. *Metab Brain Dis* **2017**.
59. Cao, Y.; Zhang, L.; Sun, S.; Yi, Z.; Jiang, X.; Jia, D. Neuroprotective effects of syringic acid against OGD/R-induced injury in cultured hippocampal neuronal cells. *Int J Mol Med* **2016,** *38*, (2), 567-73.
60. Tanaka, T.; Kawaguchi, N.; Zaima, N.; Moriyama, T.; Fukuta, Y.; Shirasaka, N. Antiosteoporotic activity of a syringic acid diet in ovariectomized mice. *J Nat Med* **2017**.
61. Wu, J.; Li, X.; Fang, H.; Yi, Y.; Chen, D.; Long, Y.; Gao, X.; Wei, X.; Chen, C. Y. Investigation of synergistic mechanism and identification of interaction site of aldose reductase with the combination of

gigantol and syringic acid for prevention of diabetic cataract. *BMC Complement Altern Med* **2016,** *16*, (1), 286.
62. Thipparaboina, R.; Mittapalli, S.; Thatikonda, S.; Nangia, A.; Naidu, V. G. M.; Shastri, N. R. Syringic Acid: Structural Elucidation and Co-Crystallization. *Crystal Growth & Design* **2016,** *16*, (8), 4679-87.
63. *United States Pharmacopeia and National Formulary*. 26th Edition ed.; Rockville, MD, USA, 2003.
64. Avdeef, A. Solubility of sparingly-soluble ionizable drugs. *Adv Drug Deliv Rev* **2007,** *59*, (7), 568-90.
65. LaPlante, S. R.; Carson, R.; Gillard, J.; Aubry, N.; Coulombe, R.; Bordeleau, S.; Bonneau, P.; Little, M.; O'Meara, J.; Beaulieu, P. L. Compound Aggregation in Drug Discovery: Implementing a Practical NMR Assay for Medicinal Chemists. *J. Med. Chem.* **2013,** *56*, (12), 5142-50.
66. Grillo, D.; Polla, G.; Vega, D. Conformational polymorphism on imatinib mesylate: grinding effects. *J Pharm Sci* **2012,** *101*, (2), 541-51.
67. Dhapte, V.; Mehta, P. Advances in hydrotropic solutions: An updated review. *St. Petersburg Polytechnical University Journal: Physics and Mathematics* **2015,** *1*, (4), 424-435.
68. LaPlante, S. R.; Aubry, N.; Bolger, G.; Bonneau, P.; Carson, R.; Coulombe, R.; Sturino, C.; Beaulieu, P. L. Monitoring drug self-aggregation and potential for promiscuity in off-target in vitro pharmacology screens by a practical NMR strategy. *J. Med. Chem.* **2013,** *56*, (17), 7073-83.
69. Banik, M.; Gopi, S. P.; Ganguly, S.; Desiraju, G. R. Cocrystal and Salt Forms of Furosemide: Solubility and Diffusion Variations. *Crystal Growth & Design* **2016,** *16*, (9), 5418-28.
70. Cherukuvada, S.; Babu, N. J.; Nangia, A. Nitrofurantoin-p-aminobenzoic acid cocrystal: hydration stability and dissolution rate studies. *J Pharm Sci* **2011,** *100*, (8), 3233-44.
71. Ueda, K.; Higashi, K.; Moribe, K. Direct NMR Monitoring of Phase Separation Behavior of Highly Supersaturated Nifedipine Solution Stabilized with Hypromellose Derivatives. *Mol Pharm* **2017,** *14*, (7), 2314-22.
72. Schultheiss, N.; Newman, A. Pharmaceutical Cocrystals and Their Physicochemical Properties. *Crystal Growth & Design* **2009,** *9*, (6), 2950-67.
73. Das, S.; Paul, S. Hydrotropic Solubilization of Sparingly Soluble Riboflavin Drug Molecule in Aqueous Nicotinamide Solution. *J Phys Chem B* **2017**, *121*, (37), 8774-87.
74. Remenar J.F.; Peterson, M. L.; Stephens P.W.; Zhang Z.; Zimenkov Y.; Hickey, M.B. Celecoxib Nicotinamide Dissociation. Using Excipients to Capture the Cocrystal's Potential. *Molecular Pharmaceutics* **2007,** *4*, (3), 386-400.
75. Guo, M.; Wang, K.; Hamill, N.; Lorimer, K.; Li, M. Investigating the Influence of Polymers on Supersaturated Flufenamic Acid Cocrystal Solutions. *Molecular Pharmaceutics* **2016,** *13*, (9), 3292-3307.
76. Wang, C.; Tong, Q.; Hou, X.; Hu, S.; Fang, J.; Sun, C. C. Enhancing Bioavailability of Dihydromyricetin through Inhibiting Precipitation of Soluble Cocrystals by a Crystallization Inhibitor. *Crystal Growth & Design* **2016,** *16*, (9), 5030-39.
77. Huang, N.; Rodriguez-Hornedo, N. Engineering cocrystal solubility, stability, and pH(max) by micellar solubilization. *J Pharm Sci* **2011,** *100*, (12), 5219-34.
78. Alhalaweh, A.; Ali, H. R. H.; Velaga, S. P. Effects of Polymer and Surfactant on the Dissolution and Transformation Profiles of Cocrystals in Aqueous Media. *Crystal Growth & Design* **2014,** *14*, (2), 643-48.
79. Childs, S. L.; Kandi, P.; Lingireddy, S. R. Formulation of a danazol cocrystal with controlled supersaturation plays an essential role in improving bioavailability. *Mol Pharm* **2013,** *10*, (8), 3112-27.
80. Surov, A. O.; Volkova, T. V.; Churakov, A. V.; Proshin, A. N.; Terekhova, I. V.; Perlovich, G. L. Cocrystal formation, crystal structure, solubility and permeability studies for novel 1,2,4-thiadiazole derivative as a potent neuroprotector. *Eur J Pharm Sci* **2017,** *109*, 31-39.
81. Peng, B.; Dutreix, C.; Mehring, G.; Hayes, M. J.; Ben-Am, M.; Seiberling, M.; Pokorny, R.; Capdeville, R.; Lloyd, P. Absolute bioavailability of imatinib (Glivec) orally versus intravenous infusion. *J Clin Pharmacol* **2004,** *44*, (2), 158-62.
82. Trevaskis, N. L.; Kaminskas, L. M.; Porter, C. J. From sewer to saviour - targeting the lymphatic system to promote drug exposure and activity. *Nat Rev Drug Discov* **2015,** *14*, (11), 781-803.
83. Lu, Y.; Tang, N.; Lian, R.; Qi, J.; Wu, W. Understanding the relationship between wettability and dissolution of solid dispersion. *Int J Pharm* **2014,** *465*, (1-2), 25-31.

84. Craig, D. Q. M. The mechanisms of drug release from solid dispersins in water-soluble polymers. *Int J Pharm* **2002,** *231*, 131-44.
85. Ross, D. L.; Riley, C. M. Physicochemical properties of the fluoroquinolone antimicrobials. II. Acid ionization constants and their relationship to structure. *Int J Pharm* **1992,** *83*, (1-3), 267-272.
86. Mesallati, H.; Tajber, L. Polymer/Amorphous Salt Solid Dispersions of Ciprofloxacin. *Pharm Res* **2017,** *34*, (11), 2425-39.
87. Li, X.; Zhi, F.; Hu, Y. Investigation of excipient and processing on solid phase transformation and dissolution of ciprofloxacin. *Int J Pharm* **2007,** *328*, (2), 177-82.
88. Lee, J.; Lee, S. C.; Acharya, G.; Chang, C.; Park, K. Hydrotropic solubilization of paclitaxel: Analysis of chemical structures for hydrotropic property. *Pharm Res* **2003,** *20*, (7), 1022-30.
89. DiNunzio, J. C.; Hughey, J. R.; Brough, C.; Miller, D. A.; Williams, R. O., 3rd; McGinity, J. W. Production of advanced solid dispersions for enhanced bioavailability of itraconazole using KinetiSol Dispersing. *Drug Dev Ind Pharm* **2010,** *36*, (9), 1064-78.
90. Ilevbare, G. A.; Liu, H.; Edgar, K. J.; Taylor, L. S. Maintaining Supersaturation in Aqueous Drug Solutions: Impact of Different Polymers on Induction Times. *Crystal Growth & Design* **2013,** *13*, (2), 740-51.
91. Chen, J.; Ormes, J. D.; Higgins, J. D.; Taylor, L. S. Impact of surfactants on the crystallization of aqueous suspensions of celecoxib amorphous solid dispersion spray dried particles. *Mol Pharm* **2015,** *12*, (2), 533-41.
92. Paidi, S. K.; Jena, S. K.; Ahuja, B. K.; Devasari, N.; Suresh, S. Preparation, in-vitro and in-vivo evaluation of spray-dried ternary solid dispersion of biopharmaceutics classification system class II model drug. *J Pharm Pharmacol* **2015,** *67*, (5), 616-29.
93. Kanaya, H.; Ueda, K.; Higashi, K.; Yamamoto, K.; Moribe, K. Stabilization mechanism of nitrazepam supersaturated state in nitrazepam/Eudragit®EPO/saccharin solution revealed by NMR measurements. *Asian Journal of Pharmaceutical Sciences* **2016,** *11*, (1), 58-59.
94. Deng, J.; Zhu, X.; Chen, Z.; Fan, C. H.; Kwan, H. S.; Wong, C. H.; Shek, K. Y.; Zuo, Z.; Lam, T. N. A Review of Food-Drug Interactions on Oral Drug Absorption. *Drugs* **2017,** *77*, (17), 1833-55.
95. Wu, Y.; Loper, A.; Landis, E.; Hettrick, L.; Novak, L.; Lynn, K.; Chen, C.; Thompson, K.; Higgins, R.; Batra, U.; Shelukar, S.; Kwei, G.; Storey, D. The role of biopharmaceutics in the development of a clinical nanoparticle formulation of MK-0869: a Beagle dog model predicts improved bioavailability and diminished food effect on absorption in human. *Int J Pharm* **2004,** *285*, (1-2), 135-46.
96. Raymond, C. R.; Sheskey, P. J.; Quinn, M. R. *Handbook of Pharmaceutical Excipients*. 6th ed.; London, UK.
97. Akimoto, M.; Nagahata, N.; Furuya, A.; Fukushima, K.; Higuchi, S.; Suwa, T. Gastric pH profiles of beagle dogs and their use as an alternative to human testing. *Eur J Pharm Biopharm* **2000,** *49*, 99-102.
98. Wiedmann, T. S.; Kamel, L. Examination of the solubilization of drugs by bile salt micelles. *J Pharm Sci* **2002,** *91*, (8), 1743-64.
99. Tsume, Y.; Matsui, K.; Searls, A. L.; Takeuchi, S.; Amidon, G. E.; Sun, D.; Amidon, G. L. The impact of supersaturation level for oral absorption of BCS class IIb drugs, dipyridamole and ketoconazole, using in vivo predictive dissolution system: Gastrointestinal Simulator (GIS). *Eur J Pharm Sci* **2017,** *102*, 126-39.
100. Rubbens, J.; Brouwers, J.; Tack, J.; Augustijns, P. Gastrointestinal dissolution, supersaturation and precipitation of the weak base indinavir in healthy volunteers. *Eur J Pharm Biopharm* **2016,** *109*, 122-29.
101. Tappouni, H. L.; Rublein, J. C.; Donovan, B. J.; Hollowell, S. B.; Tien, H. C.; Min, S. S.; Theodore, D.; Rezk, N. L.; Smith, P. C.; Tallman, M. N.; Raasch, R. H.; Kashuba, A. D. Effect of omeprazole on the plasma concentrations of indinavir when administered alone and in combination with ritonavir. *Am J Health Syst Pharm* **2008,** *65*, (5), 422-8.
102. Walwarens, J.; Brouwers, J.; Spriet, I.; Tack, J.; Annaert, P.; Augustijns, P. Effect of pH and Comedication on gastrointestinal absorption of posaconazole. *Clin Pharmacokinet* **2011,** *50*, (11), 725-34.
103. Hens, B.; Brouwers, J.; Corsetti, M.; Augustijns, P. Supersaturation and Precipitation of Posaconazole Upon Entry in the Upper Small Intestine in Humans. *J Pharm Sci* **2016,** *105*, (9), 2677-84.
104. Bevernage, J.; Hens, B.; Brouwers, J.; Tack, J.; Annaert, P.; Augustijns, P. Supersaturation in human gastric fluids. *Eur J Pharm Biopharm* **2012,** *81*, (1), 184-9.

105. Hens, B.; Corsetti, M.; Brouwers, J.; Augustijns, P. Gastrointestinal and Systemic Monitoring of Posaconazole in Humans After Fasted and Fed State Administration of a Solid Dispersion. *J Pharm Sci* **2016,** *105*, (9), 2904-12.
106. Krishna, G.; Ma, L.; Martinho, M.; O'Mara, E. Single-dose phase I study to evaluate the pharmacokinetics of posaconazole in new tablet and capsule formulations relative to oral suspension. *Antimicrob Agents Chemother* **2012,** *56*, (8), 4196-201.
107. Kraft, W. K.; Chang, P. S.; van Iersel, M. L.; Waskin, H.; Krishna, G.; Kersemaekers, W. M. Posaconazole tablet pharmacokinetics: lack of effect of concomitant medications altering gastric pH and gastric motility in healthy subjects. *Antimicrob Agents Chemother* **2014,** *58*, (7), 4020-5.
108. Mudie, D. M.; Murray, K.; Hoad, C. L.; Pritchard, S. E.; Garnett, M. C.; Amidon, G. L.; Gowland, P. A.; Spiller, R. C.; Amidon, G. E.; Marciani, L. Quantification of gastrointestinal liquid volumes and distribution following a 240 mL dose of water in the fasted state. *Mol Pharm* **2014,** *11*, (9), 3039-47.
109. Sun, D. D.; Lee, P. I. Evolution of supersaturation of amorphous pharmaceuticals: the effect of rate of supersaturation generation. *Mol Pharm* **2013,** *10*, (11), 4330-46.
110. Van Speybroeck, M.; Mellaerts, R.; Mols, R.; Thi, T. D.; Martens, J. A.; Van Humbeeck, J.; Annaert, P.; Van den Mooter, G.; Augustijns, P. Enhanced absorption of the poorly soluble drug fenofibrate by tuning its release rate from ordered mesoporous silica. *Eur J Pharm Sci* **2010,** *41*, (5), 623-30.
111. Six, K.; Daems, T.; de Hoon, J.; Van Hecken, A.; Depre, M.; Bouche, M. P.; Prinsen, P.; Verreck, G.; Peeters, J.; Brewster, M. E.; Van den Mooter, G. Clinical study of solid dispersions of itraconazole prepared by hot-stage extrusion. *Eur J Pharm Sci* **2005,** *24*, (2-3), 179-86.
112. Bevernage, J.; Brouwers, J.; Annaert, P.; Augustijns, P. Drug precipitation-permeation interplay: supersaturation in an absorptive environment. *Eur J Pharm Biopharm* **2012,** *82*, (2), 424-8.
113. Lohani, S.; Cooper, H.; Jin, X.; Nissley, B. P.; Manser, K.; Rakes, L. H.; Cummings, J. J.; Fauty, S. E.; Bak, A. Physicochemical properties, form, and formulation selection strategy for a biopharmaceutical classification system class II preclinical drug candidate. *J Pharm Sci* **2014,** *103*, (10), 3007-21.
114. Tanaka, Y.; Sugihara, M.; Kawakami, A.; Imai, S.; Itou, T.; Murase, H.; Saiki, K.; Kasaoka, S.; Yoshikawa, H. In vivo analysis of supersaturation/precipitation/absorption behavior after oral administration of pioglitazone hydrochloride salt; determinant site of oral absorption. *Eur J Pharm Sci* **2017,** *106*, 431-38.
115. Carlert, S.; Palsson, A.; Hanisch, G.; von Corswant, C.; Nilsson, C.; Lindfors, L.; Lennernas, H.; Abrahamsson, B. Predicting intestinal precipitation--a case example for a basic BCS class II drug. *Pharm Res* **2010,** *27*, (10), 2119-30.
116. Indulkar, A. S.; Gao, Y.; Raina, S. A.; Zhang, G. G.; Taylor, L. S. Exploiting the Phenomenon of Liquid-Liquid Phase Separation for Enhanced and Sustained Membrane Transport of a Poorly Water-Soluble Drug. *Mol Pharm* **2016,** *13*, (6), 2059-69.
117. Tanako, R.; Takata, N.; Saito, R.; Furumoto, K.; Higo, S.; Hayashi, Y.; Machida, M.; Aso, Y.; Yamashita, S. Quantitative analysis of the effect of supersaturation on in vivo drug absorption. *Mol Pharm* **2010,** *7*, (5), 1883-87.
118. Tanaka, Y.; Kawakami, A.; Nanimatsu, A.; Horio, M.; Matsuoka, J.; Wada, T.; Kasaoka, S.; Yoshikawa, H. In vivo evaluation of supersaturation/precipitation/re-dissolution behavior of cinnarizine, a lipophilic weak base, in the gastrointestinal tract: the key process of oral absorption. *Eur J Pharm Sci* **2017,** *96*, 464-71.
119. Tho, I.; Liepold, B.; Rosenberg, J.; Maegerlein, M.; Brandl, M.; Fricker, G. Formation of nano/micro-dispersions with improved dissolution properties upon dispersion of ritonavir melt extrudate in aqueous media. *Eur J Pharm Sci* **2010,** *40*, (1), 25-32.
120. Liu, C.; Chen, Z.; Chen, Y.; Lu, J.; Li, Y.; Wang, S.; Wu, G.; Qian, F. Improving Oral Bioavailability of Sorafenib by Optimizing the "Spring" and "Parachute" Based on Molecular Interaction Mechanisms. *Mol Pharm* **2016,** *13*, (2), 599-608.
121. Chen, Y.; Wang, S.; Wang, S.; Liu, C.; Su, C.; Hageman, M.; Hussain, M.; Haskell, R.; Stefanski, K.; Qian, F. Sodium Lauryl Sulfate Competitively Interacts with HPMC-AS and Consequently Reduces Oral Bioavailability of Posaconazole/HPMC-AS Amorphous Solid Dispersion. *Mol Pharm* **2016,** *13*, (8), 2787-95.

122. Kourentas, A.; Vertzoni, M.; Symillides, M.; Goumas, K.; Gibbon, R.; Butler, J.; Reppas, C. Effectiveness of supersaturation promoting excipients on albendazole concentrations in upper gastrointestinal lumen of fasted healthy adults. *Eur J Pharm Sci* **2016,** *91*, 11-9.
123. Dahan, A.; Miller, J. M. The solubility-permeability interplay and its implications in formulation design and development for poorly soluble drugs. *The AAPS Journal* **2012,** *14*, (2), 244-251.
124. Berben, P.; Mols, R.; Brouwers, J.; Tack, J.; Augustijns, P. Gastrointestinal behavior of itraconazole in humans - Part 2: The effect of intraluminal dilution on the performance of a cyclodextrin-based solution. *Int J Pharm* **2017,** *526*, (1-2), 235-243.